RICE UNIVERSITY

Microfabricated Poly (ethylene glycol) Based Hydrogels for Microvascular Tissue Engineering Applications

By

Michael Paul Cuchiara

A THESIS SUBMITTED IN PARTIAL FULLFILLMENT OF THE REQUIREMENTS FOR THE DEGREE

Doctor of Philosophy

APPROVED, THESIS COMMITTEE

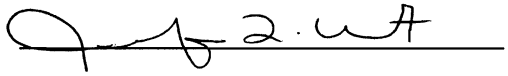

Jennifer L. West, Isabel C. Cameron
Professor, Chair Bioengineering

S. Lisa Biswal, Assistant Professor,
Chemical and Biomolecular
Engineering

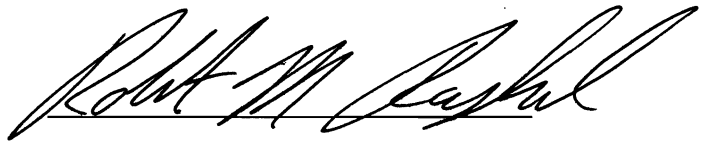

Robert M. Raphael, Associate
Professor, Bioengineering

Houston, TX

April 2011

ABSTRACT

Microfabricated Poly (ethylene glycol) Based Hydrogels for Microvascular Tissue Engineering Applications

By

Michael Paul Cuchiara

Shortages in donor organs and the lack of therapeutic treatment options to address tissue loss and end-organ failure has led to intense research into tissue engineering based therapeutics. Cellular, tissue, and organ level therapeutics hold the potential to shift clinical paradigms and drastically improve healthcare outcomes. However, to date the only successful tissue engineering therapeutics have been limited to thin and avascular tissues such as skin, cartilage and the bladder. This is primarily due to the absence of a perfusable vasculature to transport nutrients and waste during *in vitro* tissue development and inadequate host-implant vascular integration upon implantation. In this thesis we set out to develop hydrogel microfabrication technologies to (1) improve *in vitro* mass transport, (2) integrate self-assembling microvascular networks with microfabricated channels and (3) incorporate and support functional parenchymal cellular elements within *in vitro* constructs.

Application of microfabrication technologies to PEG hydrogels requires that fabrication schemes are cell compatible, robust for handling and imaging and most importantly allow for precise micron level control of both fluid perfusion and hydrogel structure fabrication. Herein we report multiple cell compatible

microfabrication schemes that employ multilayer replica molding and photolithographic hydrogel fabrication techniques. Systems designed with these techniques resulted in improved *in vitro* mass transport, integration of self-assembled microvascular networks with fabricated structures and the ability to pattern multilayer heterogeneous hydrogel structures that contain and support multiple cellular elements.

The progress reported herein has broad applicability towards the development of biomaterials with highly biomimetic structural-functional characteristics. More specifically these hydrogel microfabrication technologies hold the promise to improve the therapeutic potential of tissue engineered constructs and provide more biologically applicable pre-clinical tissue models.

ACKNOWLEDGMENTS

Thank you Jennifer for your unwavering support and willingness to support a very open and free thinking research environment. Thanks to my other committee members Lisa Biswal and Robert Rapheal. Lisa and her lab members, especially Gautam, taught me the intricacies of clean room techniques and improved my microfab tremendously. Rob, well graduate at school at Rice would not be graduate school at Rice without you. Thanks for everything.

Thanks to all West lab members past and present. Special thanks to Jordan Miller for being my mentor and Christy Franco for always having the answer. None of this would have been possible without the support of my family and my soon to be wife Maude.

TABLE OF CONTENTS

ABSTRACT 1
ACKNOWLEDGMENTS 3
TABLE OF CONTENTS 4
LIST OF TABLES 6
1. Chapter 1: Need For Regenerative Medicine-Based Therapeutics 10
2. Chapter 2: Tissue Engineering Strategies 13
2.1. Scaffolding Strategies 15
2.2. Current Success and Challenges in Tissue Engineering Therapeutics 27
3. Chapter 3: Vascularization of Tissues 30
3.1. Microvascular Physical Characteristics and Function 30
3.2. The Developing Microvasculature: Vasculogenesis 32
3.3. The Dynamic Microvasculature: Angiogensis 36
3.4. Microvascular Tissue Bed Mass Transport 39
4. Chapter 4: Microvascular Tissue Engineering (MVTE) 44
4.1. Role of Vascularization in Improved Tissue Engineering Therapeutics 44
4.2. PEG Hydrogels Modified with Vascular Biomimetic ECM Signals 47
4.3. PEG Hydrogels Modified with Pro-Vasculogenic Signaling Proteins 49
4.4. Proteolytically Degradable PEG Hydrogels for MVTE 51
4.5. Cellular Elements for MVTE 52
4.6. Current Limitations in Microvascular Tissue Engineering 56
4.7. Microfabricated Hydrogels for MVTE Applications 64
4.8. Current Limitations in Microfabricated Hydrogels for MVTE Applications 76
5. Chapter 5: Overview of Thesis Objectives 79
6. Chapter 6: Multilayer Microfluidic Poly (ethylene glycol) diacrylate Hydrogels 80
6.1. Introduction 80
6.2. Objectives 82
6.3. Materials and Methods 82
6.4. Results and Discussion 92
6.5. Conclusions 102

7. Chapter 7: Perfused Microchannel Integration with Microvascular Networks 106
7.1. Introduction 106
7.2. Objectives 107
7.3. Materials and Methods 107
7.4. Results and Discussion 116
7.5. Conclusions 129
8. Chapter 8: Softlithographically and Photolithographically Fabricated PEG Hydrogels 130
8.1. Introduction 130
8.2. Objectives 137
8.3. Materials and Methods 137
8.4. Results and Discussion 144
8.5. Conclusions 153
9. Chapter 9: Strategic Directions in Microvascular Tissue Engineering 155
10. Chapter 10: Bibliography 160
11. Chapter 11: Appendices 174

LIST OF TABLES

Table 1: Incidences of organ and tissue abnormalities and the number of procedures associated with the occurrence 11
Table 2: Cell Adhesive ECM Mimetic Peptide Sequences. 49
Table 3: Ratios and Density of Heterocellular Culture Conditions 143
Table 4: Effects of Photoinitiator Concentration and Solvent Type on Structure Formation 149

LIST OF FIGURES

Figure 1: Tissue Engineering Paradigm..... 13
Figure 2: Scaffold Processing and Fabrication Techniques. 18
Figure 3: PEG Biofunctionalization and Crosslinking Systems..... 22
Figure 4: Soluble Bioactive Factor Release from Hydrogel Scaffolds. 23
Figure 5: Effects of Multiple Heterobifunctional PEG-Biomolecule Conjugation Sites 25
Figure 6: Heterobifunctional Biomolecule Conjugation Schematic. 26
Figure 7: Schematic Representation of Photopolymerized PEGDA Network Formation. 27
Figure 8: Circulatory System with emphasis on Microvascular Component..... 30
Figure 9: Composition of Blood Vessels. 32
Figure 10: Schematic of Vasculogenesis. 34
Figure 11:Vacuole Fusion Precedes Lumen Formation. 35
Figure 12: Sprouting Mechanism of Angiogenesis. 38
Figure 13: Non-Angiogenic Mechanisms of Postnatal Vessel Formation.]..... 39
Figure 14: Schematic of Microvascular Mass Transport Pathways. 42
Figure 15: Integration of the Traditional Tissue Engineering Paradigm with Microfabrication Technologies.. 47
Figure 16: Effects of RGD on Endothelial Cell Adhesion to PEG 48
Figure 17: Immobilized Growth Factor Effects on 2D Endothelial Cell Morphology. 50
Figure 18: Proteolytically Degradable Bioactive PEG Hydrogels.. 52
Figure 19: Morphological and Functional Analysis of Self-Assembled Blood Vessel Networks.... 54
Figure 20: Schematic of Pro-tubulogenic Co-Culture in a Proteolytically Degradable PEG Hydrogel. 55
Figure 21: Effects of Distance from Vasculature on Nutrients and Bioactive Factor Concentrations. 58
Figure 22: Shifting Transport Regimes in Vascularized Constructs.. 59
Figure 23: Photolithographic Patterning of Hydrogels. 65
Figure 24: Photodegradable PEGDA Derivatives. 67
Figure 25: Soft lithography Schematic.. 68
Figure 26: PGS Microchannels.. 70
Figure 27: Mass Transport within Microfluidic Hydrogels. 71
Figure 28: Microfluidic hydrogels fabricated via a sacrificial poragen 72
Figure 29: Hydrogels inlaid within PDMS housings for controlled gradients and flow regimes..... 74
Figure 30: Hydrogel Microfabrication Approaches within PDMS housings 75
Figure 31: Integration of Microfabrication Technologies with a Self-Assembling Pro-Tubulogenic Hydrogel.. 79
Figure 32: Supporting Apparatuses for Microfluidic Hydrogels. 81
Figure 33:Reaction Schematic for Synthesis of poly(ethylene glycol) diacrylate (PEGDA). 83
Figure 34:Reaction Schematic of Acryoyl-PEG-RGDS 85
Figure 35: Fabrication schematic of PDMS/PEGDA microfluidic networks 88
Figure 36: Multilayer microfluidic PEGDA hydrogel. 93
Figure 37: Solute molecular weight effects on PEGDA spatiotemporal diffusion profiles. 95
Figure 38: PEGDA hydrogel concentration effects on transport properties..... 96
Figure 39: Volume Filling Logic Based Explanation for Polymer Concentration Effects on Diffusivity in Swelling Restricted Systems. 98
Figure 40: Encapsulated 3T3 fibroblast spatiotemporal cell viability fluorescent micrographs ... 100
Figure 41: Encapsulated 3T3 fibroblast spatiotemporal perfused and static cell viability 102

Figure 42: Schematic Demonstrating Effects of Optimal Microchannel Network Spacing on Oxygen Gradients and Cell Viability Profiles.. 105
Figure 44: Reaction Schematic of Peptides with Heterobifunctional PEG linkers to form tethered adhesion peptides and a proteolytically degradable PEG derivative..... 110
Figure 45: System Design Schematic and Microvascular Network Formation.. 111
Figure 46: Spatiotemporal Microvascular Morphology.. 119
Figure 47: Spatiotemporal Self-Assembled Microvascular Network Morphology..... 120
Figure 48: Spatiotemporal Scaffold Apoptotic Activity. 122
Figure 49: Mass Transport Regimes in Acellular and Vascularized PEG Scaffolds.. 125
Figure 50: Dextran Spatial Fluorescence Intensity Profiles. 127
Figure 51: High Molecular Weight Dextran Intensity Profiles and Extravessel Diffusion.. 128
Figure 52: Schematic of Microscope Modified for Mask Projection Photolithography and an LCD Based Exposure System..... 131
Figure 53: Schematic Diagram of Liver Functional Unit 133
Figure 54: Microfabricated, Perfusable, Multi-compartment BAL Devices.. 134
Figure 55: Multilayer Additive Photolithographic Fabrication of PEGDA Hydrogels with Encapsulated Hepatocytes. 135
Figure 56:Hepatocyte Fibroblast Microfabricated Co-Culture. 136
Figure 57: MPP System Schematic. 138
Figure 58: Multilayer Photolithographic and Softlithographic Fabrication Schematic of PDMS/PEGDA Microdevices.. 141
Figure 59: Multilayer PEGDA Hydrogels Fabricated using Mask Projection Photolithography and Softlithography.. 146
Figure 60: Effects of Photoinitiator Concentration on Cell Viability.. 149
Figure 61: Heteroculture Composition Effects on Hepatocyte Cytochrome p450 Function.. 150
Figure 62: Effect of Media Formulation on Hepatocyte Cytochrome P450 Function.. 151
Figure 63: Transient Media Conditioning on Hepatocyte Cytochrome P450 Function..... 152
Figure 70: Gel Permeation Chromatography (GPC) of Laysan-PEG-NHS conjugation to PQ peptide.. 174
Figure 72: Gel Protein Chromatography (GPC) of Laysan-PEG-NHS conjugation to RGDS.. ... 175
Figure 71: Matrix Assisted Laser Desorption/Ionization Time of Flight Mass Spectroscopy (MALDI TOF) of solid state peptide synthesis product for the collagen derived PQ peptide..... 176
Figure 64: Representative Images of 5% PEGDA Toluidine Blue Diffusion Profiles..... 177
Figure 65: Representative Images of 10% PEGDA Toluidine Blue Diffusion Profiles..... 177
Figure 66: Representative Images of 20% PEGDA Toluidine Blue Diffusion Profiles..... 178
Figure 67: Representative Images of 10% PEGDA 3kDa Dextran Fluorescein Diffusion Profiles 178
Figure 68: Representative Images of 10% PEGDA 10kDa Dextran Fluorescein Diffusion Profiles 179

LIST OF EQUATIONS

Equation 1: Fick's Second Law of Diffusion. 90
Equation 2: Solution to Fick's Second Law of Diffusion. 90
Equation 3: Dimensionless Peclet Number and Comparison to Microchannel Geometry. 90
Equation 4: Molecular Radius as a Function Solute Molecular Weight. 91
Equation 5: Solute Effective Diffusivity as a Function of Solute Molecular Radius. 91
Equation 6: Equation for Calculation of % Convection Transport Trace 116

1. Chapter 1: Need For Regenerative Medicine-Based Therapeutics

Numerous pathologies exist which lead to gross tissue abnormalities, organ failure and require organ and or tissue transplants (see Table 1) Procedures associated with these pathologies place a significant financial burden on the health care system with more than $400 billion dollars in annual expenditures resulting from treatment associated with the pathology.[1] Furthermore, of those patients seeking organ or tissue replacement most will perish while waiting for a transplant. For example, of the 30,000 patients who die from liver failure only 3,000 or 10% will receive the potentially lifesaving transplant.[1]This trend highlights a significant shortage of donor organs and tissues and gives rise for a need to radically transform current clinical paradigms associated with transplants.

Table 1: Incidences of organ and tissue abnormalities and the number of procedures associated with the occurrence Recreated from [1]

Indication	Procedures or patients per year
Skin	
Burns*	2,150,000
Pressure sores	1,500,000
Venous stasis ulcers	500,000
Diabetic ulcers	600,000
Neuromuscular disorders	200,000
Spinal cord and nerves	40,000
Bone	
Joint replacement	558,200
Bone graft	275,000
Internal fixation	480,000
Facial reconstruction	30,000
Cartilage	
Patella resurfacing	216,000
Chondromalacia patellae	103,400
Meniscal repair	250,000
Arthritis (knee)	149,900
Arthritis (hip)	219,300
Fingers and small joints	179,000
Osteochondritis dissecans	14,500
Tendon repair	33,000
Ligament repair	90,000
Blood vessels	
Heart	754,000
Large and small vessels	606,000
Liver	
Metabolic disorders	5,000
Liver cirrhosis	175,000
Liver cancer	25,000
Pancreas (diabetes)	728,000
Intestine	100,000
Kidney	600,000
Bladder	57,200
Ureter	30,000
Urethra	51,900
Hernia	290,000
Breast	261,000
Blood transfusions	18,000,000
Dental	10,000,000

*Approximately 150,000 of these individuals are hospitalized and 10,000 die annually.

The 10% of the tissues or organs that are transplanted can be divided into two categories either autologous or non-autolgous sources. Autologous sources refer to procedures which harvest tissue from healthy regions in the patient's body and transplant these tissues to the site of pathology in order to augment or replace the abnormally functioning tissue. For example, the sapehnous vein is used in vascular bypass surgery [2] to provide a patent vessel for blood flow while the hamstring tendon is often harvested to replace or augment the mechanical functions of injured ligaments in the knee joint[3]. Autologous transplant strategies offer complete biocompatibility and often help to restore a large amount of function to the diseased tissue. Unfortunately, autologous transplants result in loss of function at the site of tissue harvesting a side effect known as donor site morbidity. Furthermore, the need for multiple tissue transplant procedures may deplete the donor site supply to such an extent that the originally normal tissue

function at the donor site may be permanently damaged. Non-autologous sources such those produced form human cadavers (allografts) and from other species (xenografts), are not limited by donor site morbidity but these tissue transplants have a greatly increased risk of disease transmission, have poor biocompatibility, often illicit a strong immune response and require that the patient remain on immunosuppression therapy for the remainder of their lifetime.[4,5]

Thus there exists a need to develop tissue engineering based strategies to augment and or replace the current clinically accepted strategies surrounding organ and tissue transplantation. Tissue engineered therapeutics circumvent the need for large scale tissue harvesting from donor tissue by providing *ex vivo* culture conditions to develop the engineered tissue into clinically viable constructs. Tissue engineering effectively minimizes if not eliminates donor site morbidity and coupled with the proper choice of materials, tissue engineering holds the promise to greatly reduce the biocompatibility and disease transmissions concerns surrounding non-autologous transplantation procedures.

2. Chapter 2: Tissue Engineering Strategies

A common paradigm has emerged to integrate diverse disciplines, and mimic the *in vivo* characteristics of tissue organization and content. (Figure 1) This paradigm consists of three general branches: the recapitulation of a provisional extracellular matrix analog or scaffold; incorporation of bioactive signaling factors and the presence of cellular or multicellular components. Proper integration of all branches is necessary to facilitate the production of tissue engineering therapeutics with successful clinical outcomes.

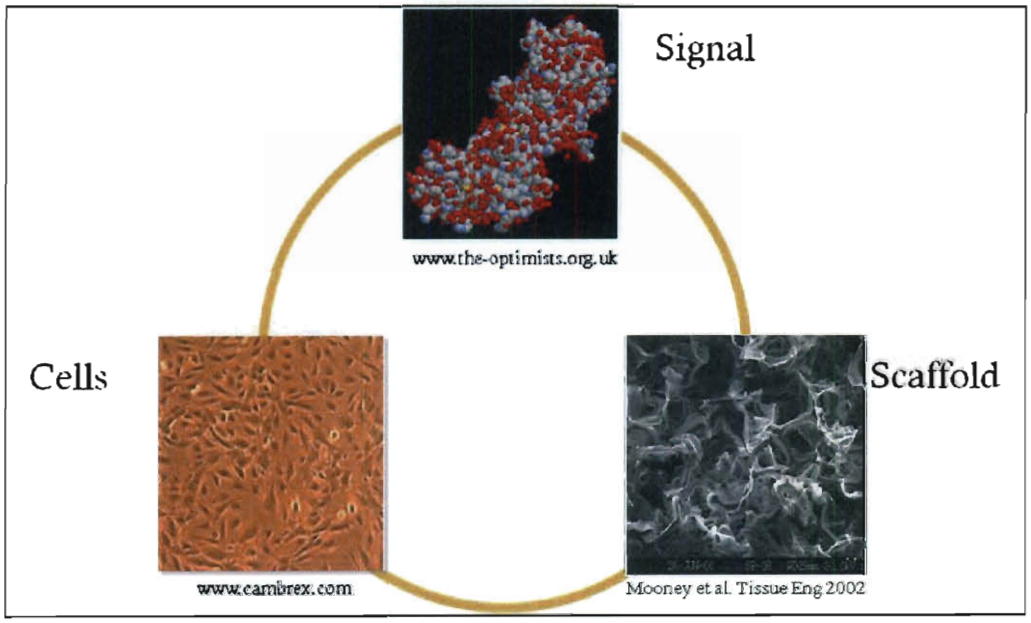

Figure 1: Tissue Engineering Paradigm. Combination of cells, bioactive signals, and scaffolding components to mimic *in vivo* tissues has governed tissue engineering system design throughout its first 20 years.

Comprehensive analysis of the scientific literature surrounding tissue engineering yields important design considerations and useful engineering parameters for recapitulating these environments. However, the highly complex

and dynamic nature of cellular, biophysical, and biochemical enactors makes highlighting the sufficient and necessary signals in tissue development a daunting task. None the less, it is important to develop an overarching strategy that includes a synergy of cellular constituents, matrix or insoluble components, and soluble signals together to drive tissue formation.

Selection of the proper cellular elements is integral in providing the correct phenotypical cellular activity as well as the functional aspect of the tissue. Cell sources must also account for the heterogeneous nature of complex tissues and often require multiple cell types to be seeded within the construct. Another approach that has recently gained interest is the use of pluripotent cell types to provide all of the cellular components of the construct. This is advantageous because it does not require multiple cell sources the seeding of multiple cell types.

Soluble signals in the form of nutrients and signaling factors are crucial to determining cell phenotype, morphology and to spatially direct tissue formation. It is not only important to determine the type and concentration of bioactive factor but it is critical that the factors be dynamically presented in the system. Furthermore spatial presentation of the factors has an important effect on tissue formation. Soluble factors whether as a product of media components, cell secreted signals or released from the matrix must be carefully controlled and characterized in order to direct tissue development.

The extracellular matrix (ECM) plays multiple important roles in providing physical scaffolding, sequestering soluble growth factors, and establishing hapotactic signaling gradients for cell adhesion and migration. Furthermore, the ability of the ECM to remodel and react dynamically to the environment is a crucial characteristic in regulating cell migration and tissue formation behaviors. Therefore when designing vasculogenic ECM biomimetic systems the researcher needs to provide a matrix substitute that provides a dynamic multifaceted interaction with the cellular elements. Although it is important to determine the optimal combination of cells, signals and ECM components, much of our research focuses on development of scaffolds to mimic the ECM.

2.1. Scaffolding Strategies

Tissue engineering scaffolds seek to mimic the native ECM by providing a physical architecture as well as a source of biochemical signals to support cellular adhesion, migration, morphology, and tissue formation. Biomimetic ECM scaffolds can be loosely categorized as either natural or synthetic based materials, with some constructs incorporating a combination of both[6]. Natural materials that are commonly used for microvascular tissue engineering are collagen[7], agarose[8], alginate [9], and fibrin[10] matrices. The use of natural materials as scaffolding constructs is advantageous due to their inherent bioactivity and biodegradation, which allows for cell-ECM signaling and tissue remodeling with minimal modification of the material. However, the ability to independently tailor the physical and biochemical properties of the material is difficult. Thus identifying and decoupling important physical and biochemical enactors is

prohibitive in natural systems. Furthermore, batch to batch variability and the risk of disease transmission and adverse host immune reactions in natural scaffolding materials makes implementing good manufacturing practices difficult and has discouraged the clinical application of these materials due to regulatory concerns. Despite these drawbacks, natural materials are commonly employed as MVTE scaffolds and at the very least provide a template for synthetic materials to mimic.

Synthetic scaffolds provide a greater degree of control over scaffold physical and biochemical properties. Unlike natural materials synthetic scaffolds have little or no risk of disease transmission with manageable immunogenicity and cytotoxicity. [11] Batch to batch variability can be reduced through proper quality control measures and common characterization techniques. However, in order to mimic the ECM, most synthetic scaffolds require the incorporation of bioactivity into inherently non-biomimetic systems. Modification of synthetic scaffolding materials with various ECM proteins is a common mechanism to precisely engineer bioactive signaling components of tissue engineering scaffolds. Proteins such as fibronectin, fibrin, agarose, gelatin, and collagen have been used to coat or impregnate the matrix of synthetic polymers such as poly(dimethyl siloxane) (PDMS), poly(caprolactone), poly(tetrafluoroethylene) (ePTFE), and Dacron.[12]

Independent of material type, the manner in which the scaffold is fabricated has a great affect on construct physical properties. A wide variety of scaffold fabrication techniques have been developed to alter scaffold bulk

properties in order to improve mass transport and cellular migration characteristics. Particulate leaching[13], polymer phase separation[14], gas foaming[15] and electrospinning[16] have all been shown to increase average pore size, facilitate pore interconnectivity, and enhance overall porosity at the nano- and micro-scale.(Figure 2) Optimal macroporous architectures should allow for tissue ingrowth and cellular migration without compromising desired scaffold mechanical properties. Examples of scaffolds with average pore diameters ranging from 10-100 μm have been shown to facilitate cellular ingrowth and migration.[13-16] (Figure 2) Furthermore, selection of optimal pore geometries and average pore diameter should reflect the native tissue type of interests and be carefully integrated with cell seeding methods and overall construct integration schemes.

Although these techniques have been shown to improve bulk mass transport properties, they provide little or no spatial control over fabricated microarchitectures. Furthermore, cytotoxic processing conditions require cell seeding to occur post scaffold processing. This methodology often results in non-homogenous cellular distribution throughout the thickness of the scaffold and limits the overall metabolic density of the construct[17-19]. Next generation fabrication technologies should provide the ability to spatially tailor scaffold architectures so as to control cell migration and tissue formation.

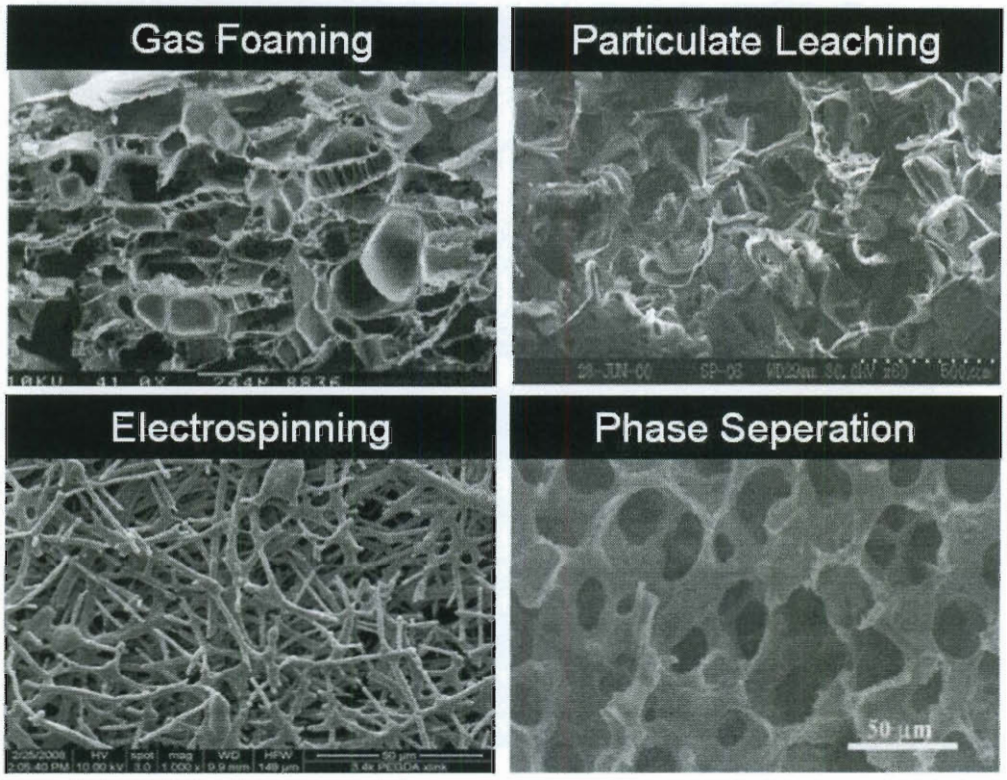

Figure 2: Scaffold Processing and Fabrication Techniques. Techniques allow for bulk tailoring of physical architecture. However current techniques are not cytocompatible and have no ability to spatial control architecture. Recreated from Mooney *et al*[47], Ma *et al.*[48] and Harris *et al.*[49]

One class of synthetic materials which shows great promise as tissue engineering scaffolds is hydrogels. Hydrogels have favorable scaffolding properties and closely mimic *in vivo* systems due to their high water content and tissue-like elastic properties. Furthermore, the large interstitial aqueous fraction of hydrogel systems facilitates rapid water soluble mass transport.[20] This property coupled with the fact that tissue engineering hydrogel systems are often less than 10% polymer fraction by mass, permits a greatly reduced effective diffusivity and improved mass transport when compared to non-hydrogel polymer scaffolds.[21] Multiple hydrophilic synthetic polymers have been used to generate

hydrogel systems for tissue engineering including, poly(ethylene glycol) (PEG), poly(hydroxyethyl methacrylate) (PHEMA), poly(vinyl alcohol) (PVA), poly(acrylic acid) (PAA), poly(methacrylic acid) PMMA, and poly(acrylimide) (PAAm).[21] Perhaps the most widely studied hydrogels system for tissue engineering applications are PEG-based scaffolds. PEG hydrogels are non-toxic, non-immunogenic, and approved by the US Food and Drug Administration for a variety of clinical applications.[21] Furthermore, PEG has been touted as a "stealth" material due to its ability to resist protein adsorption and evade adverse foreign body immune reactions.[22] In addition, PEG's intrinsically low protein adsorption provides a blank slate to specifically engineer the desired scaffold bioactivity while maintaining independent control over system physical properties.[23,24] For these reasons the remainder of microvascular scaffolding design discussions will focus on the fabrication and modification PEG hydrogel based systems.

2.1.1. PEG Hydrogel Crosslinking Techniques

Crosslinked PEG hydrogel scaffolds possess many important biomimetic properties of the extracellular matrix including high biocompatibility. This has led to intense interest in PEG-based materials as scaffolds for tissue engineering and regenerative medicine applications. However, independent of the scaffold, it is important that the conditions used to crosslink PEG pre-polymer solutions are compatible with cellular components. This is critical if cells are to be encapsulated and/or if the scaffold is to be used as an *in situ* gelling construct. Free-radical based polymerization of acrylate terminated PEG macromers and

Michel-Type addition reactions between free thiols and acrylate groups have become the most prevalent means for crosslinking PEG scaffolds.

Michael-Type addition reactions were first reported by Hubbell's research group in the late 1990's as a means for crosslinking bioactive PEG scaffolds.[25] Michael-Type crosslinking mechanisms are base-catalyzed addition of free- thiols to acrylates in a one-to-one additive fashion. (Figure 3A) The process is cytocompatible and relatively rapid, proceeding to completion in 30 min at 37 °C and a pH of 7.4.[26] Michel-Type hydrogels are degradable through hydrolysis without the need to engineering specific degradable co-polymers.[27] Another advantage of Michel-Type PEG hydrogels is that the thiol side chain on the cysteine amino acid can be systematically used as a biocompatible crosslinker and as a means to immobilize proteins and oligopeptide sequences in the scaffold.[28] Cell encapsulation within Michel-Type hydrogels at neutral pH and 37 °C often exhibit non-homogenous cell dispexing devicesrsion due to gravity driven cell settling during the slow gelation time.The use of mi to disperse cells during crosslinking or elevated pH and and/or temperatures improves cellular dispersion. Also the use of mutli-armed thiol or acrylate terminated crosslinkers increases the rate of gelation and provides a mechanism to improve gel mechanical properties.[29]

The other dominate mechanism to drive PEG hydrogel gelation is free-radical based chain elongation from acrylate terminated PEG macromers. This process is very rapid and takes advantage of hydrophobic-driven self-assembled acrylate micelles that co-localize prior to free-radical addition and promote rapid

crosslinking. Furthermore, a single free radical will add in a chain elongation mechanism crosslinking many PEG pre-polymer chains from a single radical and creating polymerization nodes or crosslink centers. [30] In this respect free-radical crosslinked PEG hydrogels form much faster (< 1min[20] vs 30 min[26]) and much stiffer (5000 Pa[31] vs 300 Pa[26]) matrices than Michel-Type at a given hydrogel concentration and PEG pre-polymer molecular weight. It should also be noted that free-radical crosslinked PEG hydrogels are not degradable by cellular proteases or hydrolysis at physical pH or temperature. Therefore it is necessary to design hydrolytically or proteolytically degradable co-polymers.

The mechanism of how a free –radical is generated greatly affects the utility and application of free-radical crosslinked PEG hydrogels. The well characterized free-radical initiator system of ammonium perfsulfate (APS) and N, N, N', N'-tetramethylethylenediamine (TEMED) is commonly used to generate free radicals and drive hydrogel crosslinking.[32] However the temperature to drive rapid initiation (> 50 °C) and both components, APS and TEMED, have been shown to be cytotoxic and significantly reduce the applicability of these systems for cell encapsulation and *in situ* gelling applications.

More recently photopolyemrizable techniques have been applied to crosslink PEG hydrogel scaffolds.[20] These systems use the combination of light and a photoiniator as a free radical generator to initiate the chain elongation process. (Figure 3B) A wide variety of photoinitiators that react to various wavelengths of light have been shown to promote rapid photopolymerization with low cytotoxicity.[33] Furthermore these systems allow for sub-micron scale

photolithographic spatial patterning of structures[34], biochemical[35] and biophysical functionalities[36] within the scaffold. This has proven advantageous for investigating fundamental cellular phenomena and for fabricating tissue mimetic microenvironments. (see section 64 Microfabricated Hydrogels for MVTE)

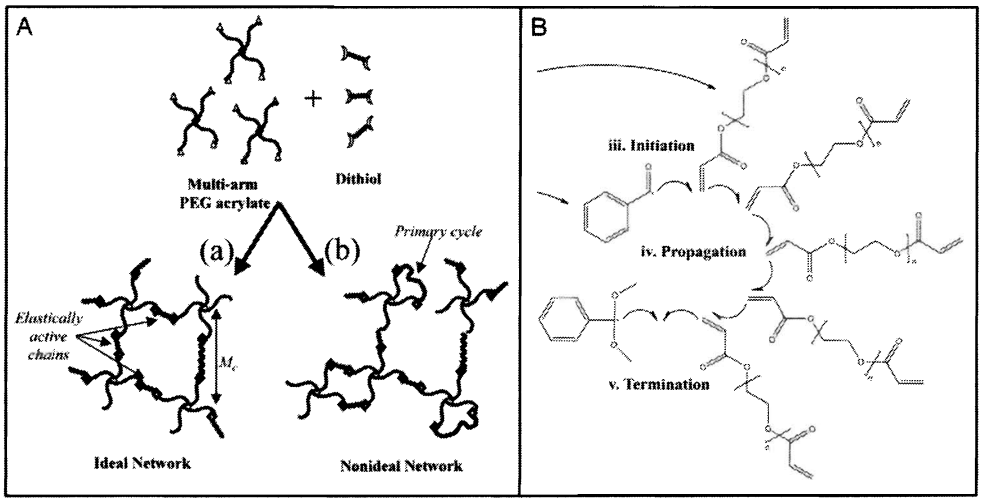

Figure 3: PEG Biofunctionalization and Crosslinking Systems. (A) Michel-Type PEG crosslinking[27] and (B) free radical photopolymerization based PEG crosslinking[37]

2.1.2. Techniques for PEG Scaffold Biofunctionalization

Often PEG materials are used to improve surface wet-ability, prevent protein adsorption, improve biocompatibility, and create "stealthy" biological interfaces. These are advantageous qualities when designing inert interfaces or improving biodistribution. However, for tissue engineering scaffold-based applications, PEG's intrinsically bioinert properties require the incorporation of bioactivity to communicate with biological and cellular environments.

Generally, biofunctionalization of PEG based scaffolds can be achieved via impregnating or non-covalently loading biomolecules into the matrix[38,39] or

through covalently crosslinking biomolecules into the matrix[40-42] and combinations of both[43]. Non-covalently loading biomolecules into the scaffold is simple and does not require development of specific chemical modification schemes to drive functionalization. This method also allows for biomolecule release from the scaffold resulting in the formation of chemotractant gradients originating from the scaffold surface and extending into the tissue space.[44] (Figure 4 A&B) This may be advantageous for facilitating native tissue ingrowth and cell infiltration. In particular this is a useful tool for MVTE because it may provide a means to recruit existing blood vessels into the scaffold and therefore improve anastomosis times.[43] (Figure 4C)

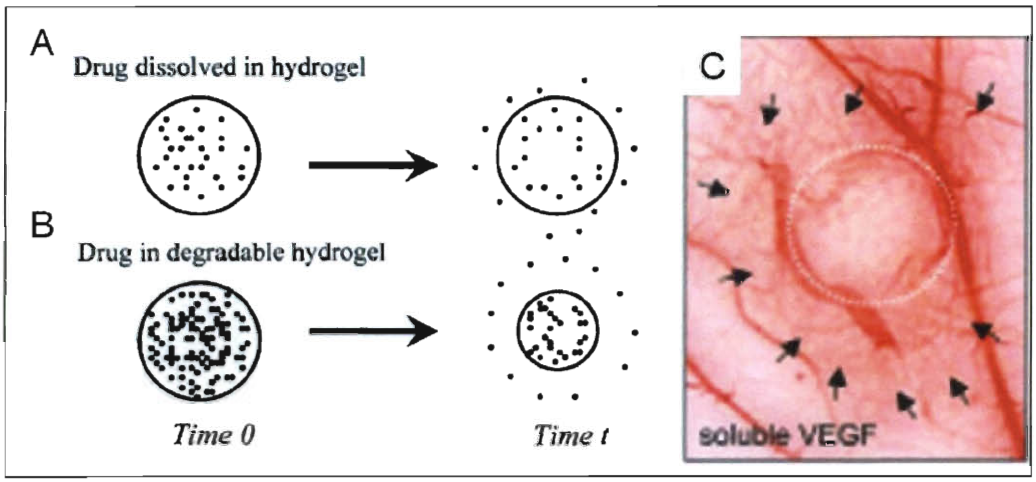

Figure 4: Soluble Bioactive Factor Release from Hydrogel Scaffolds. Soluble factor release from non-degradable hydrogels (A) and degradable hydrogels. The release from non-degradable hydrogels is not dynamic and concentration and diffusivity dependent. The release profile. from degradable hydrogels ins dynamic and will vary as a function of the mechanism of hydrogel degradation. (C) VEGF release from hydrogel scaffolds induces blood vessel growth up the concentration gradient in the surrounding tissue.Recreated from Peppas *et al.*[21] and Zisch *et al.*[28]

However, the bioactivity of non-covalently loaded biomolecules decreases over time when compared to covalently tethered biomolecule. This is due to

reduced biomolecule concentration through both diffusional release from the scaffold (Figure 4) and cellular internalization followed by breakdown via intercellular enzymatic pathways.[28] Consequently, much effort has focused on ways to covalently immobilize biomolecules to PEG hydrogels without disrupting native bioactivity. Commonly biomolecules are immobilized through heterobifunctional conjugation to primary amine terminus[45] or amino acids with free side chain amines (lysine)[46] through n-hydroxysuccinimide reactions(Figure 5), carbodiimide coupling, or other amine reactive chemistries.[47] Amino acids with free thiols (cystine)[48] have also been commonly used as the reactive sites for biomolecule conjugation to PEG scaffolds especially when Michel-Type crosslinking is employed.

Targeting native free amine or free thiol rich residues on biomolecules allows for easy bioconjugate production without the need for engineering specific conjugation domains.(Figure 5) However, close spatial localization of the conjugation site to either tertiary structure stabilizing regions (ie. disulfide bonds) or cellular binding sites has shown to reduce bioconjugate activity.[49] It is possible to avoid this drawback by optimizing the molar ratio of conjugation linker to reactive site, carefully choosing biomolecules with stable conjugation sites,[42] or by designing protein and oligopeptide sequences with specific conjugation sites through either synthetic peptide synthesis[50] or recombinant protein expression.[51] Optimization of reaction conditions commonly allows for immobilization that preserves biomolecule acitivity[52] as shown through bioconjugate bioactivity

assays used to evaluate conjugation effects and determine optimal dosage concentrations that produce desired scaffold biomimetic behavior.

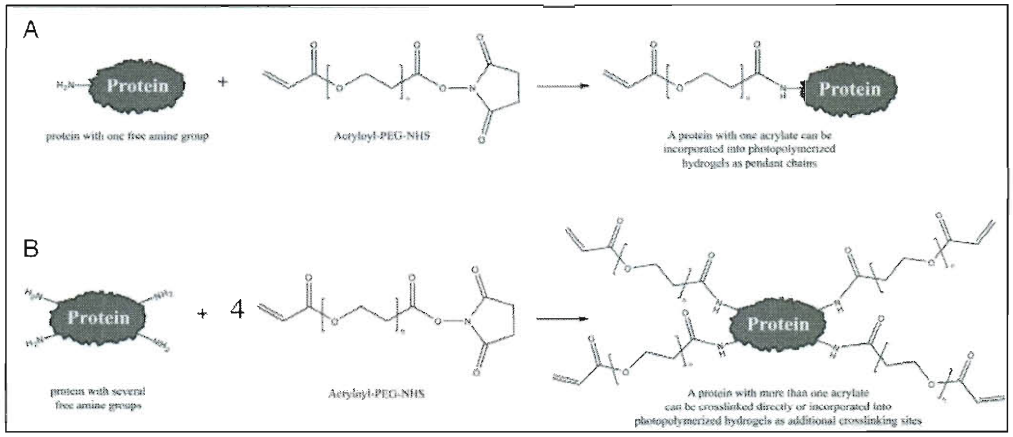

Figure 5: Effects of Multiple Heterobifunctional PEG-Biomolecule Conjugation Sites. (A) Biomolecules with only one free primary amine to react with acryoyl-PEG–N-hydroxysuccinimide act as tethered biomolecules with little steric hindrance and reduced conjugation site effects on bioactivity. (B) Biomolecules with multiple free primary amines to react with acryoyl-PEG–N-hydroxysuccinimide act as crosslinking reagents with sterically reduced access and potential for negative conjugation site effects on bioactivity. Recreated from Miller and West[37]

Independent of conjugation site effects, it has also been shown that direct covalent immobilization of biomolecules can result in decreased bioactivity due to steric hindrance of cell reactive domains.[53] The use of bioinert spacers has been shown to improve steric hindrance and provides a means to tether biomolecules into the PEG hydrogel matrix. As an example our group has shown that the use of a heterobiofunctional PEG spacer, with an amine reactive n-hydroxysuccinimide and an acrylate terminated end group can provide a robust method to covalently anchor biomolecules to the scaffold with minimal affects on bioactivity and greatly reduced streric restrictions.[23] (Figure 6)

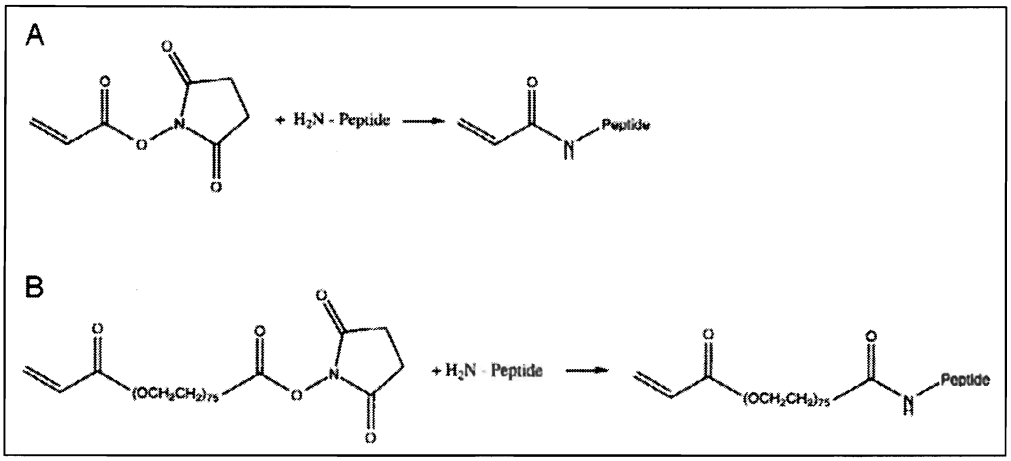

Figure 6: Heterobifunctional Biomolecule Conjugation Schematic. (A) Biomolecule conjugation using a heterobifunctional acrylate-N-hydroxysuccinimide moiety (A) without a PEG spacer and (B) with a PEG spacer. Recreated from Hern and Hubbell[23]

The use of heterobifunctional acrylate-PEG-Biomolecule moieties is compatible with cellular encapsulation using either Michel-Type[54] or free radical driven techniques[55] and allows for specific bioadhesion[45] , control over tissue formation[56], and cell migration through proteoltyic degredation[57]. A very interesting recent finding in acrylate-based hydrogel systems demonstrates that that increasing concentrations of monoacrylated PEG derivatives surprisingly enhances the free radical based PEG crosslinking process. This finding emphasizes the importance of thermodynamically stabilizing the hydrophobic acrylate micelle on scaffold crosslinking properties. (Figure 7)and enables the development of PEG scaffolds systems with increasing amounts of bioactivity and biomimetic components without compromising scaffold physical properties.[30]

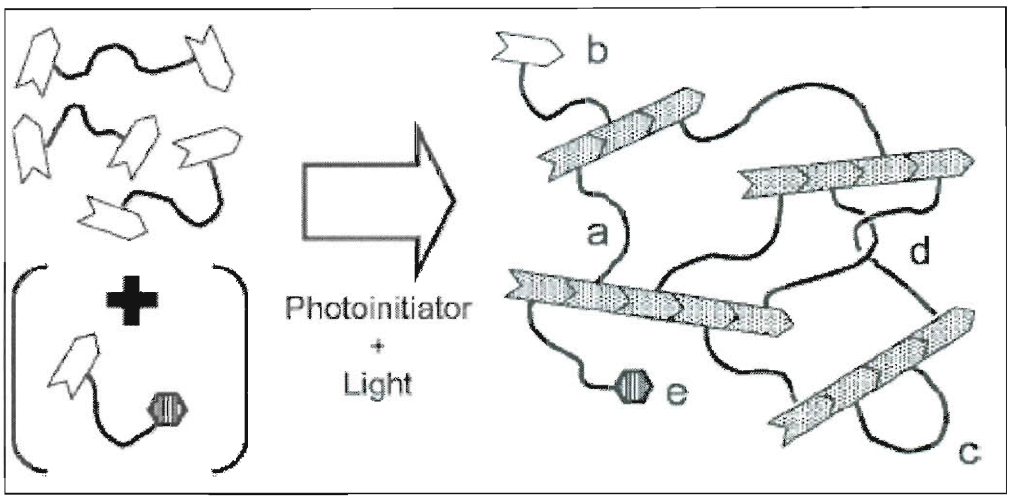

Figure 7: Schematic Representation of Photopolymerized PEGDA Network Formation. (a) PEGDA crosslink, (b) un-reacted acrylate, (c) cyclic crosslinks, (d) chain entanglements and (e) PEG tethered biological moiety. Reproduced from Beamish *et a.l*[30]

2.2. Current Success and Challenges in Tissue Engineering Therapeutics

The concept of directly engineering tissues for the development of therapeutics which seek to substitute, restore, maintain and or improve tissue function was born in the late 1980's and began to take root with the publishing of a ground breaking article in a 1993 issue of Science by Robert Langer and Joseph Vacanti's aptly titled Tissue Engineering. Since then the field has experienced significant growth with annual industrial and scientific research and development expenditures totaling $600M in 2001.[58] However, to date the only successful tissue engineering therapeutics have been limited to those seeking to augment skin, cartilage or the bladder. [59,60] The chief reason theses tissues have been successfully engineered is due to either their intrinsically low metabolic activity and or the constructs are sufficiently thin to allow nutrient and waste

transport to occur by either host vasculature integration or by purely diffusional process. Implanted tissues with greater thicknesses and metabolic consumption rates require that the host vasculature provide nutrient transport. However, vessel in growth occurs on the order to tens of micrometers per day[61] which would require weeks to months in order to vascularize constructs on the order of millimeters to centimeters. During this time hypoxic conditions followed by cellular necrosis will occur in regions furthest from the implant surface. Furthermore, heterogeneous nutrient and waste concentration gradients across cellular layers of the implant will lead to non-uniform cellular differentiation and behavior ultimately leading to a reduction in therapeutic potential.[62] Such mass transfer properties dictate that implanted tissue engineering therapeutics without perfused vasculature are limited to thicknesses on the order of 150-200 um.[63,64]

In order to develop bulkier more complex tissues with high metabolic activity such as heart, lung, liver, muscle, or neural tissue it is necessary to provide tissue engineering constructs that are vascularized pre-vascularized *in vitro* prior to implantation. Pre-vascularized constructs with perfused microvascular networks improve nutrient and waste transport by providing mass transport in the form of vessel supported convection followed by extra vessel diffusion. Appropriate vessel design parameters such as microvascular network geometry, density, and perfusion rates can provide fundamental design parameters that limit cellular necrosis *in vitro* by controlling the number of cell layers between perfused vessel networks. More importantly, perfusable microvascular networks within the pre-vascularized implant will allow for both

microvascular surgical connection to the implant and reduce the effective distance of host vessel in-growth to the surface of the implant. It is important then to take a step back and study the biology and physiology of how tissues are vascularized.

3. Chapter 3: Vascularization of Tissues

3.1. Microvascular Physical Characteristics and Function

Blood vessel networks or the systemic vasculature functions to deliver nutrients and remove metabolic waste products from tissue. These networks can be generally classified into three groups; the arterial circuit, the capillary networks or microvasculature, and the venous circulation. Each network component has diverse cellular and extracellular matrix (ECM) compositions as well as physical characteristics that reflect their unique biological functionality.

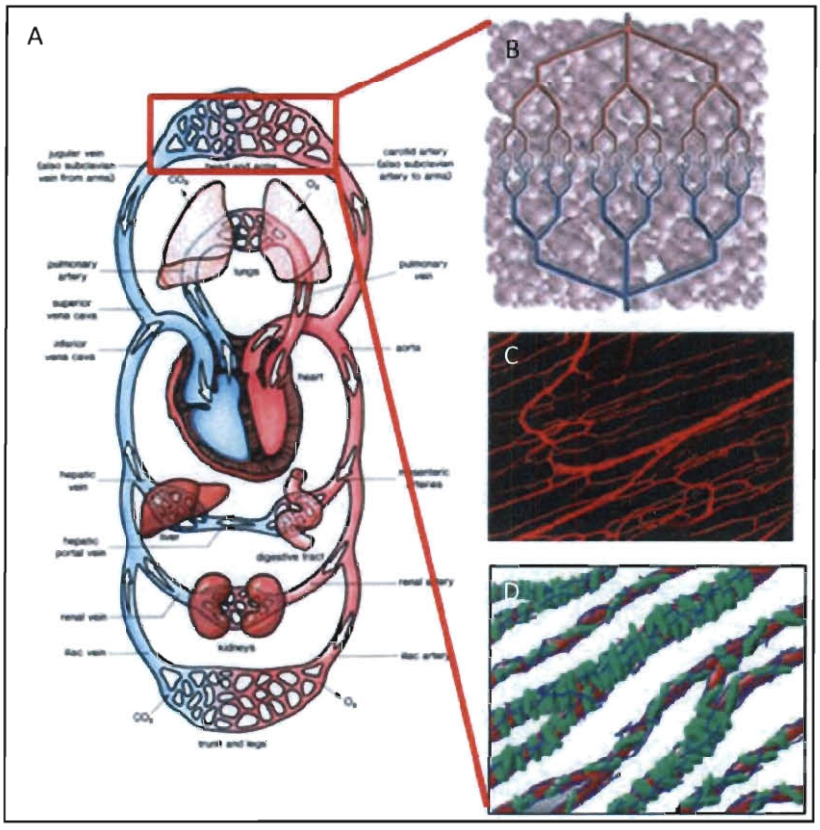

Figure 8: Circulatory System with emphasis on Microvascular Component. (A)The circulatory system composed of the arterial and venous circuit bridged by capillary bed. (B) Microvascular networks depicting regular branching. (C) Cherry stain of skeletal muscle vasculature. (D) Schematic of vasculature (red), pericytes (green), and basement membrane (blue).

Derived from Jain *et al.*[182]

The arterial network provides pressurized delivery of oxygenated blood from the heart to the tissue. The venous system returns deoxygenated blood

passively from the peripheral circulation back into the central circulation and ultimately back to the heart. Both function primarily as highly dispersed, large diameter, convective based transport vessels with little to no exchange of solutes across the vessel into the tissue space. Connecting the two networks are intricate, ultra high surface area, capillary beds. These microvessels are small in diameter commonly consisting of two to three endothelial cells in diameter. (Figure 8)

The EC networks found within the microvasculature are surrounded by a laminin and collagen rich basement membrane reinforced by a single layer of pericytes.[65] The thin basement membrane, lack of confluent pericyte presence, inherently leaky EC cell-cell contacts coupled with the high surface area of capillary networks provides a highly permeable element of the circulatory system where exchange of nutrients and waste from the tissue space can occur freely. (Figure 9) Much of the following discussion will focus on the rationale design of systems which seek to mimic the function of the microvasculature within *in vitro* systems.

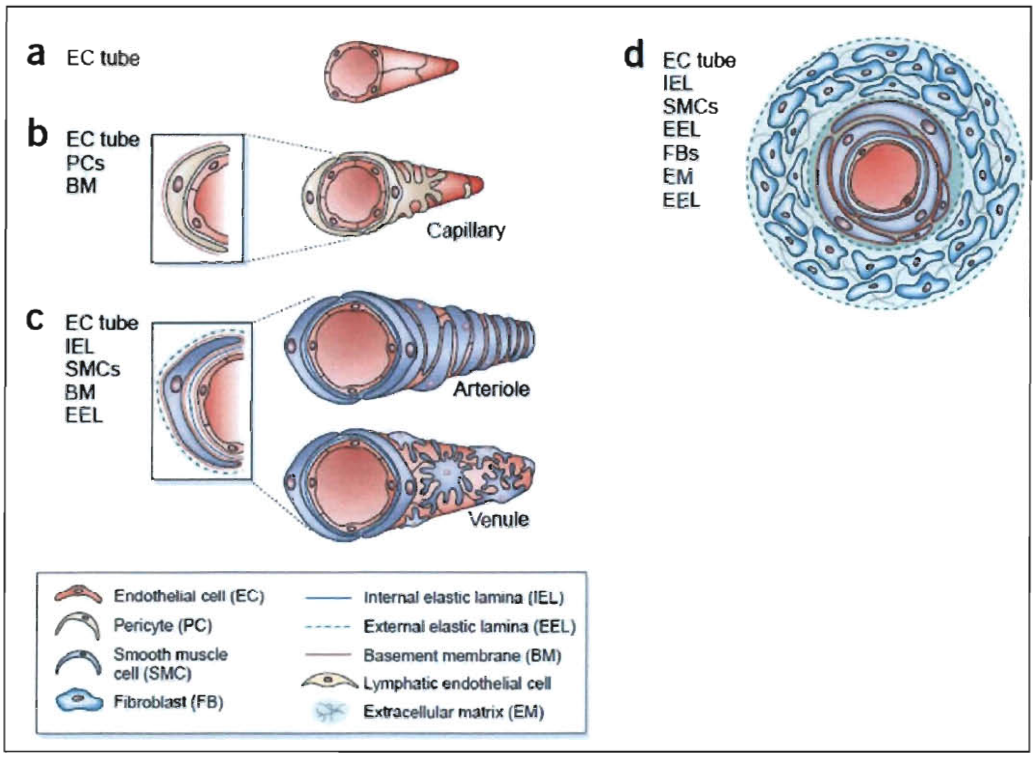

Figure 9: Composition of Blood Vessels. (a) Early EC tubes mature into (b) capillary structures containing an EC tube surrounded by the matrix rich basement membrane and sparse vessel stabalizign pericutes.As percicte coverage thickens pericytes begin to differentiate into smooth muscle cells capillaries form arterioles and venules (c). The walls of the largest vessels (d) are divided into three distinct layers the intima, media and adventitia. Mature vessels also contain their own blood supply, vaso vasorum, to support cellular nutrient demands. Recreated from Jain *et al.*[66]

3.2. The Developing Microvasculature: Vasculogenesis

The formation of blood vessels is thought to occur in multiple distinct morphogenic processes. Vasculogenesis is thought to primarily occur in a prenatal environment during embryo development and in the most general of terms refers to the *de novo* formation of vascular networks from mesodermal progenitors. In contrast postnatal vessel development occurs when EC are activated, such as during wound healing, hypoxia, and metastasis. Postnatal vessel development refers to the formation of a new sprout from an existing

vessel (angiogenesis) or the bifurcation of a larger diameter parent vessel into two smaller diameter daughter vessels (intussusceptions). Recently, evidence has arisen that suggests during times of tissue repair circulating multipotent stem cells or endothelial cell precursors (EPC) in the circulatory system contribute to vessel formation in a process that resembles lymphoid lineage homing combined with embryonic vasculogenesis.[67] Although post- and pre-natal vessel development are governed by unique signaling events, together they provide key rational design information and parameters utilized in the development of microvascular networks *in vitro*.

Vasculogenesis occurs in the embryo when mesodermal progenitors begin to differentiate into EC precursors. This specialization is marked by the coalescence of progenitors into structures referred to as blood islands. The fusion of adjacent blood islands results in the formation of primitive tube like networks known as the capillary plexus. [65] (Figure 10) Branching and remodeling of the plexus leads to the development of a mature vessel network while the initiation of blood flow is thought to further develop the network and drive the hierarchical organization into larger diameter venules and arterioles.[68]

Molecular regulation of initial plexus formation is thought to be governed by both soluble and insoluble factors provided within the local microenvironment. Fibroblast growth factor (FGF)[14], vascular endothelial growth factor A (VEGF-A)[69], Indian hedgehog (Ihh)[70], and Quaker[71] signaling have all been implicated in the differentiation of mesodermal progenitors to the EC phenotype found in the primary capillary plexus. Proper transient expression profiles of these soluble

factors and their target receptors provides the regulation necessary to not only promote the initial EC cell phenotype from progenitors, but also balance physical network characteristics such as network density and tubule diameter.

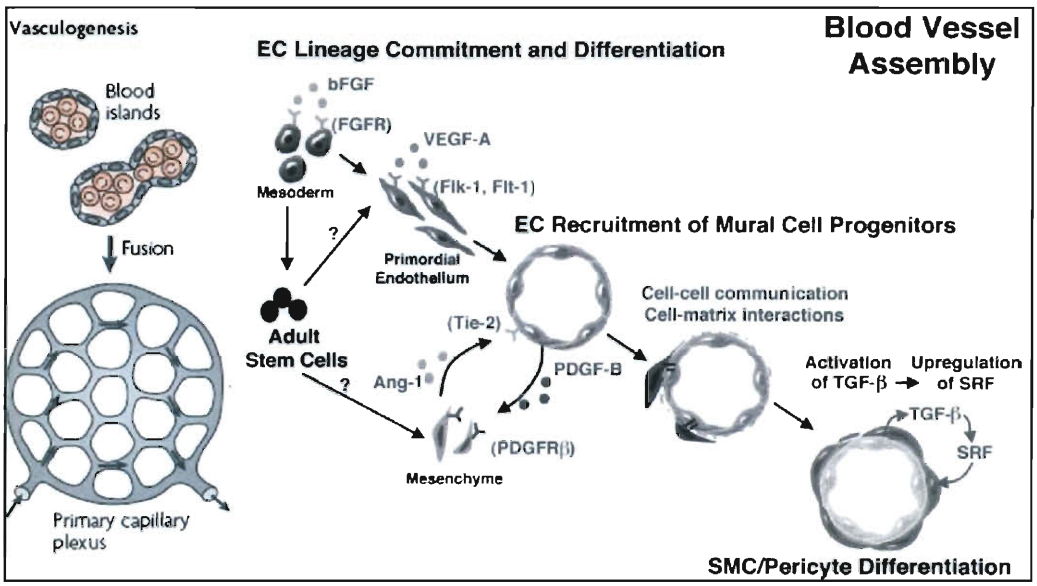

Figure 10: Schematic of Vasculogenesis. (left) Coalescence of EC precursors into blood islands and subsequent organization in the primary capillary plexus. (right) EC lineage and differentiation with role of signaling factors and mural cell progenitors. Recreated from Hirschi *et al.*[13] *and* Jain *et al.*[16]

The driving force behind the formation of the primary capillary plexus with distinct vessel lumens from blood islands is thought to be governed in part by intercellular vacuole fusion.[72] Recent *in vivo* studies in zebrafish and *in vitro* studies of human EC on collagen gels indicate that longitudinal intracellular vacuole compartments fuse to form intracellular lumens. [73] (Figure 11)

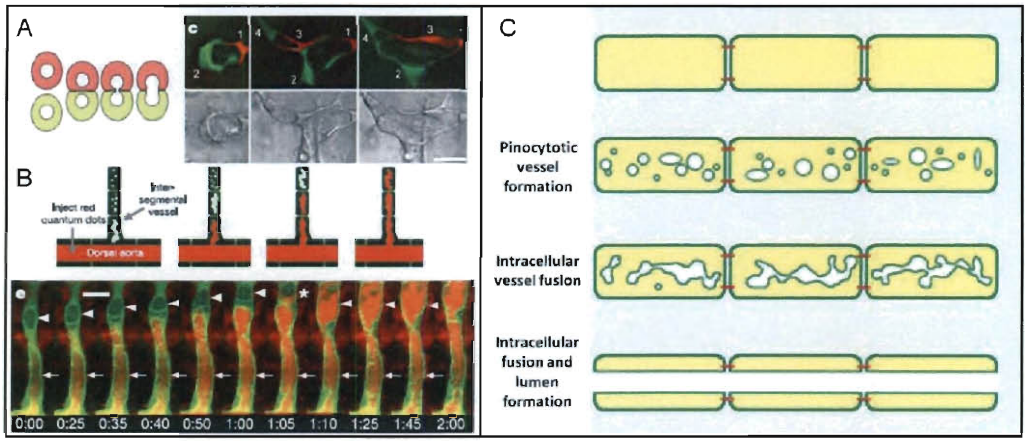

Figure 11:Vacuole Fusion Precedes Lumen Formation. (A) HUVEC on collagen gels fuse vacuoles to form lumens. (B) Zebra fish dorsa aorta vessel outgrowth via vesicular fusion. (C) Mechanism for lumen formation. Reproduced from Kamei *et al.* [73]

Development of the primary plexus into mature capillary beds is thought to be partly controlled through EC interaction with mural cells or pericytes. Recruited pericytes regulate vessel blood flow via contractile forces and also function to stabilize the nascent endothelial vessel via both physical interactions and signaling cascades that promote EC viability and suppress EC proliferation.[74] Endothelial cells attract pericytes from the mesoderm chiefly via the secretion of platelet derived growth factor-beta (PDGF-β). Furthermore, PDGF-β is known to be a powerful mitogen and chemotractant and is thought to be responsible for the differentiation of pericytes down the smooth muscle cell (SMC) lineage. [75] Upon EC-pericyte contact, transforming growth factor beta (TGF-β) is thought to become activated due to the heterocellular receptor interactions. Activated TGF-β directly up regulates gene expression of SMC marker SM-α-actin and indirectly up regulates other SMC markers, SM-γ-actin, SM22-actin, and calponin through activation of serum response factor (SRF). [65] These soluble effectors present in

the capillary microenvironment are crucial to developing stable microvascular networks *in vitro*.

3.3. The Dynamic Microvasculature: Angiogensis

As previously described, postnatal vessel development is thought to occur via angiogenesis or the sprouting of new vessels from existing vessel networks. Also there are non-angiogenic mechanisms in postnatal vessel development such as intussusceptions or the bifurcation of a parent vessel into two smaller diameter daughter vessels, and the spontaneous formation of vessels form circulating multipotent stem cells. Although the contribution of non-angiogenic neovessel formation is thought to be minor[68], each mechanism involves unique chemotaxic, haptotaxic and cell mediated signaling events which provide important rational design considerations for *in vitro* microvascular tissue engineering strategies.

Perhaps the most widely recognized and dominant mechanism of postnatal neovessel formation is the sprouting of vessels from existing vasculature or angiogenesis. This process involves the selection/activation of endothelial cells known as “tip cells” via Notch-Delta like 4 ligand (DLL4) cell-cell contacts. These cells undergo a drastic change in phenotype from quiescent behavior to highly invasive and migratory activity with up regulation of both soluble and membrane bound proteases in addition to apical basal polarity changes. Local degradation of the basement membrane by the tip cells is thought to release pro-quiescent factors to adjacent ECs while local

concentration gradients of VEGF-A either through the release of the matrix bound isoform (VEGF 165) or as soluble enactor (VEGF 121) is thought to spatially direct and encourage sprout elongation.[76] Stabilization of the growing sprout is thought to occur by the recruitment of pericytes through secretion of PDGF-β by the sprouting EC.[68] The nascent sprout is thought to continue growth until the "tip cell" encounters another "tip cell" or an existing capillary where stable cell-cell contacts must occur. Subsequent lumen formation is necessary to encourage blood flow and perfusion. There is a growing body of evidence to suggest that vessel lumen formation is closely tied to pinocytosis and or vacuole formation. Where polarity of the lumen is established by integrin-matrix contacts and fusion of vesicles precedes polar exocytosis and subsequent lumen formation.[77] (Figure 12) It is also thought that lumen formation occurs co-currently with sprout elongation.

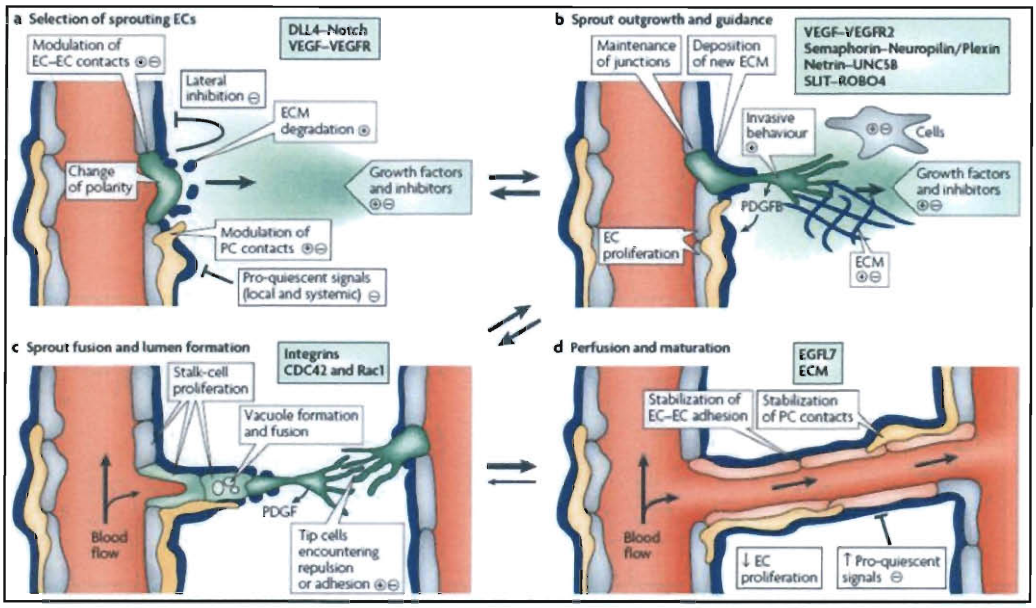

Figure 12: Sprouting Mechanism of Angiogenesis. (a) Initial change of EC polarity and expression of invasive phenotype. (b) Sprout outgrowth and degradation of ECM. (c) Proliferation of sprout cells and pre-lumen vacuole formation. (d) Perfusion of neo-vessel and stabilization by PC contact and ECM synthesis. Recreated from Adams *et al.*[68]

The contribution of non-angiogenic neovessel formation provides insight into additional mechanisms which promote neo vessel formation. Circulating endothelial precursor cells (EPC) have been implicated in the formation of the sprout themselves and also function to signal existing EC to begin the sprouting process.[78] Intussusception is the most poorly characterized mechanism of vessel formation. (Figure 13) This process involves the excessive proliferation of EC, degradation of basement membrane matrix and polarity changes which lead to the formation of a tissue pillar or bifurcation site. It is reasonable to assume that the pinocytotic and the vacuole based lumen mechanism may function along with the tissue pillar generation to develop the bifurcation site.

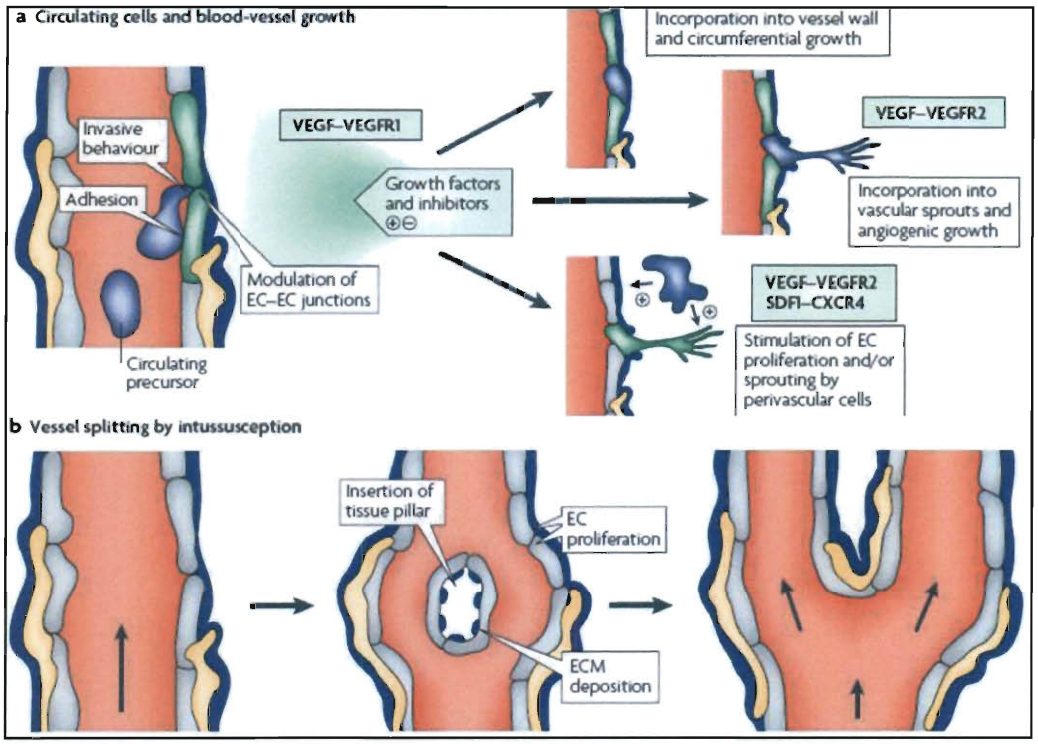

Figure 13: Non-Angiogenic Mechanisms of Postnatal Vessel Formation. (a) Circulating cells initiate sprout formation by adhering and displaying invasive phenotype. (b) Insertion of a tissue pillar by excess secretion of matrix by EC. Recreated from Adams *et al.* [68]

3.4. Microvascular Tissue Bed Mass Transport

The most important function of the microvasculature is the ability to transport molecules from the circulation into the interstitial tissue space. This critical mass transfer functionality is supported by an ultra high surface area of 500-700 m^2 in adult humans and high vessel density where on average no functional cell is greater than 30 um from a capillary[79]. Furthermore the capillary walls are extremely thin tubular structures often containing only one cell layer surrounded by a basement membrane with a total thickness of 500 nm. Together these characteristics provide favorable physical system for the efficient exchange of nutrients in a tissue bed.

The mechanism of molecular transport out of the vessel lumen into the interstitial space is highly dependent upon the molecule of interest. Small lipid soluble molecules such as oxygen and carbon dioxide can diffuse directly across the capillary endothelium and therefore move at a much higher rate than other solutes.[79] Small molecules that are water soluble but lipid insoluble cannot pass through the cell membrane but instead rely on interendothelial cell clefts as passageways out of the microcirculation. Molecules such as water and glucose and electrolytes such as sodium and potassium ions are thought to rely on this mechanism for transport.[79]

Macromolecular microvascular transport is less understood and there a multiple theories proposing transport mechanisms. Larger molecules, such as the plasma protein albumin (MW = 67 kDa, radius = 3.55 nm), have molecular radii that approach size of intercellular clefts (6-7 nm). Therefore molecules on this size order experience both significant hydrodynamic drag and steric hindrance within the clefts resulting in a decrease in vascular permeability with an increase in molecular size. However, increases in molecular weight beyond albumin result in only a modest decrease in permeability that is not consistent with purely intercellular cleft based transport. This suggests a mechanism of transport other than the small intercellular clefts or pores. Rippe and Haraldsson proposed a two pore theory suggesting that there was a second, larger diameter, population of intercellular clefts responsible for the enhanced transport of larger diameter macromolecules.[80] Still others have proposed that macromolecules can be transported across the microvascular endothelium via a traditional vesicle

supported transcytosis pathway. This process can occur through passive endocytosis or for common serum proteins such as albumin through active receptor mediated endocytosis.[81] Still other research proposed that macromolecular transport is a combination of both transcytotic vesicular transport and fusion of vesicles to form a trans-endothelial pathway.[82] (Figure 14) The broad range of proposed mechanisms present in the literature for over 100 years still requires more in depth fundamental biology studies to identify key mechanistic trends across tissue types and to develop an integrated paradigm of microvasculature structure and function relationships. Several comprehensive reviews by Michel and colleagues[82-84] provide an in depth look at microvascular permeabilities that is beyond the scope of this discussion.

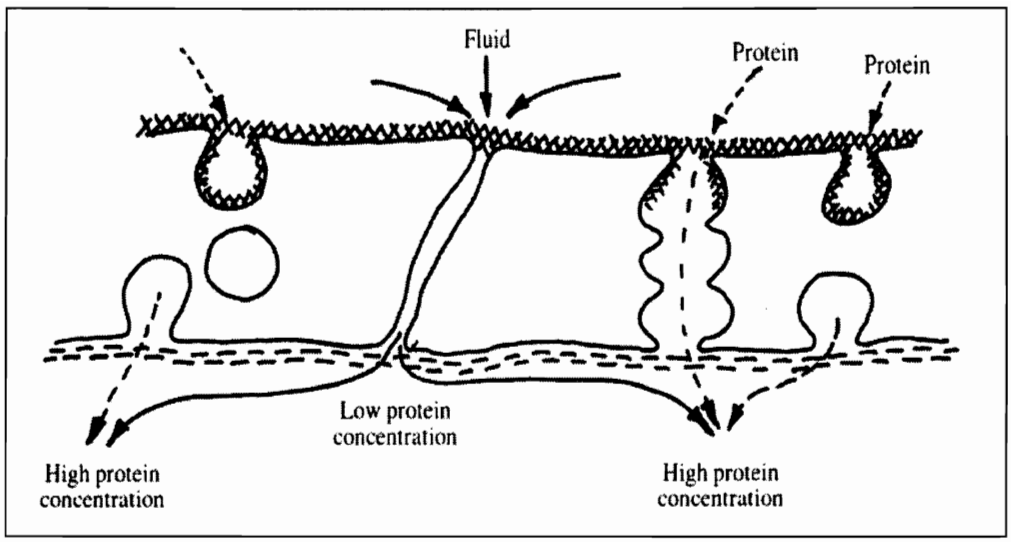

Figure 14: Schematic of Microvascular Mass Transport Pathways. Multiple mechanisms likely contribute to macromolecular mass transport across capillary endothelium. The transcytotic pathway contribute via passive or receptor mediated vesicular fusion (left). In some cases transcytotic pathways can fuse to form a trans-endothelial pathway (right). Transport between endothelial junctions or in the some cases the larger fenestration also contribute to mass transport (center). [83]

Given the heterogeneity of tissue function, and the parenchymal and microvasculature architectures that support this function, it is likely that an amorphous fusion of all macromolecular transport process occur to a greater or lesser degree depending on the needs of the tissue of interest. It is therefore important to consider the heterogeneity of microvascular permeabilities across tissue types. For example, liver capillary membranes are very porous to all solutes freely allowing passage of plasma proteins while the renal glomerular membranes is highly permeable to electrolytes and water but is selectively impermeable to plasma proteins.[79] This heterogeneity is an example of a strong structure-function transport relationship that likely dictates the type and level of transport mechanism present for a given tissue type. Vascularized tissue development *in vitro* must carefully consider design parameters to drive specific

microvascular formation directly related to the tissue type of interest. Cellular elements, provisional scaffold properties, soluble signals and hydraulic perfusion regimes must be carefully selected and tailored for the given tissue type in order to ensure proper tissue structure and function.

4. Chapter 4: Microvascular Tissue Engineering (MVTE)

4.1. Role of Vascularization in Improved Tissue Engineering Therapeutics

Development of robust, *in vivo*-like tissues *in vitro* holds the potential to create regenerative medicine therapeutics, provide more physiologically significant pre-clinical models and supply a pharmacological and toxicological screening platform that reflects *in vivo* systems in both complexity and function. Despite significant progress, tissue engineering research has largely failed to produce tissue or organ level systems *in vitro*. This is thought to be primarily due to difficulty translating systems from 2D to 3D. The most significant challenge when developing 3D systems is the mass transport limitations encountered when scaling up to metabolically dense constructs over clinically relevant length scales.

Reliance on passive diffusion of nutrients to sustain cellular metabolic activity limits overall construct size and metabolic density. Passive diffusion inadequately delivers nutrients over large length scales and limits the size and metabolic density of the construct. Furthermore, build up of nutrient and waste gradients within the construct reduces cell viability and disrupts cellular phenotype[85]. Inadequate transport of nutrients and waste has been correlated with a decrease in tissue quality as a function of distance from the nutrient source with the most distant regions becoming metabolically inactive or necrotic[62,86]. Due to these limitations, much effort in tissue engineering the fabrication has focused on strategies to enhance the mass transport properties of the construct, to maximize cellular viability and modulate signaling gradients for the control of cellular behavior and tissue formation.

Pure diffusional transport of nutrients and waste from cellularized tissue engineering systems limits the maximum geometric length of engineered tissues to between 150-200 μm and restricts system metabolic density.[11, 12] The development of complex, highly metabolic, tissue engineering therapeutics with clinically relevant dimensions requires the presence of pre-vascularized networks which transport nutrients and waste via convection and minimize the length over which diffusional processes occur.[87] Design of tissue engineering constructs that incorporate microvascular networks with sufficient mass transport characteristics holds the potential to increase both the size of *in vitro* tissue analogs and the capacity of the construct to support metabolically dense and clinically relevant cellular environments. Furthermore, implanted pre-vascularized tissue engineering constructs provide the ability to be surgically connected to host vasculature and reduce the effective distance for which invading host vessels must migrate in order integrate with the pre-vascularized networks. Optimization of these properties is essential to the *in vitro* development of complex tissues and organs such as the liver, brain, lung, and heart which require immediate perfusion post implantation for successful clinical outcomes.

One approach to engineering vascularized tissues is the development of a functional pre-vascularized network *in vitro* prior to the implantation. Pre-vascularization approaches may provide surgical anastomosis sites between the implant and the host and or facilitate rapid integration of the implanted vasculature with existing host vasculature networks to provide perfusion of nutrients and removal of waste from the implanted tissue. Perhaps the most

daunting task of this approach is the generation of functional perfusable microvascular networks *in vitro*. Development of these networks requires a highly multidisciplinary approach integrating concepts from cell and developmental biology with technologies from various material science sectors, all under the governing umbrella of fundamental engineering, fluid, and mass transport principles.

Strategies for developing biomimetic PEG hydrogel systems for microvascular tissue engineering applications operate under the traditional tissue engineering paradigm. This strategy combines a dynamic ECM mimetic provisional scaffold; immobilized and free pro-vasculogenic signaling factors, and pro-vasculogenic cellular elements within a culture regime. More recently spatially mimicking the tissue microenvironment and recapitulating its structure-function relationship has placed an emphasis on applying microfabrication technologies to biomaterial development. This adds an additional component to the traditional tissue engineering paradigm and suggests that synergistic benefits may occur if components are integrated under a structure function relationship. (Figure 15) In the following sections, each component of the tissue engineering paradigm will be discussed with respect to their application in microvascular tissue engineering.

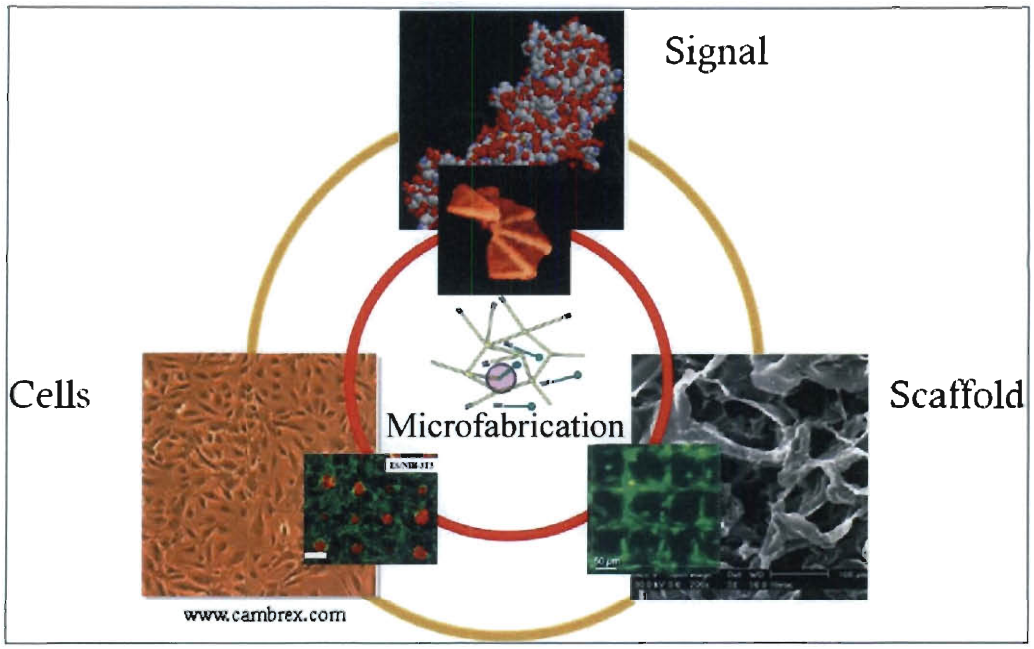

Figure 15: Integration of the Traditional Tissue Engineering Paradigm with Microfabrication Technologies. Functional synergies arise when signals, cells and scaffolding are spatially integrated using microfabrication technologies to mimic the *in vivo* tissue microenvironment. Recreated from Hahn *et al.*[36], Khademhosseini *et al.*[88] and Tayalia *et al.*[89].

4.2. PEG Hydrogels Modified with Vascular Biomimetic ECM Signals

Initial biofunctionalization of PEG scaffolds incorporated whole ECM proteins, such as fibrinogen, into the polymer matrix.[90] However, whole proteins present multiple adhesion and signaling domains that make elucidating specific bioactive mechanisms and targeting cell specific signaling difficult. Moreover, whole proteins are subject to denaturation during scaffold processing steps and isolation of whole protein extracts is costly and carries the risk for disease transmission.[91] Therefore much interest has focused on the design of synthetic oligopeptide analogs that mimic the bioactive properties of their larger parent molecules. Multiple peptide sequences have been derived and have been shown

to bind to cell surface receptors and mediate cell adhesion and migration.[92] (Table 2 and Figure 16)

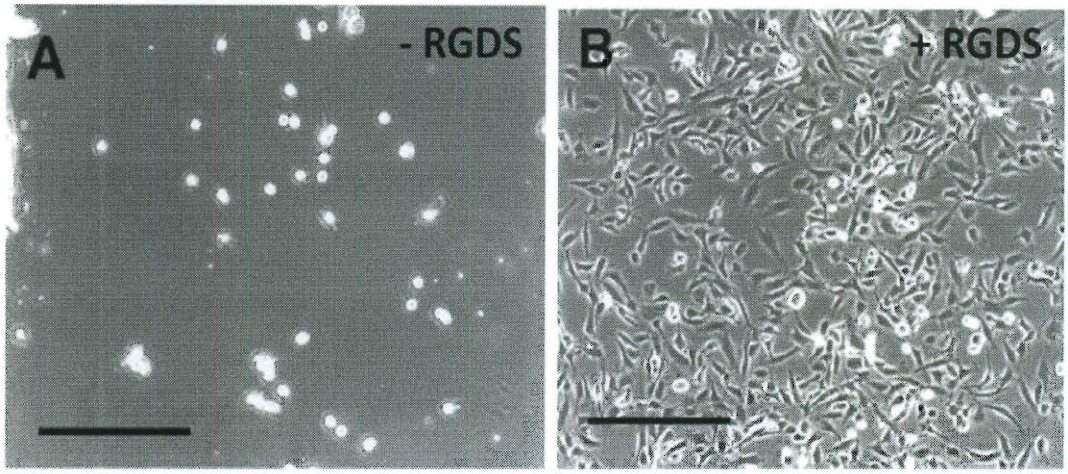

Figure 16: Effects of RGD on Endothelial Cell Adhesion to PEG. Recreated from Hern *et al.*[23]. Scale bar = 100μm

Peptide selection for MVTE scaffold biofunctionalization should mimic the matrix content of the vascular microenvironment. The microvascular matrix environment is known to be rich in both collagen and laminin and therefore the RGD peptide represents a robust option to promote both EC and pericyte adhesion. In addition it may be advantageous to employ peptides that exhibit selective or preferential cell adhesion. For example, REDV was shown to be selective for EC, while VAPG was shown to be adhesive for smooth muscle cells with little cross talk between adhesive domains.[38,39] Matrix based cell adhesion selectivity may be advantageous to help independently direct the response of EC and pericytes during vessel formation and maturation independent of soluble factors.

Table 2: Cell Adhesive ECM Mimetic Peptide Sequences. Recreated from West *et al.* [92].

Cell Adhesive ECM Mimetic Peptide Sequences	
Peptide Sequence	**ECM Source**
RGD	Fibronectin, vitronectin, laminin, and collagen
YIGSR	Laminin
IKVAV	Laminin
REDV	Fribronectin
DGEA	Collagen
KQAGDV	Fibrinogen
VAPG	Elastin

4.3. PEG Hydrogels Modified with Pro-Vasculogenic Signaling Proteins

Multiple pro-angiogenic signaling proteins have been covalently immobilized into PEG hydrogel scaffolds. VEGF, PDGF, and bFGF have been immobilized into PEG hydrogels and been shown to promote vascularized tissue growth.[51,93,94] The combination of VEGF and PDGF is particularly attractive due to its ability to mimic the signaling feedback necessary to favor stable pro-tubulogenic phenotypes instead of the rapidly proliferating cobblestone morphology often seen in EC culture.[95] Functionalization of PEG scaffold surfaces with pegylated PDGF and RGDS in the presence of soluble VEGF has been shown to direct human umbilical vein endothelial cells (HUVECs) to form tubules instead of the cobblestone morphology observed with RGDS functionalization alone.[52] (Figure 17 A&B)

In addition to growth factors, cell-cell signaling molecules are thought to play a role in the formation of tubule like structures during vasculogenesis.[12] This cell-cell affect has been mimicked within synthetic PEG hydrogels by the covalent attachment of Ephrin-A1 into the scaffold. It was observed that HVUECs spontaneously formed tubule like structures with hollow lumens on the surface of PEG hydrogels functionalized with Ephrin-A1 and RGDS.[56] (Figure 17 C&D) This is a very interesting finding suggesting that the combination of adhesive ligands with pro-angiogenic proteins provides a bioactive signaling regime for spontaneous microvasculature formation.

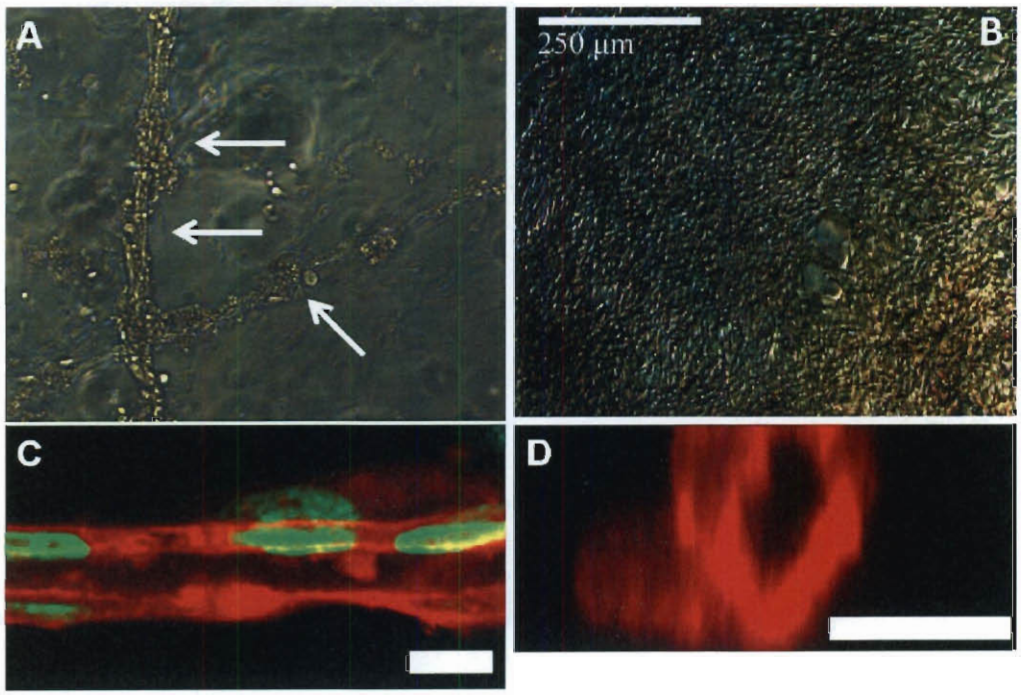

Figure 17: Immobilized Growth Factor Effects on 2D Endothelial Cell Morphology.(A) Light microscope images of Human Umbilical Vein Endothelial cells (HUVECs) on PEG hydrogels with immobilized PEG-PDGF-BB and PEG-RGDS (A) and PEG-RDGS alone (B) after 18 days of culture. Recreated from Saik *et al.*[52] Phalloidin-TRITC (red) and DAPI (green) confocal fluorescent micrographs of HUVECs seeded on PEG scaffolds with immobilized PEG-Ephrin A1 and PEG-RGDS Lumenized structures can be seen in length (C) and cross section (D) scale bar 10 µm. Recreated from Moon *et al.*[56]

4.4. Proteolytically Degradable PEG Hydrogels for MVTE

Although the bioinert nature of PEG hydrogels allows for high biocompatibility and low immunogenic responses it also renders the hydrogel not degradable by proteolysis. Furthermore, the stable ester linkages within the backbone of PEG make it non-degradable to hydrolysis at physiologic pH. Therefore in order to allow cellular migration and tissue formation to take place within a 3D PEG hydrogel matrix, it is necessary to engineer degradable domains into PEG hydrogels.

Hydrolytically degradable PEG co-polymers are relatively simple to synthesize and allow for degradation, cell migration, and ultimately for tissue formation.[72,73] However, the degradation mechanism of these systems is controlled by polymer type, crystallinity, co-polymer ratios, hydrophilicity of the matrix, access of water to the polymer, and the pH of the environment. This myriad of factors makes modeling and prediction of polymer degradation difficult. Furthermore, hydrolytically degradable systems are not responsive to cell based proteolysis and therefore these systems struggle with the ability to match matrix degradation to tissue formation. Conversely, the degradation of proteolytically degradable PEG copolymers is directly related to the proteolytic activity of the cellular constituents within the scaffold. Therefore proteolytically degradable systems behave like an *in vivo* provisional matrix which allows for scaffold degradation at a rate that matches tissue formation.

Recently our group and others conjugated proteolytically degradable peptides sequences to PEG macromers. The system was designed with the degradable peptide sequence flanked by polymerizable PEG macromers to produce a PEG-Peptide-PEG block co-polymer capable of rapid polymerization followed by proteolytic degradation.[2441] (Figure 18) The degradation of the hydrogel can be further tailored by designing a peptide sequence with variable substrate reactivity and cell specificity.[54]

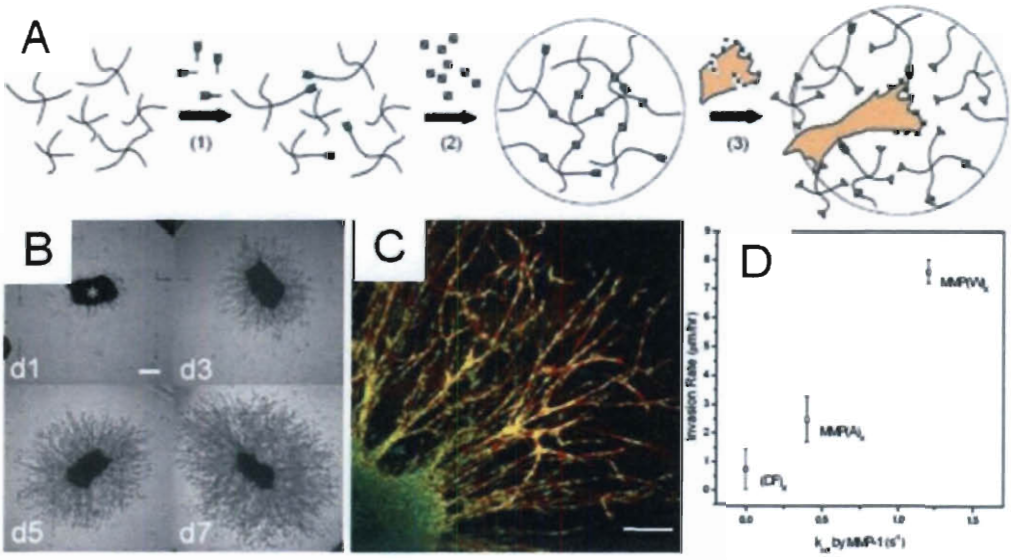

Figure 18: Proteolytically Degradable Bioactive PEG Hydrogels. (A) Michael Type crosslinking of PEG hydrogels with adhesion peptides and MMP degradable linkers. (B,C) Invasion of fibroblasts into MMP sensitive hydrogel from 1-7 days. (D) Cell invasion rate depended on proteolytic activity of the peptide. Derived from Lutolf *et al.* [54].

4.5. Cellular Elements for MVTE

Development of vascularized tissue *in vitro* requires a multicellular system consisting of the organ functional parenchymal cells with the necessary cellular elements to facilitate blood vessel formation *in vitro*. Review of biology literature surrounding blood vessel development (see Figure 10-Figure 13) suggests that

the process is chiefly governed by endothelial and mural cells. Various endothelial cell (EC) types have been employed as the singular vessel forming elements. Human umbilical vein endothelial cells (HUVEC),[96] rat lung microvascular endothelial cells,[97] human dermal microvascular endothelial cells (MDMEC),[98] and human embryonic stem cells (HESC)[99] have been used to generate vessel like structures *in vitro*. Unfortunately, single cell type *in vitro* systems often suffer from regression due to lack of stabilization over long culture periods.[43] Co-culture systems including a mural cell type along with EC have been utilized to generate long lasting and stable vessels. Human perivascular cells (PC)[51], neural progenitors cells[52], and smooth muscle cells[42], have been incorporated into co-culture environments and have been shown to stabilize vessel formation with respect to controls.

A very interesting finding by Rakesh Jain's research group demonstrated that a co-culture of human umbilical vein endothelial cells (HUVECs) and 10 T ½ (murine pericyte pre-cursors) self-assembled to form long lasting blood vessels within collagen hydrogels after implantation *in vivo*. The 10T ½ cells were shown to differentiate into pericytes in presence of HUVECs, and stabilize vessel structures where cultures without 10T ½ regressed shortly after self-assembly.[100]

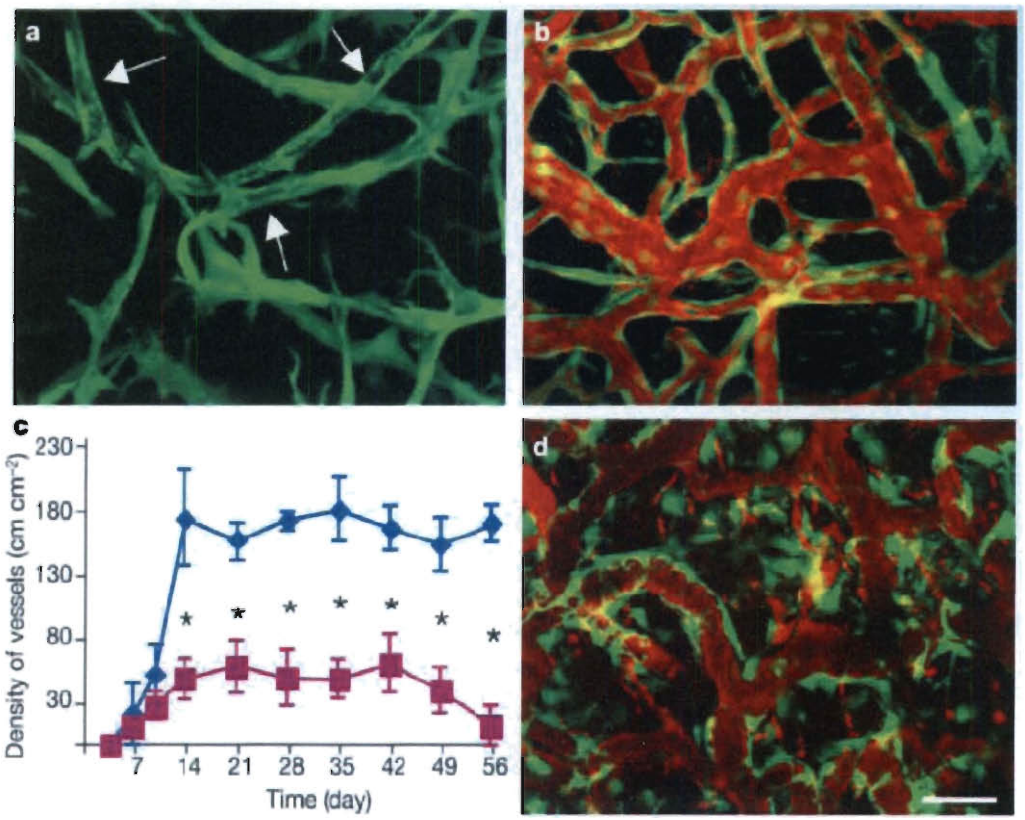

Figure 19: Morphological and Functional Analysis of Self-Assembled Blood Vessel Networks. (A) Fluorescent micrographs of E-GFP expressing HUVECs (green) and (B) E-GFP expressing HUVECS (green) vessels perfused with rhodamine dextran (red) *in vivo*. (C) Temporal analysis of vessel density in co-culture (blue trace) and HUVEC only (red trace) constructs. (D) Co-culture of E-GFP expressing 10T ½ pericytes (green) and rhodamine dextran perfused vessels (red) at 4 weeks of culture.

This was an important proof of concept demonstrating the vasculogenic potential of the co-culture. However, the results were limited to *in vivo* tubulogenesis within a natural hydrogel Our research group has recently developed a fully synthetic photopolymerizable PEG hydrogel that drives the rapid self-assembly of stable HUVEC and 10T ½ microvascular networks in vitro. This novel hydrogel is fabricated with a PEG tethered biomimetic integrin peptide (PEG-RGDS) and a proteolytically degradable PEG derivative. The self-assembled pre-vascular networks were shown to degrade the provisional

synthetic scaffold, secrete characteristic microvascular extracellular matrix proteins, laminin and collagen IV, and remain stable in culture for up to 30 days.[43] (Figure 20) This was a very important finding demonstrating that tubulogenesis could occur without functionalizing the scaffold with bioactive signaling proteins. This research represents a model for the proper integration of bioactive factors, synthetic hydrogel matrix, and co-culture system that is essential for recapitulating *in vivo* microenvironments capable of spontaneously generating microvascular networks.

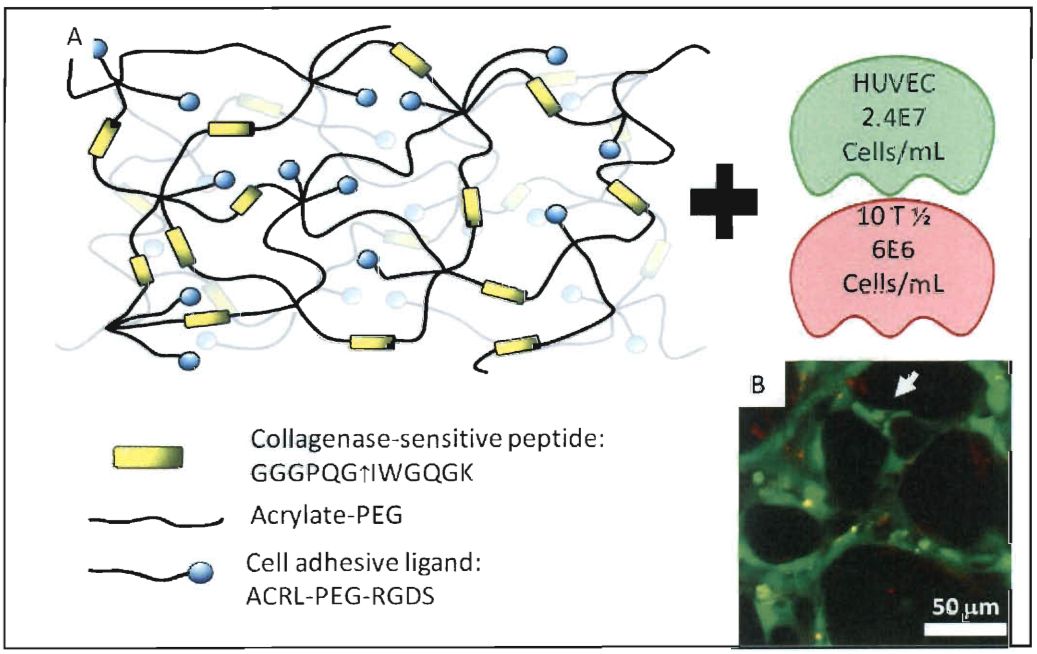

Figure 20: Schematic of Pro-tubulogenic Co-Culture in a Proteolytically Degradable PEG Hydrogel. (A) Schematic showing idealized hydrogel network fabricated with proteolytically degradable PEG derivative and ECM mimietic PEG-RGDS peptide conjugate and encapsulated pericyte precursoss (10 T ½ and human umbilical vein endothelial cells (HUVECs). (B) Pro-tubulogenic hydrogel shows tubule formation at 72 hr (green; HUVEC, red; 10 T ½ and arrow indicating pre-lumen vacuole) Recreated from Moon *et al.*[43]

4.6. Current Limitations in Microvascular Tissue Engineering

Much progress has been made towards the development of vascularized constructs *in vivo* and *in vitro*.[101] Rapidly forming and long term stable networks have been produced on 2D substrates and within 3D constructs across a range of natural and synthetic materials within both *in vitro* and *in vivo* systems.[102] However, current approaches have fallen short on several key aspects that are necessary for developing complex, bulky, vascularized tissues for regenerative medicine therapeutics and more pre-clinically relevant *in vitro* tissue models. These factors are divided into three areas described below:

1.) Perfusable vasculature integrated across length scales

The predominant body of work surrounding the growth and development of vascularized tissues *in vitro* has employed constructs with non-clinically relevant size scales. This is likely due to the experiments' early investigational nature and the scarcity of novel materials. Therefore a significant remaining challenge is scaling up the vascularized systems to bulky, organized and perfused constructs for therapeutic transplant or more robust *in vitro* tissue analogs. However, *in vitro* vessel scale up requires design considerations beyond increases in material quantities and overall dimensions; with unique scale up challenges to be considered at each stage of vessel nucleation, vessel growth, and maturation.

During the initial vessel nucleation and early vessel development, advanced bioreactors are required to provide adequate mass transport of

nutrients, waste and key signaling molecules across large (mm-cm) length scales. Furthermore, the high cell seeding density required to drive early vessel nucleation (> $30x10^6$ cells/mL) creates a highly regenerative but also pro-necrotic transport regime likely to have non-homogenous cell viability and tubulogenic activity. (Figure 9) Large scale bioreactor designs incorporating perfusion[103], pulsatile pumping[103] and a combination of both [104] have been reported to improve mass transport and alleviate detrimental nutrient and waste gradients. Other bioreactors have focused on microfabricated biomimetic designs with microchannels in poly(dimethyl siloxane) (PDMS)[87,105] and collagen scaffolds[106] to improve mass transport. However, these systems have not been directly applied to control and optimize vessel nucleation and growth. Therefore it is important to develop bioreactors specifically designed to optimize spatial tubule growth.

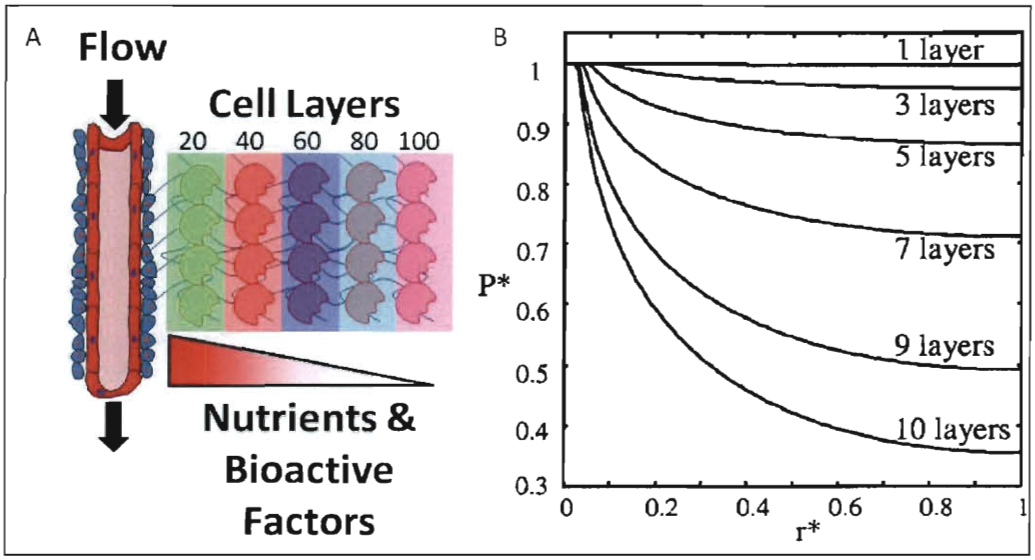

Figure 21: Effects of Distance from Vasculature on Nutrients and Bioactive Factor Concentrations. (A) Schematic demonstrating the affect of cells as metabolic sinks model on spatial distribution of nutrients and bioactive factors. (B) Kroghian based experimental modeling of oxygen profiles as a function of distance from a nutrient sources and number of cell layers. Recreated from Malda *et al.*[62]

2.) Integration of vessel networks with *in vitro* perfusion sources

Once the vessels networks have formed, it is critical that the networks integrate with a perfusion source across length scales (Figure 22). This will shift transport regimes from passive diffusion through the construct to lumen supported convection or flow through the vessel networks. This shift in transport mechanisms will enhance overall system transport properties (see Figure 22; $Flux_{Diff} << Flux_{Vascularized}$) and shorten the constructs characteristic diffusion length (see Figure 22; D>>d) resulting in spatially homogenous cell viability and prevention of vessel network regression. Furthermore, integration of vessel networks with a perfusion source across length scales will provide an opportunity to engineer a pro-anastomotic interface for rapid integration upon transplantation.

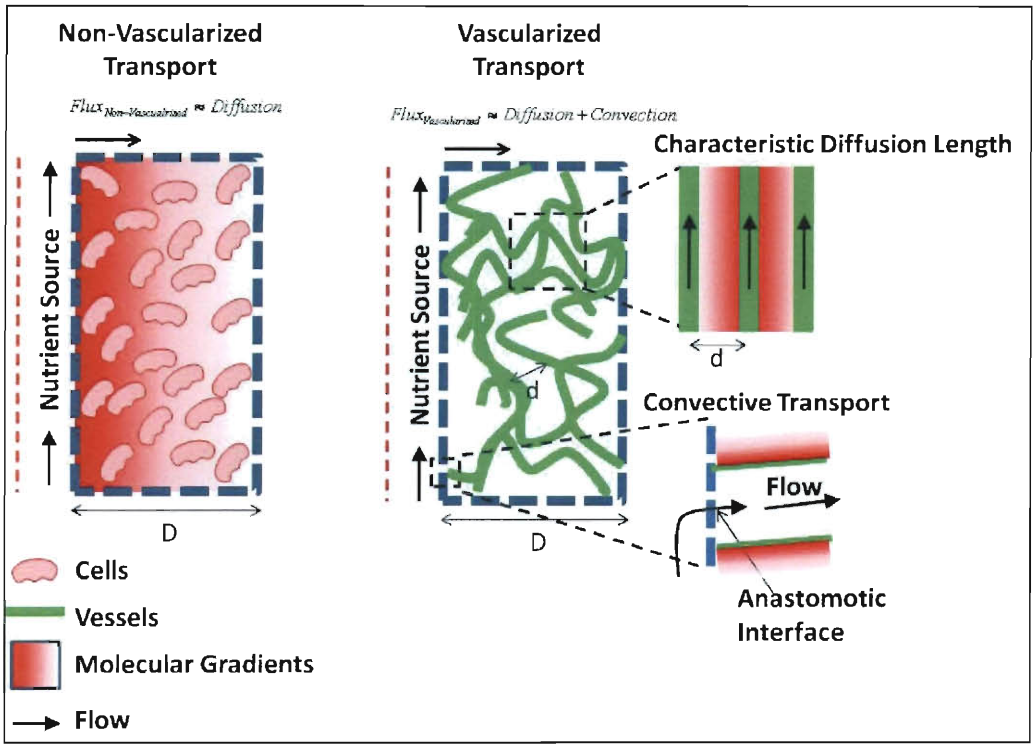

Figure 22: Shifting Transport Regimes in Vascularized Constructs. Non-vascularized transport is limited to diffusion-based transport with characteristic diffusion lengths (D) determined by the size of the overall construct size. Vascularized transport is utilizes perfusable vessel networks to transport mass via convection over large distances and diffusion over short distance. Characteristic diffusion lengths (d) in this system are defined by the distance between vessels.

Beyond improving transport regimes and providing a pro-anastomotic interface for rapid integration *in vivo*, hierarchical organization and perfusion of vessel networks may also help to mature and generate tissue specific vessel networks. It has been previously shown within *in vivo* models that flow based maturation of early capillary plexuses leads to a more stable vessel network with appropriate physiologic transport functions.[107-109] Furthermore, flow based maturation communicated through pressure driven circumferential strain and shear stress on the endothelium is thought to be responsible for tissue specific microvascular specialization.[110-112]

Together these factors outline the framework for a new paradigm to improve the quality of *in vitro* vascularized constructs. Beyond the well cited and exploited factors found to drive initial vessel self organization and network formation, vascularization strategies must allow for external perfusion and hierarchical organization across large dimensions. Such considerations will help to transition vascularized constructs from the early proof of concept stage to robust, bulky and clinically relevant systems.

3.) Physiologic functionality of microvascular networks

Development of cellular, biomaterial and bioreactor technologies to grow, perfuse, and integrate vessel beds across length scales provides a significant improvement over the current state of the art. However, these characteristics alone do not necessarily assure the physiologic functionality of microvascular networks. The hallmark function of the microvascular is to provide an ultra high surface area mass exchange system with the ability to be selectively permeable to various solutes depending on the tissue type the vasculature is supporting. Furthermore the microvasculature's transport properties are dynamic and can autoregulate to tissue demand for oxygen and nutrients as well as respond to systemic small molecule stimuli such as nitric oxide or humoral regulation via a variety of vasoconstrictor or vasodialator agents.[79] However, very little research has focused on applying and testing the mass transport functionally of *in vitro* microvascular networks, instead only focusing on single vessel constructs[113]. Therefore one of the remaining challenges in engineering microvascular

networks *in vitro* is validating their ability function as a dynamic mass exchange system.

4.) Incorporation of parenchymal cellular elements

Much work has focused on the choice of scaffold, bioactive and cellular elements for the development of microvascular networks. However, these approaches often neglect the incorporation strategies and nutrient and signaling needs of tissue specific parenchymal cellular elements. The parenchymal cellular elements provide physiologic functionality for a given tissue type and therefore represent the most significant therapeutic contribution for regenerative medicine based therapeutics and are often the targets for pre-clinical drug development models *in vitro*. For example, a construct with highly functional and biomimetic liver vasculature *in vitro* provides very little hepatic function unless hepatocytes are present to metabolize waste and secrete hepatic compounds. Likewise, a liver cancer drug tested against a highly biomimetic microfabricated construct without hepatocytes carries little physiologic significance. Often the set of culture and tissue engineering parameters that are pro-vasculogenic may not support viability and function of the parenchymal elements. Therefore it is necessary to design a system that can support both microvascular network formation and parenchymal cell viability and physiologic function.

The distinct soluble signaling, matrix components, and nutrient needs of parenchymal and pro-vasculogenic cells coupled with the dynamic nature of tissue development makes culture of heterogeneous cell populations non-

obvious and requires special design considerations beyond simple combinatorial approaches. Some techniques have used systems seeded with pluripotent cellular elements that can differentiate into the pro-vasculogenic, pericyte, and parenchymal cellular elements.[6,114] These approaches employ dynamic multi-step culture conditions that first drive vessel formation and then direct differentiation into the parenchymal phenotype. In any case care must be taken to design systems that can independently direct formation of stable and functional microvascular networks while supporting parenchymal viability and preservation of phenotype in order to maintain tissue specific physiologic functionality.

Another function of the parenchymal cells other than tissue specific function may be their ability to orchestrate or promote microvascular network formation and maturation.[115] It is unclear during organism development, whether vessel networks and the nutrient and bioactive gradients they determine stipulate tissue specific formation or if parenchymal cells function to direct microvascular network properties. Regardless of the temporal development order, heterotypic cell interactions will likely play an important role in biomimetic tissue development.[66] Developmental biology studies have provided useful insight into the temporal and hierarchal order of parenchymal and stromal cell roles during tissue development. It is important that *in vitro* tissue design must account for these relationships in developing whole tissue systems.

5.) Rapid *in vivo* anastomosis

The largest remaining tissue engineering challenge for regenerative medicine based applications is the need for rapid construct anastomosis *in vivo*.[60] Although biomimetic and physiologic functional transport regimes *in vitro* can increase construct size and performance, the lack of rapid anastomosis with the host vasculature *in vivo* will result in low overall implant viability and non-homogenous tissue function across the thickness of the implant.[62] Much effort has focused on recruitment of host vessels through growth factor and other biochemical release from the implant.[93]Despite this effort, host vessel anastomosis is still plagued by slow integration times. Moreover, the biochemical conditions that improve the anastomosis times often negatively affect both implant and host vessel quality [2851] and carry concerns about systemic toxic effects associated with very high and non-physiologic growth factor concentrations.[116,117]

Another approach to improving anastomosis times *in vivo* is the engineering of a pro-anastomotic interface. One embodiment of an improved pro-anastomotic interface could result from the hierarchal integration of microvascular networks from single cell capillaries to larger diameter arterioles that are on the adequate size range for surgical anastomosis. Another example of a potentially pro-anastomotic interface could result from the presence of guidance microchannels at the implant interface that could allow for more rapid host vessel ingrowth into the construct. Furthermore, this approach can guide tissue in growth to specific strategically important anastomosis sties that will

facilitate rapid whole network perfusion. Both of these approaches have yet to be demonstrated *in vivo* or *in vitro* and are an intense topic of interest in our research group.

4.7. Microfabricated Hydrogels for MVTE Applications

Application of microfabrication technologies to hydrogels may provide a useful tool set to address some of the remaining challenges in MVTE. In particular hydrogel microfabrication technologies provide a means to spatially recapitulate the tissue microenvironment and help drive tissue formation. More specifically with respect to bridging length scales in MVTE constructs microfluidic hydrogels may provide sources to improve *in vitro* transport regimes and act as higher order conduits to facilitate biomimetic mass transfer across large length scales. The remainder of this chapter focuses on these technologies and their potential applications to MVTE.

4.7.1. Direct Photolithographic Patterning of Hydrogels

Photolithography refers to the process by which photons are spatially directed or focused to drive, either directly or indirectly, a photochemical reaction. This technology was developed by the semi-conductor industry to pattern integrated circuits with micron resolution. Spatially directed exposure of the photosensitive material can be achieved through a physical photomask, by focusing light via a laser scanning microscope[118], or through the use of a liquid crystal display projector[119]. Direct patterning of biomolecules within the hydrogel matrix has been shown by multiple groups to control cellular localization and

migration in 3D.[36,120,121] (Figure 23 C & D) PEG hydrogel structures have also been fabricated via additive photo patterning.[34,122] This technique enables the independent control of hydrogel content (cellular, biochemical, and biomechanical) and structure geometry.(Figure 23 A&B)

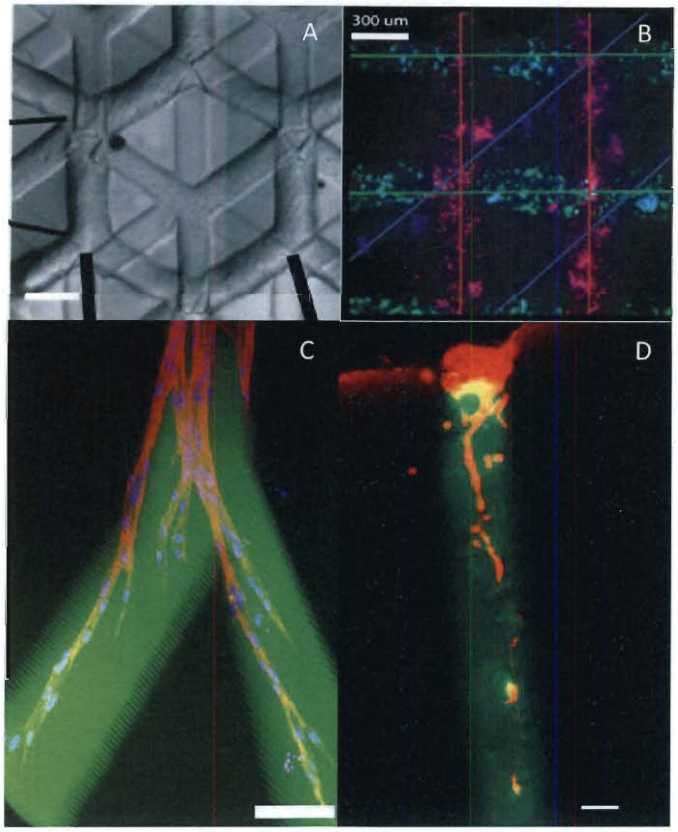

Figure 23: Photolithographic Patterning of Hydrogels. (A,B) Additive photopatterning of PEGDA for the formation of multiple independent cellularized structures[34,122] (C) Two photon laser photo patterning of PEG-RGDS into proteolytically degradable hydrogels directs cell migration in 3D (green=flourecent RGDS, Blue=DAPI, and red=phalloidin).[121](D) Photopatterning of GRGDS in agarose hydrogels directs cellular migration (green fluorescent GRGDS, red=phalloidin)[120]

Direct photolithographic hydrogel patterning for the fabrication of microvascular networks has largely remained absent from the literature for multiple reasons. Although cells can be patterned and their migration spatially

directed, the formation of patent EC lumens using this techniques has not been reported. Furthermore, it is conceptually and practically difficult to connect lithographically patterned cell structures to macroscale perfusion apparatus necessary to promote perfused vascularized tissue engineering constructs. Finally, although cellular migration can be spatially directed using this technique, the additive fabrication of patent microchannel requires the exposure of large non-channel areas. This region of interest (ROI) patterning via laser scanning lithography (LSL) is difficult due to the time associated with pattering large ROIs using the iterative raster scanning algorithm. More recently, Kloxin et al has developed a photocleavable PEGDA hydrogel derivative.[123] (Figure 24A) In this work the author demonstrated the ability to photocrosslink hydrogels with one wavelength of light and photodegrade the bulk hydrogel with as conventional UV lamp or spatially tailor 3D regions using a two-photon light source and a laser scanning microscope. (Figure 24 B & C) This is a breakthrough in the development of 3D hydrogel microchannels in a material removal scheme compatible with large structure fabrication.

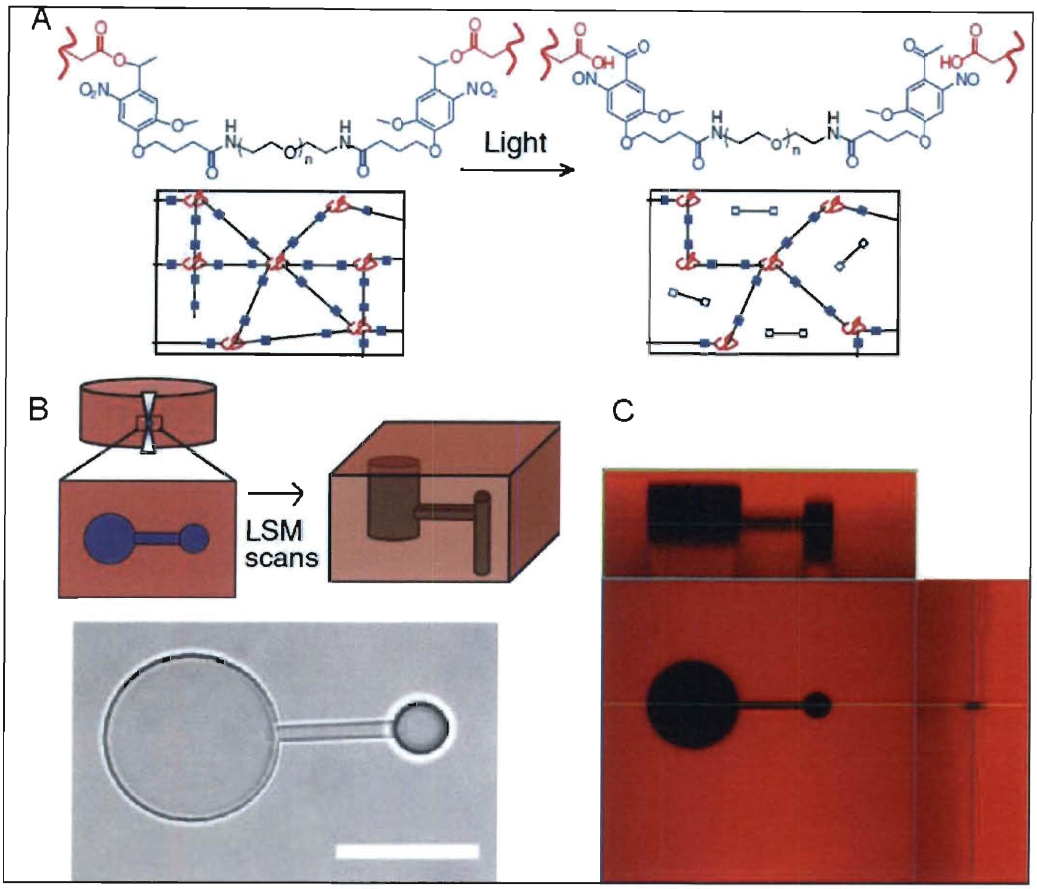

Figure 24: Photodegradable PEGDA Derivatives. (A) Schematic of photocleavable PEG derivative ad network before and after cleavage . (B) Schematic of two photon irradiation and 3D channel patterning in phase contract and (C) fluorescent imaging modes Adapted from Kloxin et al [123]

4.7.2. Replica Molded Hydrogels

Perhaps a more direct method to fabricate microarchitectures within PEG hydrogels is through soft lithographic replica molding of pre-polymer solutions. Soft lithography was introduced by. Whitesides' research group as a means to fabricate microfluidic channels within PDMS. The general process is outlined in Figure 25 where the photo resist is deposited on the substrate (a-b), a mask is fixed in place and the photosensitive material is exposed to UV (c-d), liquid pre-

polymer is poured over the mold with structures in relief and cured. Finally the cured polymer is peeled from the photoresist master to observe microarchitectures in relief (e-f).[124]

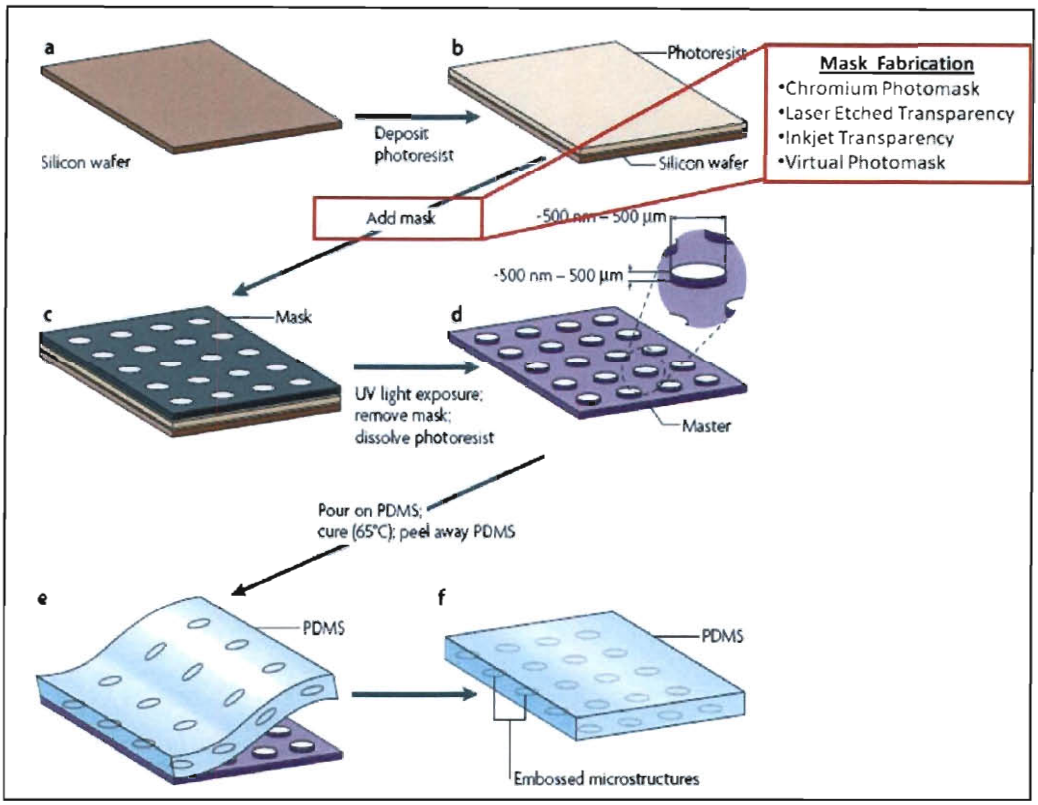

Figure 25: Soft lithography Schematic. photo resist is deposited on the substrate (a-b), a mask is fixed in place and the photosensitive material is exposed to UV (c-d), liquid prepolymer is poured over the mold with structures in relief and cured, cured polymer is removed to observe microarchitectures in relief (e-f) Recreated from Weibel *et al*[124].

This technique has been broadly applied to a wide range of polymer system for applications ranging from whole organisms sorting[125],automated microfluidic cell culture systems[126], to microarrayed pillars for biosensing and cellular diagnostic applications[127,128].

Recently it has been shown that hydrogels and other attractive biomaterials can be fabricated into microchannel networks using this same

technique. These networks have been used to facilitate convective and diffusive mass transport [129], spatiotemporally introduce reagents into the scaffold bulk from perfused channels [130] and direct cell localization within the microchannel lumen [131] and the scaffold bulk [132,133]. Most recently, multilayer microfluidic devices have been developed combining poly(dimethylsiloxane) (PDMS) and hydrogel microarchitectures to study cell migration [134] and spatially control microenvironment properties within perfused channels [135].

Early fabricated system in this field involved the micromachining of silicon and pyrex [87] to build microchannel architectures. The materials utilized in these devices performed poorly as tissue engineering scaffolds and did not encourage microvascular formation. However, replica molding techniques using a sucrose sacrificial coating and poly(glycerol sebacate) (PGS) as the molding material produced microchannels that supported media perfusion, EC adhesion, and yielded a confluent monolayer at 14 days of culture.[136] (Figure 26)

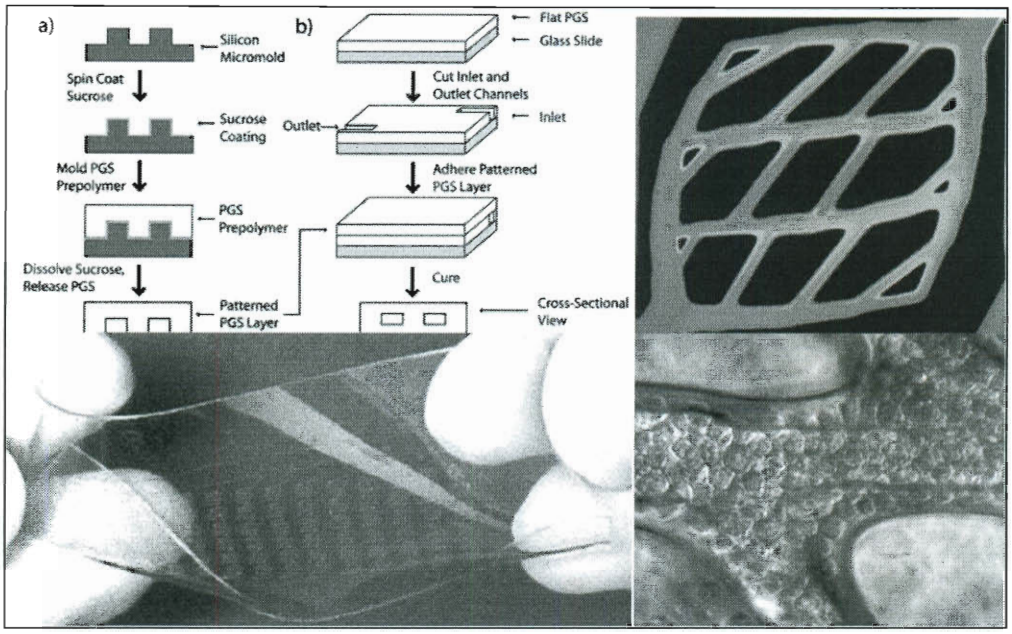

Figure 26: PGS Microchannels. (A) Replica molding fabrication schematic (B) Microchannel Network geometry (C) flexible and parallel microchannel networks (D) endothelialized microchannel networks at 14 days. Recreated from Fidkowski et al[136].

The first replica molding of perfusable hydrogel microchannels began to allow for cells to be encapsulated within the hydrogel bulk and for evaluation of system mass transport properties. These systems probed spatiotemporal mass transport and cell viability characteristics associated with microchannel networks within agarose[129] and calcium alginate[130] tissue engineering scaffolds as a function of cell type, cell seeding density, and perfusion rate. (Figure 27) Although this research laid the ground work for microfluidic hydrogel fabrication, these systems do not exhibit any tendency of the scaffold to direct tissue formation or produce microvascular tubule networks composed of cells. This was primarily due to the lack of biofunctionality of PGS, agarose, and calcium alginate based materials.

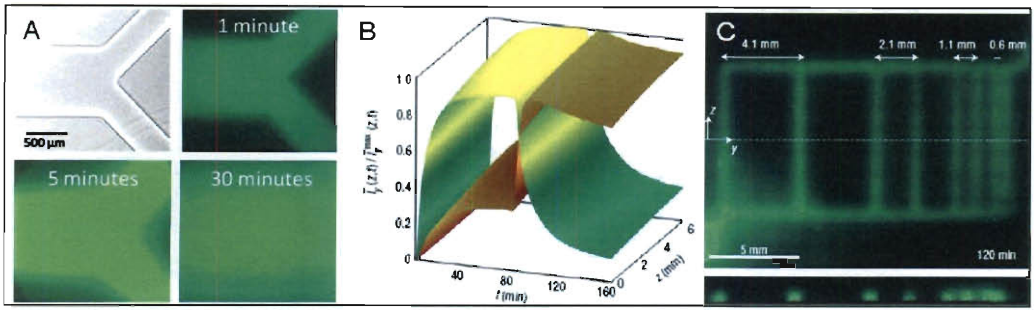

Figure 27: Mass Transport within Microfluidic Hydrogels. (A) FITC BSA diffusion from perfused agarose hydrogels as a function of time.[129] (B) Spatial temporal diffusion of fluorescein (green) and rhodamine (red) of perfused calcium alginate hydrogels.(C) Calcein AM (green, positive cell viability stain) only labels cells in regions nearest the perfused channel.[130]

A novel method for the fabrication of microchannel networks within highly bioactive hydrogel matrices was introduced by the Golden *et al*[133]. in 2007. This method utilized replica molding to fabricate a sacrificial gelatin microstructure mesh which was embedded within both collagen and fibrin hydrogels and dissolved away to yield a microchannel. (Figure 28) This work re-iterated the capability to seed EC within the microchannel network but also encapsulated a second cell type, fibroblasts, in the hydrogel bulk.[133]

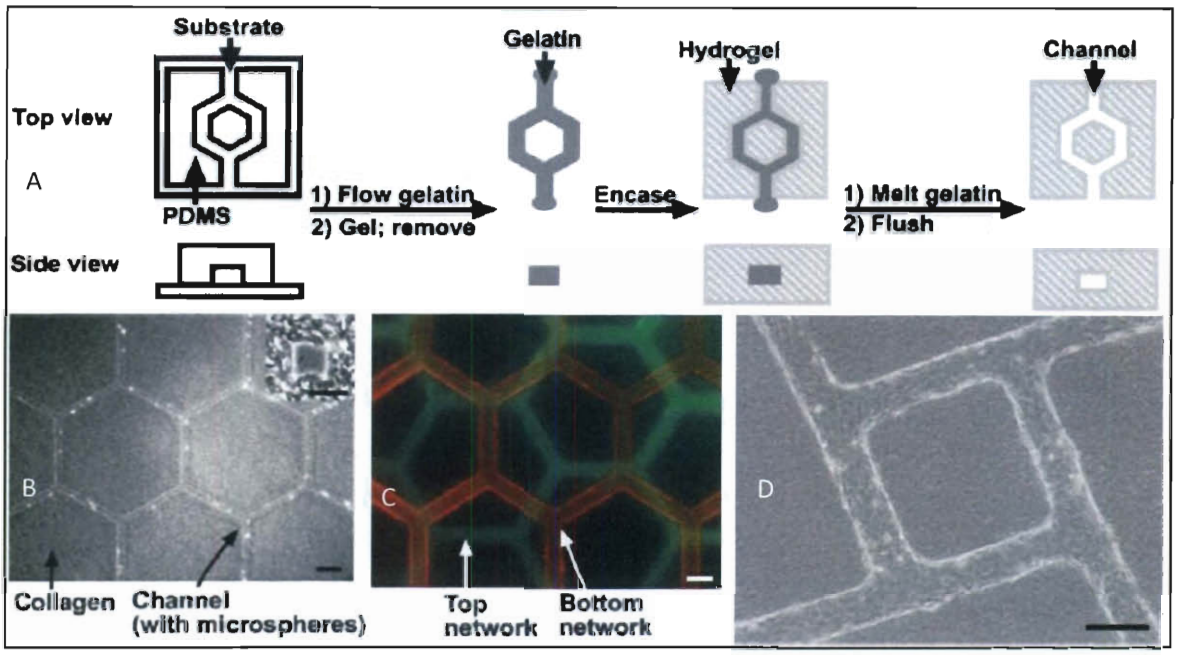

Figure 28: Microfluidic hydrogels fabricated via a sacrificial poragen. (A) Schematic illustrating use of replica molded gelatin meshes as a sacrificial poragen. (B) Collagen hydrogel with microspheres flowing through channels. (C) Layering of two microchannel networks to form a pseudo 3D system. (D) Endothelialized microchannel networks after culture for 5 days. Recreated from Golden *et al*[133]

This application of a biocompatible sacrificial poragen process to highly bioactive hydrogel materials (Collagen, Fibrin and Matrigel) was an important contribution to the literature. However this work fell short in addressing several key limitations in developing vascularized tissues *in vitro*. Most importantly the author did not encapsulate any tubule forming cellular elements within the hydrogel bulk and therefore failed to demonstrate the systems potential to support self-assembled microvascular networks *in vitro*. Coinciding with this the researcher didn't show the ability to integrate fabricated and endothelialized channels with interstitial tubule forming elements located within the hydrogel bulk. This is important when trying to design systems that integrate perfusion components across length scales.

4.7.3. Microfabricated Hydrogels Embedded within PDMS Housings

In vivo organization of microvascular tissue hierarchies is often composed of spatially distinct heterogeneous physical and biochemical regions. Each region provides a specific function that is unique to the tissue and important to a maintaining a structure function relationship at the tissue and organ level. (see section 4.6 Current Limitations in Microvascular Tissue Engineering - #3 Role of Parenchymal cell) Often spatial and temporal recapitulation of physical, biochemical and cellular elements in biomimetic patterns cannot be accomplished with a single microfabrication technique and therefore it is often necessary to employ multiple microfabrication modes within a single construct.

One strategy that is being employed to address some logistical problems associated with microfluidic hydrogels is the use of an external PDMS housing. Despite the significant limitations of PDMS alone as a microfluidic scaffold, PDMS has advantages in composite hydrogel-PDMS systems. PDMS provides a readily fabricated, transparent, imaging compatible, robust outer housing for easy handling and maintenance of a sterile culture environment without the use of complex support apparatus (see Supplemental material Choi et al[130]).[137] Furthermore, the combination of PDMS microfluidic networks with inlaid regions of cell laden hydrogels provides a means to precisely control spatial gradients and flow regimes while harnessing the biomimetic aspects of a hydrogel as a favorable scaffolding material.[134,135,138] (Figure 29)

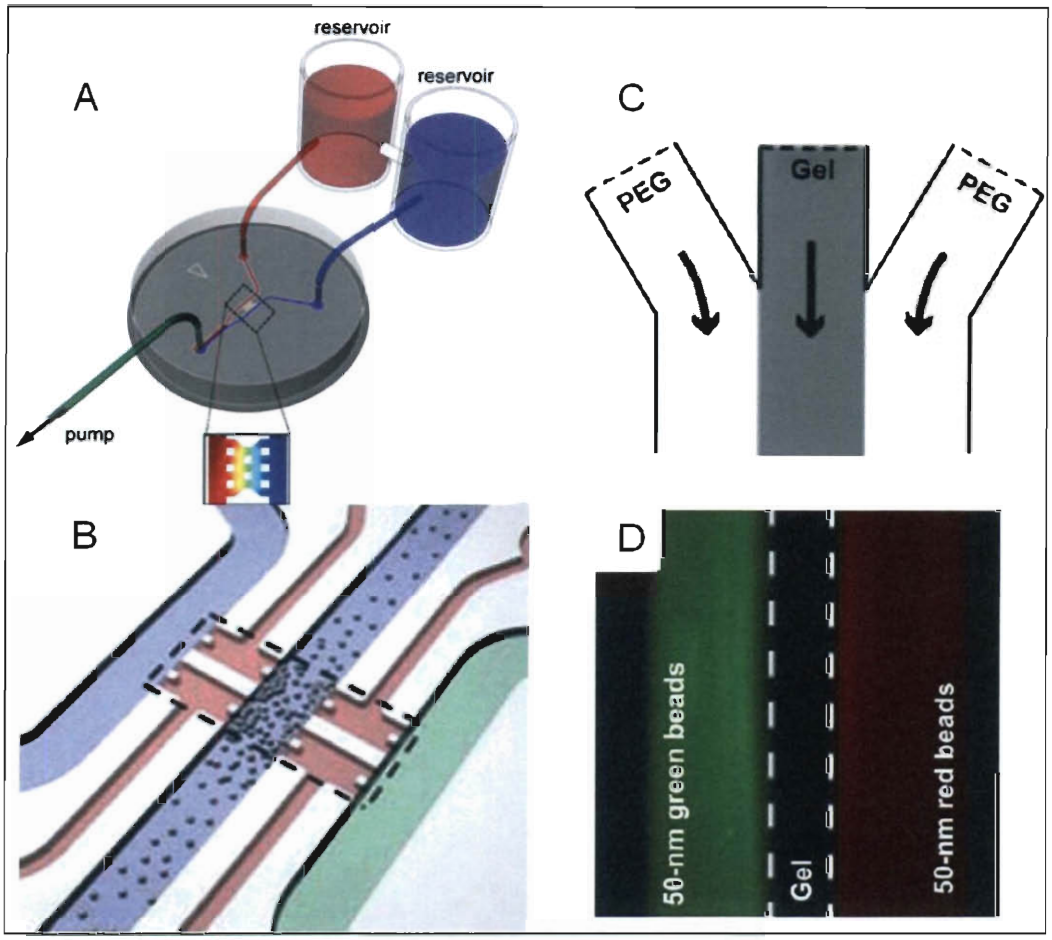

Figure 29: Hydrogels inlaid within PDMS housings for controlled gradients and flow regimes. (A) Use of a dual channel approach to establish controllable concentration gradients.[138] (B) A similar dual channel system with hydrogel elements (red) microinjected within a region between cell seeding regions (middle;blue) and perfused channels (edges blue and green).[134] (C) Use of laminar flow regimes to spatially control thermal polymerization of PEG pre-polymers for partitioning of reagents within PDMS microfluidic channels.[135]

This techniques result in systems with interesting properties and the ability to study fundamental cell interaction in a highly repeatable in vitro environment. A noticeable weakness of these systems is the reliance on thermal polymerization. In the case of Chun *et al*[134]. (Figure 29A,B) the inlaid hydrogel geometry is determined by the shape of the PDMS housing and this system requires separate microinjection access ports. In the case of Wong *et al.*[135] (Figure 29

C,D) fabrication of hydrogel structures is limited to simple straight segments directly related to the partitioning of fluid due to laminar flow regimes within PDMS microchannels.

Development of fabrication techniques that allow for independent control over PDMS housing and hydrogel geometry would be advantageous to the development of complex multi layer tissue analogs *in vitro*. Recent efforts have combined softlithography and photolithography as a method to fabricate PEG hydrogel microstructures within PDMS microfluidic channels for fabrication of cellular arrays[139] multi-component patterns[140] and robust hydrogel microparticles of easily tunable geometries within microfluidic channels.[141-143]. (Figure 30)

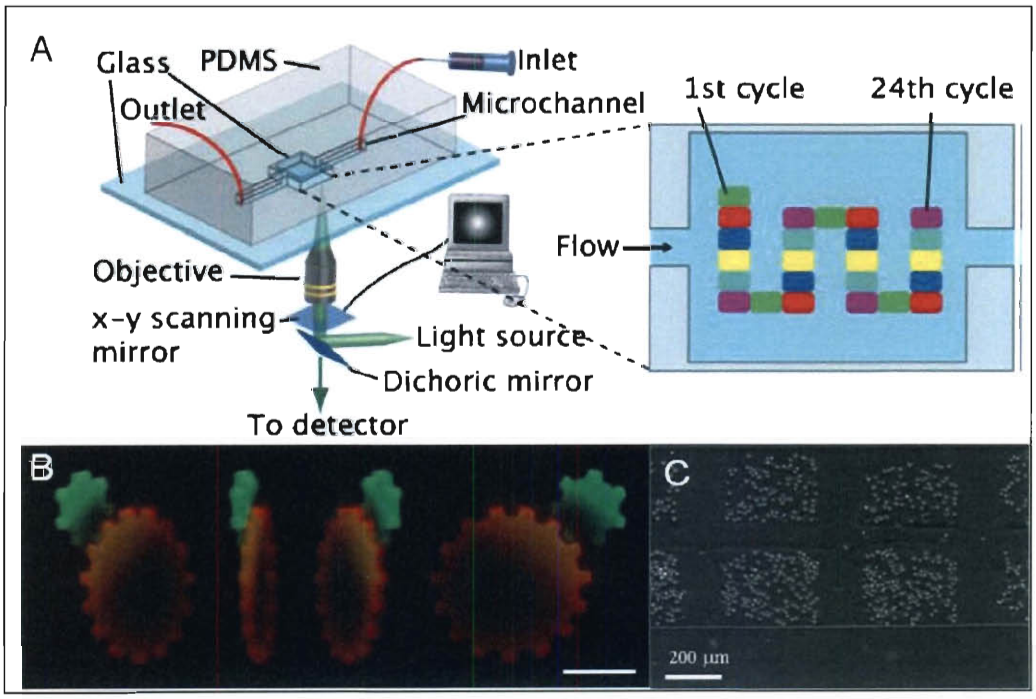

Figure 30: Hydrogel Microfabrication Approaches within PDMS housings (A) Schematic of photolithographic patterning of PEG structures within PDMS housing and (B) representative images of structure fidelity. [140] (C) Micromolded cell laden PEG structures within a PDMS microfluidic channel.[139]

Although these studies report high cell viability, the hydrogel molecular weight (< 1000 Da), hydrogel concentration (>50 wt%), and photoinitiator concentration (>1%) employed have been found to be inhibitive of tissue formation and scaffold remodeling by cellular elements. Furthermore, the use of free-radical photopolymerized poly(ethylene glycol) dimethacrylate (PEGDMA) or poly(ethylene glycol) diacrylate (PEGDA) does not allow for proteolytic or hydrolytic degradation under physiologic conditions. This severely limits the ability of these systems to allow for cell driven *in vitro* tissue development and ultimately the applicability to recapitulate the cellular microenvironments. Much of our current work has focused on adapting these fabrication methods to highly biomimetic and bioactive hydrogels that support tissue formation.

4.8. Current Limitations in Microfabricated Hydrogels for MVTE Applications

1.) Application of microfabrication techniques to hydrogels that support and guide tissue formation

Early application of hydrogel microfabrication techniques focused on natural materials, such as agarose [129] and calcium alginate[130], that have not been shown to possess vasculogenic potential. More recently, pro-tubulogenic materials such as, collagen I and the reconstituted basement membrane analog, Matrigel, have been replica molded to form microfluidic networks.[133] However, all of these natural materials suffer from batch to batch variability and with the exception of alginate carry immunogenic concerns due to their generation from

animals. In particular, Matrigel possess a variety of ECM components at unknown quantities and purities. This severely limits the ability to tailor biochemical and biomechanical properties and reduces clinical applicability. In order to maintain clinical significance, microfabrication techniques should be applied to hydrogel materials that are highly biocompatible and non-immunogenic but retain the ability to drive microvascular network formation. This is a critical remaining challenge to translating pro-vasculogenic hydrogels from the laboratory to the clinic.

2.) Fabricated Microfluidic Channel Integration with Self-Assembled Vessel Networks

A wide variety of microfluidic hydrogel network designs have been employed to mimic the *in vivo* microvasculature. Models have been developed to mimic *in vivo* flow regimes[136], minimize energy considerations [144,145], preserve wall shear stress and[146] maximize system mass transport[147] However, efforts to develop hierarchal organization and integration of fabricated channels with self-assembled vessel networks has been largely absent from the literature. Vessel network integration with fabricated microchannels would allow for controlled perfusion to occur across large length scales and would represent a material science breakthrough demonstrating integration of fabricated structures with self-assembled microvascular networks. In order to accomplish this task much care must be taken to engineer the interface between the perfused microchannel solution and the hydrogel wall containing microvascular networks. It is likely that an interplay between physical structures, proper flow and pressure conditions, as

well as biochemical considerations must be optimized in order to achieve an *in vitro* anastomotic interface between microvascular networks and fabricated structures.

3.) Incorporation, Integration and Support of Parenchymal Cellular Elements

Development of materials and techniques that are conducive to microfabrication, microvascular network formation and have been engineered to integrate across length scales still neglect considerations to incorporate the functional parenchymal elements into the tissue. Furthermore, special concern must be taken to assure that culture conditions that support microvascular network formation and integration with microfluidic networks also support parenchymal cell viability and normal physiologic functions. Finally, whether parenchymal cells are incorporated in separate fabrication steps or are concurrently seeded with pro-vasculogenic cultures, care must be taken to facilitate parenchymal integration with microvascular networks.

5. Chapter 5: Overview of Thesis Objectives

Although significant progress in pre-vascularized materials and microfluidic hydrogels has been demonstrated, there is little or no results showing that these technologies can be combined to recapitulate hierarchical vascular organization *in vitro* and improved anastomotic constructs *in vivo*. Moreover, the mass transport functionality of self-assembled microvascular networks has not been shown *in vitro* due mostly to the lack of ability to externally perfuse *in vitro* microvascular networks. Finally, although functional microvascular networks alone provide advantageous *in vitro* culture systems and have therapeutic potential, these systems have not incorporated the tissue specific parenchymal cellular elements. Together these factors have inspired a governing research objective to integrate microfabrication technologies with robust perfusion apparatus and pro-tubulogenic hydrogels. (Figure 31) Subsequent chapters will focus on novel research that begins to address these limitations and advance hydrogel microfabrication technologies for microvascular tissue engineering applications.

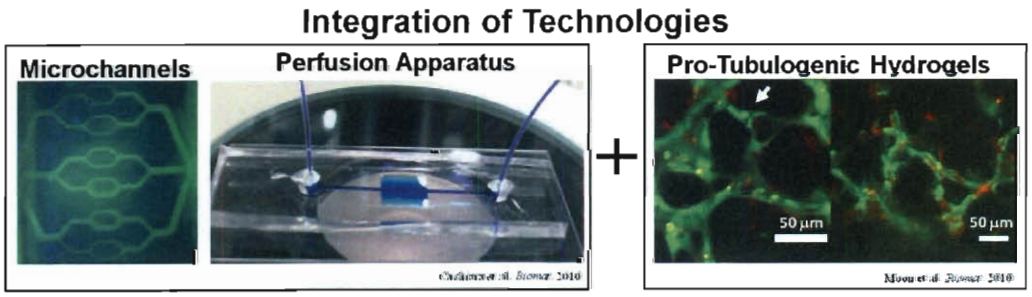

Figure 31: Integration of Microfabrication Technologies with a Self-Assembling Pro-Tubulogenic Hydrogel.

6. Chapter 6: Multilayer Microfluidic Poly (ethylene glycol) diacrylate Hydrogels

6.1. Introduction

Development of robust, *in vivo*-like tissues *in vitro* holds the potential to create regenerative medicine therapeutics, provide more physiologically significant pre-clinical models and supply a pharmacological and toxicological screening platform that reflects *in vivo* systems in both complexity and function. Pure diffusional transport of nutrients and waste from cellularized tissue engineering systems limits the maximum geometric length of engineered tissues to between 150-200 μm and restricts system metabolic density.[11, 12] Design of tissue engineering constructs that incorporate microvascular networks with sufficient mass transport characteristics holds the potential to increase both the size of *in vitro* tissue analogs and the capacity of the construct to support metabolically dense and clinically relevant cellular environments.

Multiple microfabrication techniques have been employed to improve mass transport properties in tissue engineering scaffolds. Perhaps the most important microfabrication technique to improve scaffold mass transport properties is the fabrication of microfluidic networks in tissue engineering constructs using softlithographic replica molding techniques. Despite this significant advancement, application of microfluidic channels to photopolymerizable synthetic hydrogel materials has remained absent from the literature. This is likely due to the logistical challenges associated with general handling and reliably connecting perfusion apparatuses to microfluidic hydrogels.

Systems employed to address these limitations were complex and cumbersome to the spread of the technology (Figure 32A). A more amenable and robust system design that can be rapidly tailored would allow for a broader adoption of microfluidic hydrogels. A novel system introduced by Chorbak et al utilized a microfabricated PDMS housing to control perfusion to the hydrogel. (Figure 32)

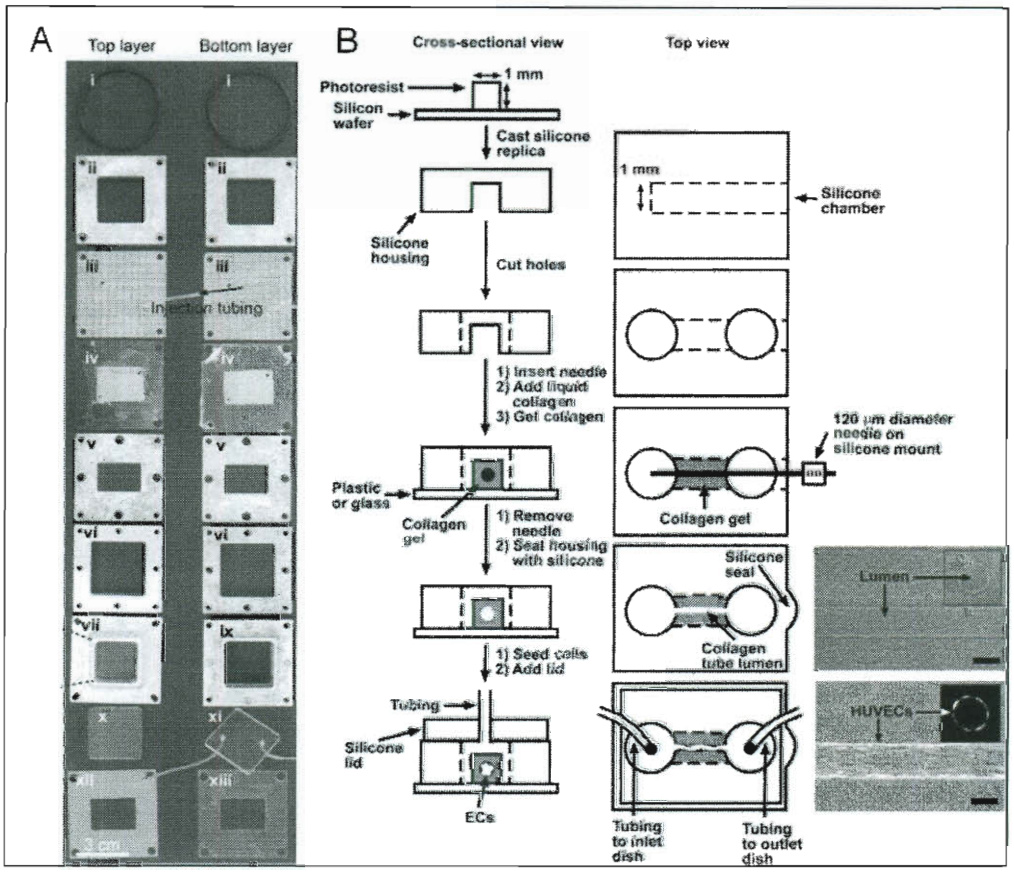

Figure 32: Supporting Apparatuses for Microfluidic Hydrogels. (A) Complex machined components needed to perfuse and handle a microfluidic hydrogel. (B) A simpler system utilizing a PDMS housing to control perfusion of collagen tube. Recreated from Choi *et al*[130] and Chrobak *et al.*[137]

We report a simple, robust, multilayer replica molding technique in which PDMS and poly(ethylene glycol) diacrylate (PEGDA) are serially replica molded

to develop microfluidic PEGDA hydrogel networks embedded within independently fabricated PDMS housings. This technique allows for the production of perfusable PEGDA networks independent of overall scaffold geometry. *In* addition, we show the ability to quantify and modulate spatial temporal construct mass transport properties and cell viability. Together these techniques represent a significant contribution towards the development of metabolically dense, complex 3D tissue analogs *in vitro*.

6.2. Objectives

The objective of this study was to fabricate perfusable microfluidic networks within PEGDA hydrogels. More specifically it was our aim to characterize the mass transport characteristics of the system by:

- Analyzing spatiotemporal mass transport across a range of molecular weight solutes and various hydrogel formulations
- Determining spatiotemporal cell viability profiles in perfused PEGDA hydrogels when compared to static culture systems
- Determine optimal microfluidic channel spacing for maximum cell viability

6.3. Materials and Methods

6.3.1. Cell Maintenance

NIH 3T3 fibroblasts, passages 3-10, (ATCC, Manassas, VA, USA) were cultured in Dulbecco's Modified Eagle Medium (DMEM; Sigma) supplemented

with 10% (v/v) heat inactivated fetal bovine serum (FBS; Biowhittaker, Walkersville, MD, USA), 2mM L-glutamine, 500 U penicillin, and 100 mg/mL streptomycin at 37° C in 5% CO_2 to 90% confluence prior to seeding.

6.3.2. Poly(ethylene glycol) Diacrylate (PEGDA) Synthesis

6 kDa PEGDA was synthesized according to previously published methods[35]. Briefly, PEGDA with a molecular weight (MW) of 6000 g/mol was prepared by combining 0.1 mmol/mL dry poly(ethylene glycol) (MW 6000 g/mol, Fluka), with 0.4 mmol/mL acryloyl chloride, and 0.2 mmol/mL triethylamine in anhydrous dichloromethane (DCM, Sigma) and stirred under argon overnight. The resulting solution was washed with 2 M K_2CO_3 (Sigma) and separated into aqueous and DCM phases to remove hydrochloric acid. The DCM phase was subsequently dried with anhydrous $MgSO_4$ (Sigma), and PEGDA was precipitated in diethyl ether (Fisher), filtered and dried under vacuum. (Figure 33)

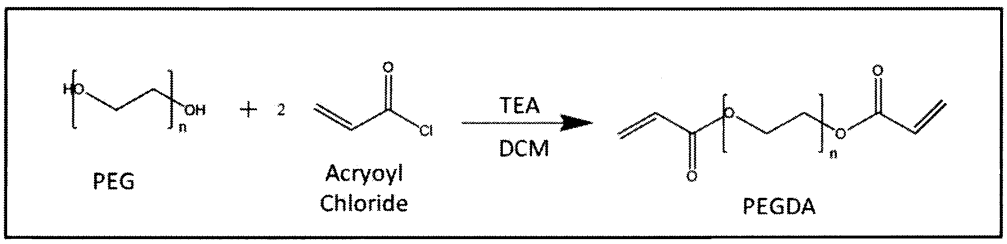

Figure 33: Reaction Schematic for Synthesis of poly(ethylene glycol) diacrylate (PEGDA).

6.3.3. Preparation of PEGDA pre-polymer solutions for Spatiotemporal Transport Studies

Solutions were prepared containing 6 kDa PEGDA in PBS (pH 7.4) to yield final concentrations of 5, 10 or 20% (w/v). Irgracure 2959 (Ciba, 100 mg/mL in 100% ethanol) was added to the hydrogel pre-polymer solution at 30 µL/mL.

6.3.4. Preparation of PEGDA pre-polymer solution and acryloyl – PEG - RGDS for Spatiotemporal Cell Viability Studies

6 kDa PEGDA was dissolved in sterile PBS (pH 7.4) to yield a final concentration of 10% (w/v). 3 mM acryloyl-PEG-RGDS, synthesized according to previously reported methods[41] (Figure 34), was added to the pre-polymer solution to allow for cell adhesion and promote cell cycle progression.(see Appendix for bioconjugate characterization) NIH 3T3 fibroblasts were trypsinized, counted and suspended within the PEGDA pre-polymer solution at 11 $x10^6$ cells/mL. The cell/PEGDA pre-polymer solution was replica molded to yield a microfluidic hydrogel as described in section 2.1.3 Fabrication of Multilayer Microfluidic Hydrogel. Cylindrical cell laden (11 $x10^6$ cells/mL) hydrogel constructs, 3 mm in diameter and height, were placed in well plates containing 1 mL of DMEM and used as static controls. Encapsulated cells were cultured for 0-72 hr under perfused or static conditions.

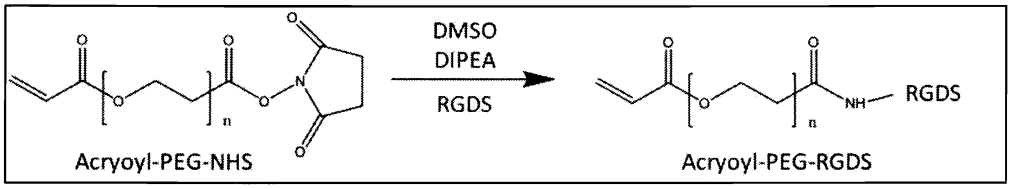

Figure 34:Reaction Schematic of Acryoyl-PEG-RGDS. The amino acid sequence RGDS is reacted with acryoyl-PEG-N-hydroxysuccinimide in anhydrous dimethylsulfoxide (DMSO) in the presence of base for 24 h at room temperature protected from light.

6.3.5. Multilayer Microfluidic Device Fabrication

6.3.5.1. Fabrication of SU-8 Photoresist Masters

Glass slides were cleaned and hydroxylated in piranha solution (7:3 v/v solution of H_2SO_4: 30% H_2O_2) for 30 minutes and dehydrated for 15 minutes at 200° C prior to spin coating. SU-8 2100 (Microchem) was spun coat at 1000 rpm for 40 seconds to generate a 350 µm thick substrate and SU-8 2050 (Microchem) was spun coat at 1000 rpm for 40 seconds to generate a 100 µm thick substrate. Photoresist substrates were exposed via a Mask Aligner (SUSS) using 20,000 dpi transparency masks (CAD/ART Services). All other photoresist processing parameters were derived from manufacture recommended protocols. 350 µm photoresist masters used to mold the PDMS housings, were cleaned with 100% ethanol, dried with filtered air, and molded to PDMS. 100 µm photoresist masters used to mold the PEGDA microchannels were cleaned with 100% ethanol, dried with filtered air and coated with SigmaCote (Sigma) to prevent adhesion of PEGDA structures to photoresist masters.

6.3.5.2. PDMS Housing Fabrication

PDMS (Sylgard 184) was mixed (10:1; silicone elastomer : curing agent), degassed, and cured to 350 µm photoresist masters for 3 hours at 65° C (Figure

35, Step 3). PDMS housings were removed from the photoresist master, access ports were bored with a 1 mm biopsy punch and then polyethylene tubing was inserted into the access ports and sealed through compression fitting. All PDMS housings were treated with the photoinitiator (2,2-dimethoxy-2-phenyl acetophenone in n-vinylpyrrolidone, 300 mg/mL) (Sigma) for 5 min to promote free radical induced interfacial polymerization of the PEGDA prepolymer solution to the PDMS housing. Excess photoinitiator was removed via sequential rinsing with 100% ethanol followed by ultrapure H_2O and then dried with filtered air.

6.3.5.3. Fabrication of Multilayer Microfluidic Hydrogels

Acetophenone-coated PDMS housings were aligned and overlaid with the SU-8 2050 photoresist masters treated with SigmaCote. PEGDA prepolymer solutions containing cells or PEGDA alone were injected into the housing around the channel mold and exposed to a long wavelength UV lamp (365 nm, 10 mW/cm^2) for 2.5 minutes (Figure 35, Step 5). In order to form 3D microfluidic networks, acetophenone-coated PDMS housings were sealed against a flat substrate and PEGDA prepolymer solutions were injected into the housing and under crosslinked via a 1 minute UV exposure to form a blank slab (Figure 1, Step 8). The PDMS/PEGDA microchannel mold and the under exposed blank slab were brought into contact and exposed to UV for 2.5 minutes to graft the hydrogel blank slab to the hydrogel with channel in relief (Figure 35, Step 9). For all experiments reported herein, the PDMS housing with an embedded PEGDA microfluidic hydrogel was conformally sealed to cover glass; polyethylene perfusion tubes were connected to the inlet reservoir and outlet syringe pump.

Perfusion was initiated at 600 µL/hr using a syringe pump (Harvard Apparatus) in withdrawal mode.

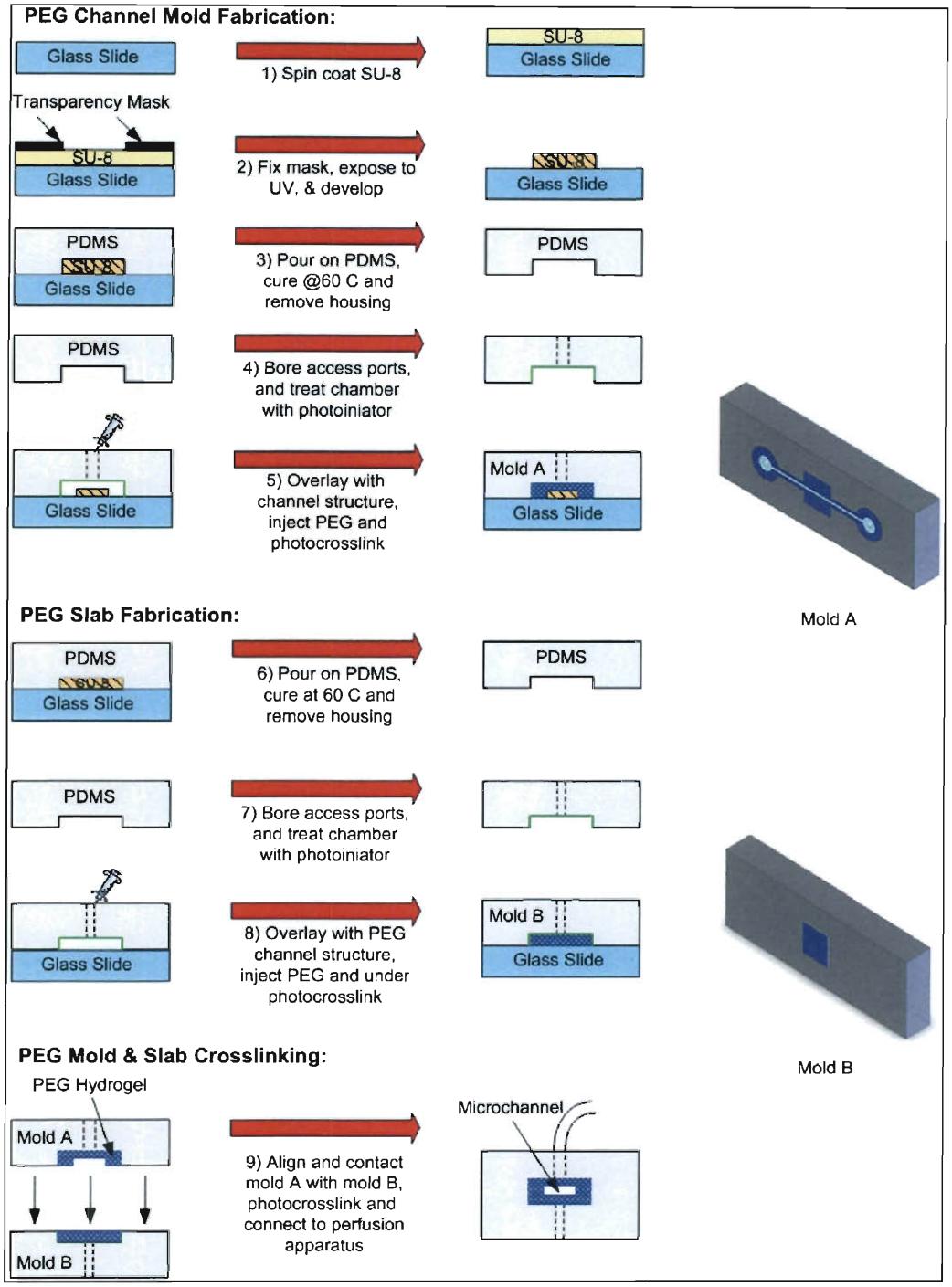

Figure 35: Fabrication schematic of PDMS/PEGDA microfluidic networks. Serial replica molding of PDMS and PEGDA to photoresist masters produces a perfusable PEGDA microfluidic channel embedded within an exterior PDMS housing. The PDMS/PEGDA construct, Mold A, can be sealed to coverglass for imaging after step 5 or crosslinked to a PEGDA blank slab, Mold B, to produce a 3D microchannel environment (Step 9).Recreated from Cuchiara *et al.*[148]

6.3.6. Spatiotemporal Diffusion Profile Analysis

Immediately post device fabrication and sealing to coverglass, acellular PDMS/PEGDA microfluidic hydrogels were perfused (600 μL/hr) with model transport molecules at various molecular weights (305 Da toluidine blue, 3 kDa dextran fluorescein, or 10 kDa dextran fluorescein). Images of the spatiotemporal fluorescent diffusion profiles were taken at 0, 1, 2, 4, 8, and 12 hours post perfusion using a fluorescent stereoscope (Zeiss Discovery V 8 Stereo Scope, 1x, EXFO X-cite light source) and a color CCD camera (Jenoptik, 5 megapixel, 16-bit). Images were analyzed using ImageJ (NIH) and spatial intensity profiles were generated using the plot profile function to determine spatial fluorescent intensity at each time-point. Intensity profiles were normalized to maximum intensity and plotted as a function of distance from the microchannel wall, perfusion time, and molecular weight of the transport molecule.

6.3.7. Mass Transport Models and Effective Diffusivity Parameter Fitting

The diffusion of solutes from the perfused microchannel was assumed to occur in only one dimension (outward from the channel). This assumption leads to the application of Fick's Second Law of Diffusion to the system (Equation 1) and its solution (Equation 2). Where C_s is the concentration of solute, D_{eff} is the effective diffusivity as a function of solute molecular weight (S) and PEGDA matrix concentration (M). C_0 is the concentration of the solute within the perfused microchannel.

$$\frac{dC_s}{dt} = D_{eff}(S,M)\frac{d^2C_s}{dx^2}$$

Equation 1: Fick's Second Law of Diffusion.

$$C(x,t) = C_0 erfc\left(\frac{x}{\sqrt{4D_{eff}t}}\right)$$

Equation 2: Solution to Fick's Second Law of Diffusion.

The assumption of diffusion only occurring in one dimension is validated by operating the perfusion system at high Peclet numbers (Pe) which show convective forces far exceeding diffusive forces. (Equation 3) For the toluidine blue and dextran system, Peclet numbers ranged from 1400-4300 respectively. These values are much larger than the ratio of channel length to channel height (L/h_C = 100) therefore suggesting that solute concentration does not vary as a function of length along the channel.

$$Pe = V_C h_c / D_{s,c} >> L / h_c$$

Equation 3: Dimensionless Peclet Number and Comparison to Microchannel Geometry.

Effective diffusivity of the hydrogel-solute system was determined by iterative parameter fitting of the measured spatiotemporal diffusion profiles to the solution of a one dimensional, non-steady state, first order Fickian diffusion equation using Igor Pro (WaveMetrics) software package. All data sets converged to the given solution for effective diffusivity across a range of initial estimates

Effective diffusivity as a function of solute molecular weight (toluidine blue MW=305 Da, 3 kDa and 10 kDa dextran) in water was determined using the

Stokes- Einstein relationship [149]. Through methods presented by Fournier *et al.*[149], where solute molecular radius (a) can be calculated by assuming the solute has a given molecular weight (MW), is spherical in shape and has a uniform density (ρ) (Equation 4). Substituting the molecular radius (a) into the Stokes-Einstein equation (Equation 5) provides values for effective diffusivity in water as a function of molecular weight. Here R is the ideal gas constant, T is temperature in degrees Kelvin, μ is the viscosity of water at temperature T, and N_A is Avogadro's number.

$$a = \left(\frac{3MW}{4\pi\rho N_A} \right)^{1/3}$$

Equation 4: Molecular Radius as a Function Solute Molecular Weight.

$$D_{Water} = \frac{RT}{6\pi\mu a N_A}$$

Equation 5: Solute Effective Diffusivity as a Function of Solute Molecular Radius.

6.3.8. Spatiotemporal Cell Viability Analysis

Spatiotemporal cell viability profiles were obtained at 0, 24, 48, and 72 hr post encapsulation at regions ranging from 0-1500 μm from the perfused microchannel or from the edge of the static tissue cylinder. 3T3 cell viability was assessed using a Live/Dead assay (Calcein AM/Ethidium homodimer, Invitrogen). The viability staining was imaged using a confocal microscope (Carl Zeiss Inc. LSM 5 Live, 20X (NA 0.8) objective, FOV= 318 x 318 μm, vertical z-stack: 1 μm slices, 50 slices per region). Images were tiled outward from the microchannel wall at 300 μm intervals between 0-1500 μm to determine cellular

viability as a function of distance from the microchannel. At each region the ratio of live cells (Calcein AM positive) to total cells (Calcein AM + Ethidium homodimer) was analyzed as a function of radial distance from channel and culture time.

6.4. Results and Discussion

6.4.1. Fabrication of Multilayer Microfluidic Hydrogels

Here we describe a multilayer softlithographic fabrication technique wherein PDMS and PEGDA were serially replica molded to form a microfluidic PEGDA hydrogel embedded within an external PDMS housing. Serial replica molding of PDMS followed by PEGDA, formed robust, perfusable hydrogel microchannel networks with channel diameters ranging from 50-500 μm and aspect ratios from 5:1 to 1:2. (Figure 36). This fabrication process, along with the rapid and mild photocrosslinking conditions utilized for PEGDA hydrogel formation, allowed for encapsulation of cells within the hydrogel matrix with minimal cytotoxicity (Figure 40 & Figure 41, t=0 hr).

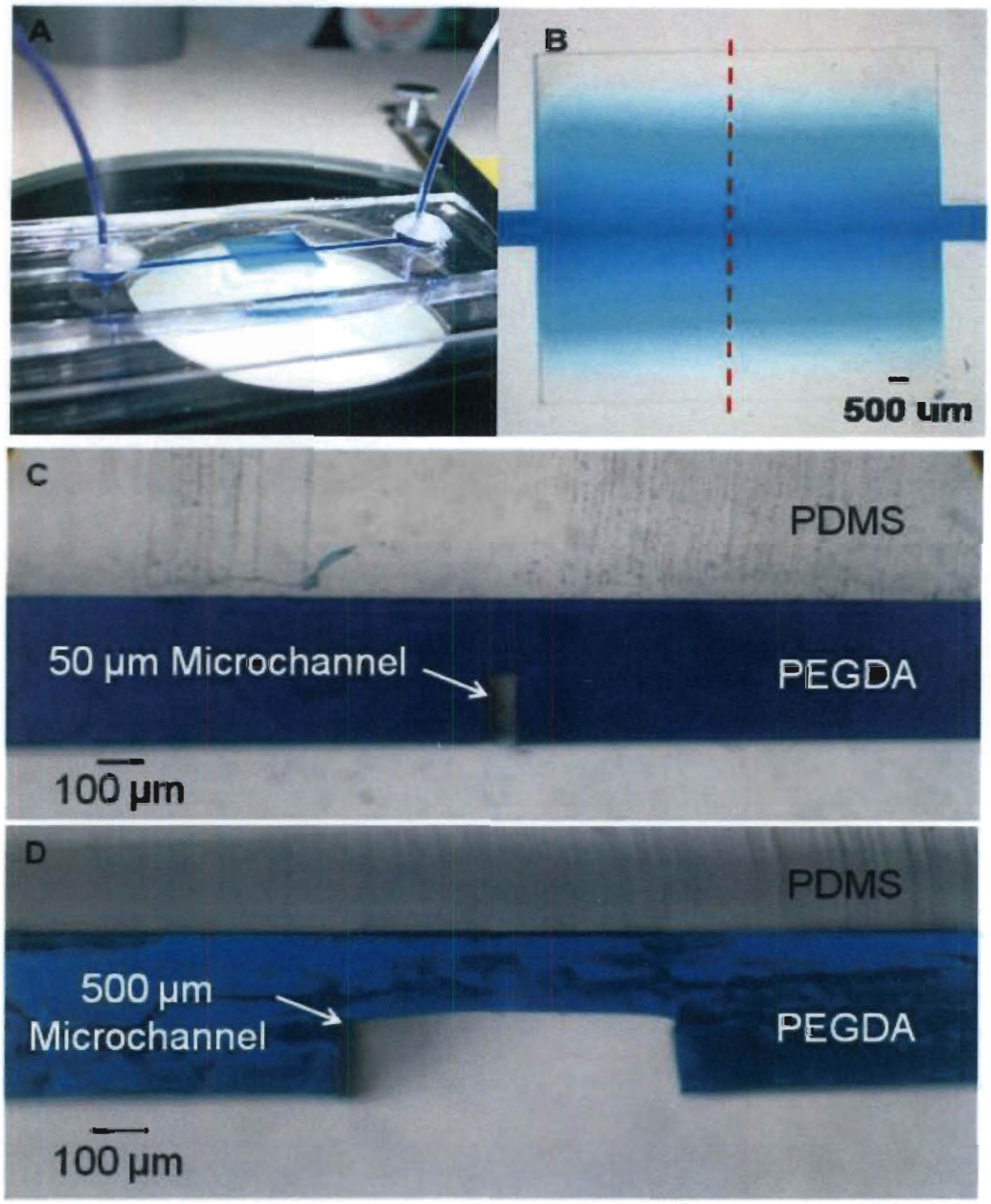

Figure 36: Multilayer microfluidic PEGDA hydrogel. (A) Isometric view of PDMS/PEGDA microchannel device perfused with toluidine blue, (B) Diffusion of toluidine blue into PEGDA diffusion chamber (10 x 10 mm) from a single 50 µm channel with red hashed line indicating location of cross sections in C & D. Recreated from Cuchiara *et al* [148] PDMS/PEGDA device cross sections with a (C) 3:1 and (D) 1:2 PEGDA microchannel aspect ratio.

6.4.2. Molecular Weight Effects on Spatiotemporal Transport Gradients

Inadequate nutrient and waste mass transport limits the size, complexity and clinical functionality of tissue engineered constructs. Optimization of nutrient and waste mass transport coupled with control over spatiotemporal signaling gradients provides the ability to maximize cell viability, spatially control cell behavior and direct tissue formation. We demonstrated a microfluidic PEGDA hydrogel system that supports pressure driven convective transport as well as diffusional transport mechanisms. Spatiotemporal molecular gradients were shown to vary as a function of solute molecular weight (Figure 37) and hydrogel concentration (Figure 38). As expected, diffusional transport of higher molecular weight solutes with larger hydrodynamic radii occurred at a slower rate when compared to that of lower molecular weight solutes (Figure 37 & Figure 38). Toluidine blue (MW=305 Da) exhibited the highest effective diffusivity (1.75×10^{-5} cm^2/sec) while 3 kDa dextran fluorescein (1.23×10^{-7} cm^2/sec) and 10 kDa dextran fluorescein (2.6×10^{-9} cm^2/sec) exhibited lower effective diffusivities in proportion to their increasing molecular radius. (Figure 38D)

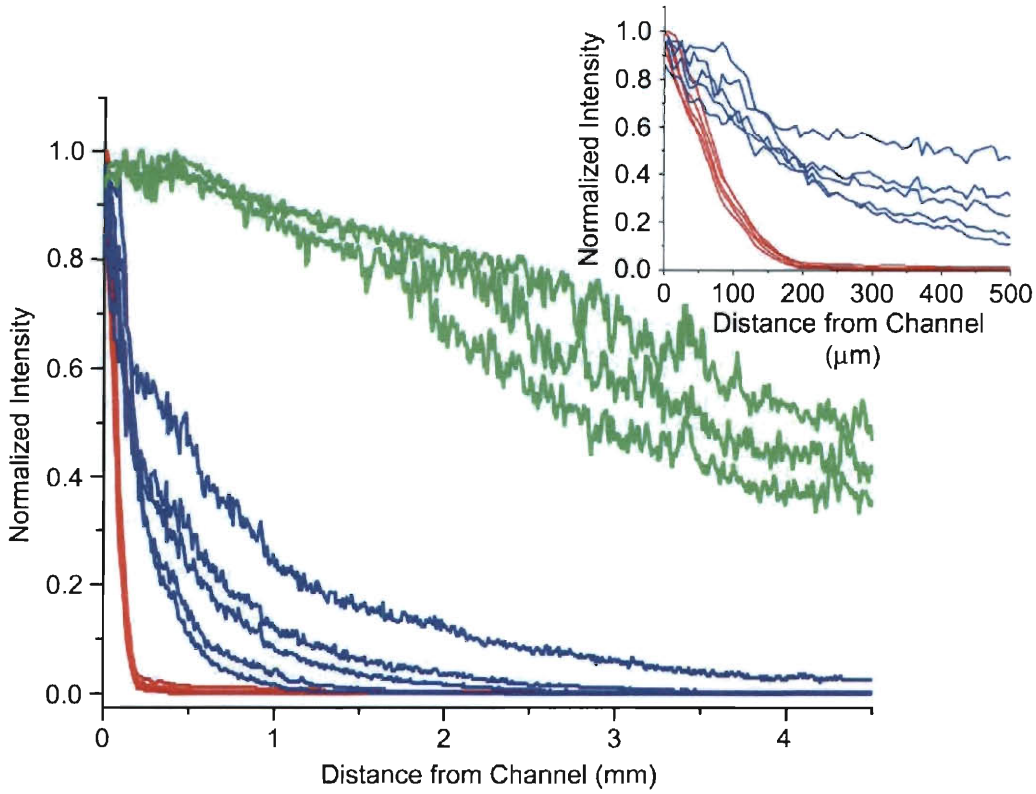

Figure 37: Solute molecular weight effects on PEGDA spatiotemporal diffusion profiles. Diffusion of multiple molecular weight solutes; toluidine blue (green, MW= 305 Da), 3 kDa Dextran fluorescein (blue) and 10 kDa Dextran fluorescein (red) in 10% (w/v) 6 kDa PEGDA hydrogels. Advancing profiles represent increasing time from 1 to 12 h (Inset) Expanded view of diffusion profiles shows dextran hydrogel penetration depths on the order of hundreds of microns compared to millimeters for low molecular weight toluidine blue. Reproduced from Cuchiara *et al.*[148].

In addition to solute molecular weight effects on spatiotemporal molecular diffusion gradients, PEGDA hydrogel concentration was shown to affect system transport properties (Figure 38). Increases in hydrogel concentration from 5 to 20% (w/v) were shown to be inversely related to solute diffusion rate and the effective diffusivity of the hydrogel-solute system (Figure 38D). At the low hydrogel concentration (5 %), toluidine blue had the highest effective diffusivity (1.86×10^{-5} cm^2/sec). However, when increasing the hydrogel concentration to 10 and 20% the effective diffusivity of toluidine blue decreased to 1.75×10^{-5} and

8.45 x10^{-6} cm^2 /sec respectively (Figure 38D). This trend was attributed to the decrease in average hydrogel pore size as a function of increasing PEGDA concentration. Modulation of diffusion gradients by varying polymer physical properties and solute molecular weight provides a useful tool to control soluble spatiotemporal signaling gradients and to direct cell migration and tissue pattern formation *in vitro.*

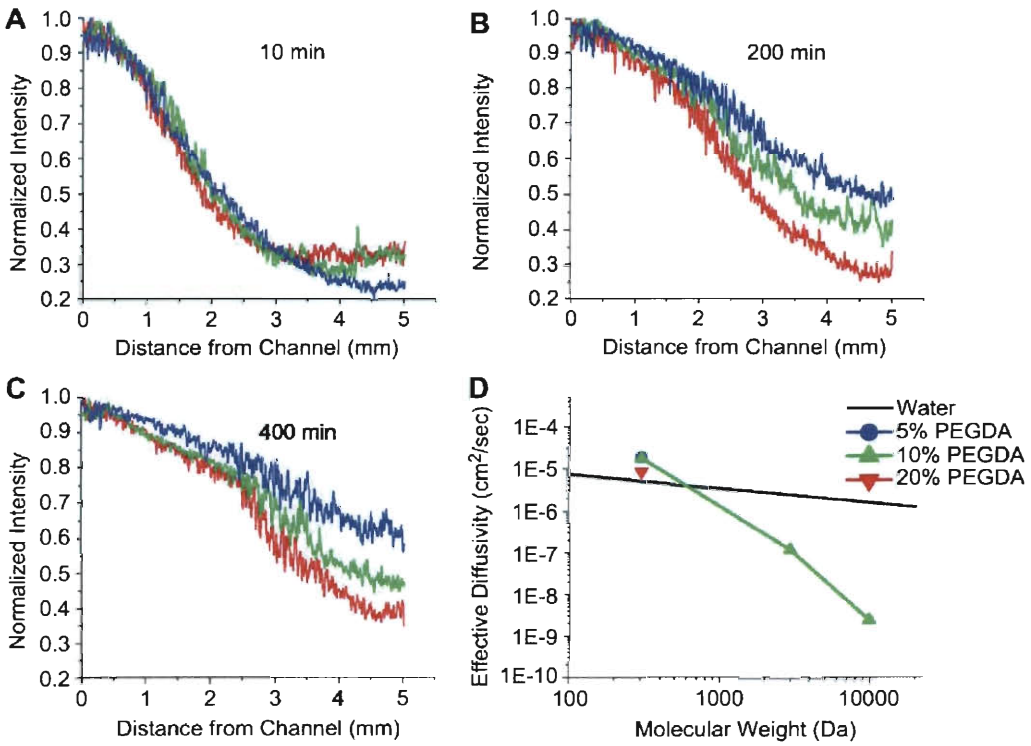

Figure 38: PEGDA hydrogel concentration effects on transport properties. (A-C) Spatiotemporal toluidine diffusion profiles at 10, 200, and 400 min of perfusion for 20% (red), 10% (green) and 5% (w/v) (blue) PEGDA hydrogels, (D) Measured effective diffusivity, fit from a 1D non-steady state Fickian diffusion model, plotted as a function of solute molecular weight and PEGDA hydrogel concentration. Recreated from Cuchiara *et al.*[148]. A low molecular weight solute (toluidine blue MW= 305 Da), at all hydrogel concentrations, had similar effective diffusivities to that of the solute in water. Increasingly larger molecular weight solutes (3 kDa and 10 kDa dextran fluorescein) exhibit decreased effective diffusivity when compared to the solute's diffusivity in water. This behavior is indicative of steric hindrance effects between the solute and the PEGDA hydrogel pore network. Diffusivity in water as a function of molecular weight was generated from the Stokes-Einstein equation Fournier *et al*[149]

6.4.3. Determination of PEGDA Network Properties

Sub-micron characterization of hydrogel physical structures is difficult to directly measure through electron microscopy techniques due to the need for high vacuum environments. Commonly the presence of a high vacuum has deleterious effects on hydrogel structures and provides an artifact laden representation of physical structure. Therefore much effort has focused on empirical swelling based models to determine the physical structure of hydrogel networks. The most important parameters these models generate to characterize hydrogel network structure are the molecular weight between crosslinks (M_C) and the corresponding average mesh or pore size (ξ).

A model that has gained particular traction is the Flory-Rehner theory[150]. This theory models a hydrogel that is immersed in a fluid medium at swelling equilibrium experiences only two thermodynamically driven forces (1) the entropically driven force to mix or solubilize in the immersed medium (ΔG_{mixing}) and the elastic recoil forces of the polymer chains ($\Delta G_{elastic}$). However, the lynchpin assumption of the Flory-Rehner model assumes swelling equilibrium with the surrounding solutions. Unfortunately, embedding PEGDA within the much stiffer PDMS housing invalidates this assumption and prohibits the application of this model to the PDMS/PEGDA microfluidic hydrogel. Due to the lack of adequate models describing network structure in swelling restricted hydrogel systems and in order to justify our conclusion that a decrease in PEGDA effective diffusivity occurs with increasing polymer concentration we

have employed a logic based explanation of how PEGDA pore size and diffusivity decrease with an increase in PEGDA concentration (Figure 39).

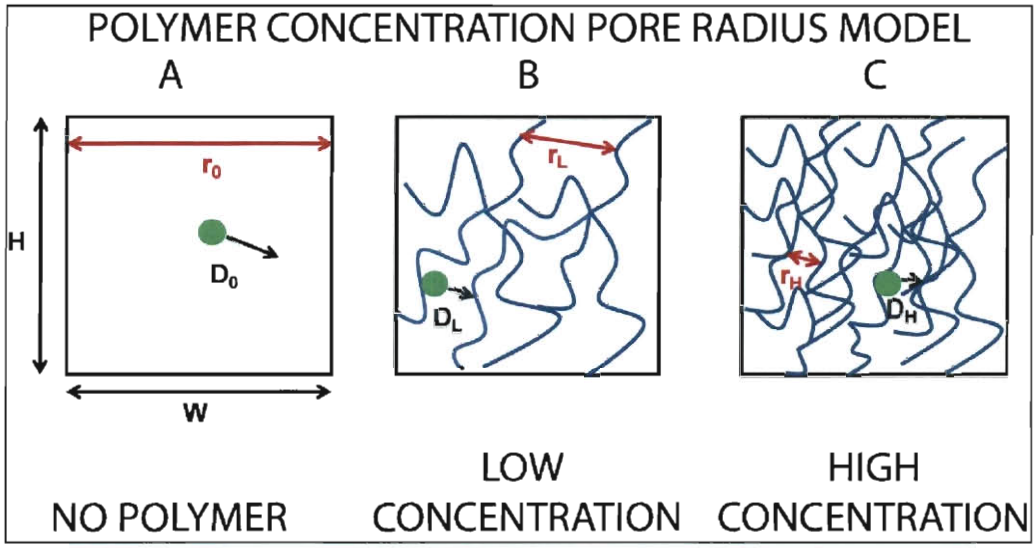

Figure 39: Volume Filling Logic Based Explanation for Polymer Concentration Effects on Diffusivity in Swelling Restricted Systems.

In brief we are suggesting that the system is of a fixed volume across all hydrogel concentration experiments. This volume can then be filled with various concentrations or volumes of PEGDA polymer. In one extreme case there is no polymer, the area available for solute diffusion is not limited and the effective diffusivity of the solute is the same as that in water (Figure 39A.). As small amounts of polymer begin to fill the fixed volume (Figure 39B) the volume is now occupied in part by water and in part by polymer. With the polymer void fraction being the only space available for diffusion. The solute effective diffusivity in this system is a fraction of value in water due to the reduced area available for diffusion or the reduced average pore size. As more polymer begins to fill the same fixed volume (increasing concentration; Figure 39C), the polymer void

fraction, the area available for diffusion and subsequently the average pore size decreases. This can be also seen as a decrease in effective diffusivity and we believe is the most likely mechanism explaining the mass transport changes observed in our system.

6.4.4. Spatiotemporal Cell Viability Gradients

Optimization of nutrient and waste gradients through rational microfluidic network design provides a tool to maintain cell viability and increase overall scaffold metabolic density. Viability of encapsulated 3T3 fibroblasts was shown to vary as a function of culture time, distance from perfused channel, and static vs. perfused culture (Figure 40 & Figure 41). A trend of decreasing cell viability with increasing distance from the microchannel wall was observed between 24-72 hrs of culture (Figure 40 & Figure 41). Regions closest to the channel (0-600 μm) were shown to have significantly higher cellular viability than the external regions (600-1500 μm) at both 48 and 72 hr of culture (paired t-test, $n=3$, $p < 0.05$). This trend was not observed at early time points and only became pronounced later in the culture (Figure 40 & Figure 41).

Necrotic region (cell viability < 30%) size as well as the overall system viability was improved in perfused systems when compared to static controls (Figure 41). 3T3 fibroblast viability in perfused systems was significantly higher compared to static controls at all time points greater than zero for distances between 0-900 μm from the microchannel wall (paired t-test, $n=3$, $p < 0.05$) (Figure 41). Necrotic regions in static systems, at late timepoints ($t = 72$ hr), were

shown to occur throughout the entire thickness of the scaffold while necrotic cores in perfused systems were confined to the regions of the scaffold farthest from the nutrient source. (distances > 600 μm) (Figure 41). Increased cell viability in perfused systems was attributed to convection-driven renewal of nutrient concentration gradients that are otherwise depleted over time in static systems. Furthermore, removal of waste products that otherwise build up in static systems was thought to also positively affect cell viability.

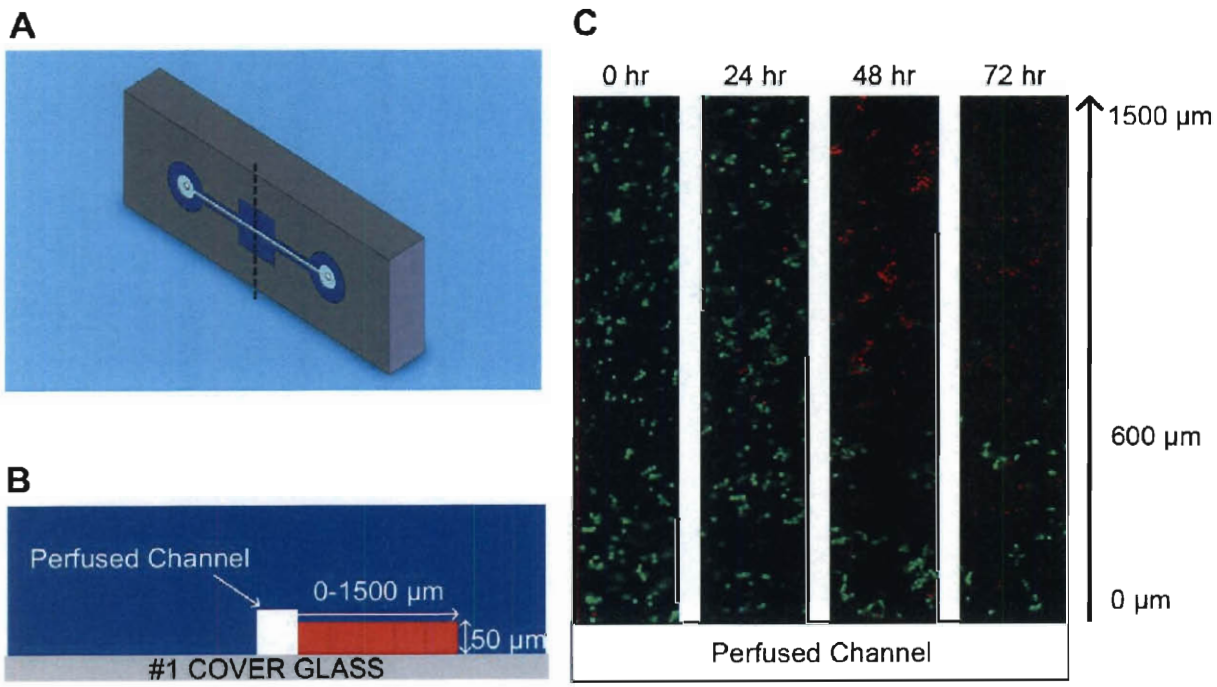

Figure 40: Encapsulated 3T3 fibroblast spatiotemporal cell viability fluorescent micrographs. (A) Isometric schematic of PDMS/PEGDA microchannel device with dashed line indicating location of cross section shown in panel B, (B) Cross section schematic of PDMS/PEGDA microchannel device indicating the size and location of the confocal z-stacks relative to the perfused channel, (C) Live/Dead (Calcein AM/Ethidium Homodimer) confocal fluorescent micrographs (20x, 318 x 318 mm FOV) of 3T3 fibroblasts encapsulated in 10% (w/v) 6 kDa PEGDA hydrogels as a function of distance from perfused microchannel (0-1500 μm) and culture time (0-72 h). At early time points (t=0 and 24 h), cell viability is high and homogenous at distances between 0 and 1500 μm from the channel. At later time points (t=48 and 72 h), a distinct necrotic core (viability <30%) forms at distances greater than 600 μm from the perfused channel. Recreated from Cuchiara *et al.*[148]

Spatiotemporal cellular viability profiles closely reflected conclusions derived from models which assume that cells act as metabolic sinks with intrinsic properties such as metabolic consumption rate and extrinsic factors such as cell seeding density[62,151,152]. These assumptions allowed cell laden hydrogel scaffold systems to be modeled as having an initial average metabolic density defined as the product of cellular metabolic consumption rate and cell seeding density. However, when scaffold metabolic densities exceeded the rate at which critical solutes are delivered to the system, inadequate nutrient and cytotoxic waste gradients develop and cellular elements become quiescent and or apoptose. This results in metabolic density profiles that parallel cell viability and ultimately generates a construct with reduced overall metabolic density. In order to maximize scaffold metabolic density, careful attention must be paid to design mass transport regimes that minimize necrotic regions and conserve the regenerative potential of the construct.

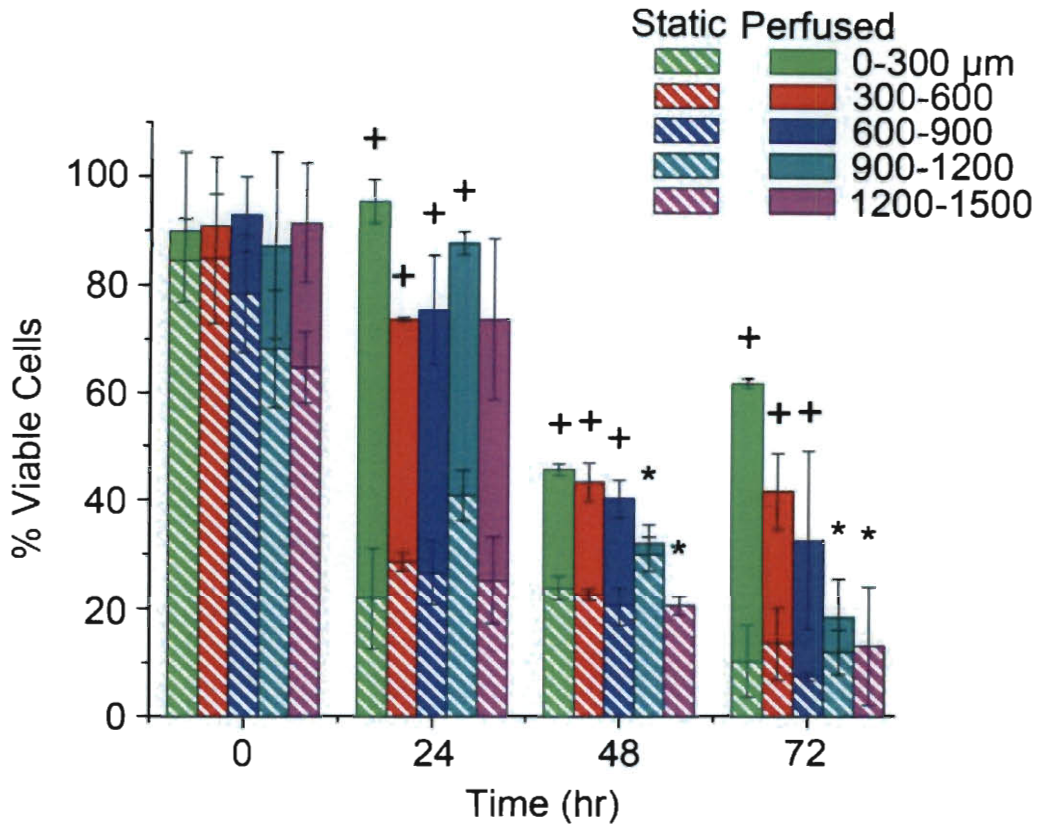

Figure 41: Encapsulated 3T3 fibroblast spatiotemporal perfused and static cell viability. Ratio of live positive cells (Calcein AM) to total cells (Calcein AM + Ethidium Homodimer) as a function of perfusion time (0-72 h), distance from perfused microchannel (0-1500 µm) and perfused (solid bar) vs. static (hash bar) culture conditions. Perfused viability was shown to be significantly less in the outermost regions (900-1500 µm) at 48 and 72 h of culture when compared to the inner regions as indicated by (*). Perfused cell viability was shown to be significantly higher (paired t-test, $p < 0.05$) than static cultures at the inner most regions (0-900 µm) at all time points greater than 0 h as indicated by (+). Recreated from Cuchiara *et al.*[148]

6.4.5. Applicability of Krogh Tissue Models

Often when analyzing mass transport to a tissue bed, especially with respect to the affects of oxygen concentration on cell viability, a Krogh tissue cylinder model is applied. Krogh based models assume that solute concentration (C) in a bed of capillaries in a tissue can be represented as a series of cylindrical layers of tissue at radial distances (r) and axial distance (z) from the capillary with an average porosity (ε^{gel}), intrinsic effective diffusivity of the tissue space (D_{gel})

and a metabolic consumption rate governed by Michaelis-Menton kinetics that can be simplified to a maximum or average metabolic consumption rate (Γmet). (Equation

$$\varepsilon^{gel}\frac{\partial C^{gel}}{\partial t} = D_{gel}\left[\frac{1}{r}\frac{\partial}{\partial r}\left(r\frac{\partial C^{gel}}{\partial r}\right)+\frac{\partial^2 C^{gel}}{\partial z^2}\right]-\Gamma_{met}$$

Equation 6: Krogh Tissue Cylinder Model

Although this is a very useful model, it assumes that the resonance time for blood in the capillaries is on the same order as the tissue effective diffusivity and therefore axial variation of solute concentration (z) in the capillary is impressed upon the tissue space. We have specifically engineered our microchannel flow regimes such that flow rate, which is related to resonance time, is much greater than the rate of diffusion into the tissue space (see Equation 3, high Peclet Number1400-4300). This operating parameter allows us to neglect axial changes in concentration and simplifies the Krogh tissue model to a non-steady state 1D-diffusion equation with a metabolic sink or consumption term that is a function of cell type (c) and cell seeding density (ρ).

$$\frac{\partial C^{gel}}{\partial t} = D_{gel}\left(\frac{\partial^2 C^{gel}}{\partial r^2}\right)-\Gamma_{met}(c,\rho)$$

Equation 7: Simplified Krogh Tissue Cylinder Model

6.5. Conclusions

In summary we have demonstrated a novel multilayer softlithographic fabrication scheme in which PDMS and PEGDA were serially replica molded to form enclosed perfusable microfluidic hydrogel networks. Furthermore, we

demonstrated the ability control spatiotemporal solute diffusion profiles by varying hydrogel concentration and solute molecular weight. Interestingly, varying PEGDA concentration had a minimal effect on toluidine blue (MW= 305 Da) effective diffusivity at all PEGDA hydrogel concentrations with values similar to that of the solute in water alone. However, higher molecular weight solutes to (3 kDa and 10 kDa dextran fluorescein) had a dramatic effect on effective diffusivity. The effective diffusivity of 3 kDa and 10 kDa dextran fluorescein decreased to 5.3% and 0.11% of their values in water respectively. This reduced transport of dextran through the PEGDA hydrogel matrix was thought to be primarily due to sterically hindered diffusion of dextran through the PEGDA pore structure. Spatiotemporal modulation of nutrient and signaling gradients provides a mechanism to control cellular phenotype and differentiation state as a function of distance from the perfused microchannel. This tool has the potential to provide much needed insight into soluble factor control over cell phenotype and can be implemented to direct tissue pattern formation within *in vitro* culture systems.

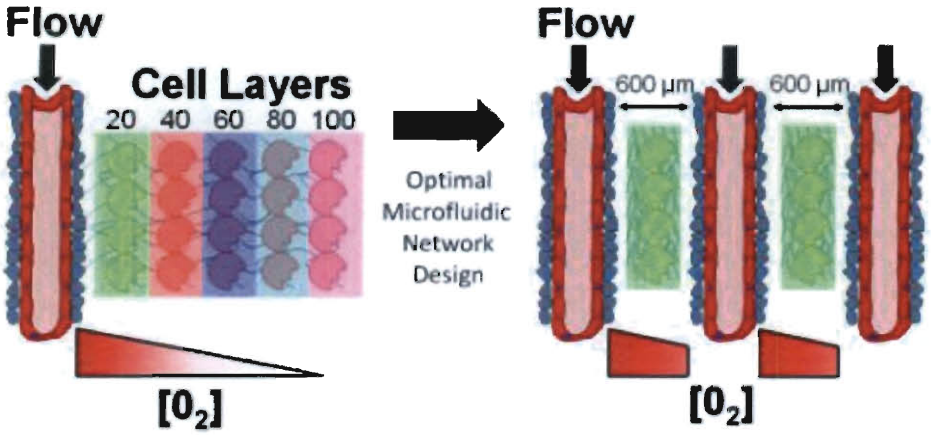

Figure 42: Schematic Demonstrating Effects of Optimal Microchannel Network Spacing on Oxygen Gradients and Cell Viability Profiles. (Left) Oxygen levels and cell viability decreases as distance from the microchannel or number of cell layers increases until oxygen levels reach necrotic levels (white; gradient bar). (Right) Optimal spacing of microfluidic networks maintains oxygen concentration at adequate levels to support cell viability across.

Our observations support that perfused PEGDA microfluidic hydrogel systems have higher cellular viability and subsequently enhanced metabolic density over static culture systems. Detailed understanding of metabolic gradients as a function of cell type and seeding density provides useful rational design parameters, such as channel spacing, that allows for maximization of cellular viability and scaffold metabolic density. For example, a channel spacing of 600 µm for 3T3 cultures seeded at 11 x 10^6 cells/mL would lead to greater than 60% average construct viability which is nearly a six fold increase over the static system (Figure 40 & Figure 41). This work provides an important tool set to reduce transport limitations in tissue engineering constructs and promote the formation of robust and complex tissues *in vitro*.

7. Chapter 7: Perfused Microchannel Integration with Microvascular Networks

7.1. Introduction

Despite significant progress, clinically viable regenerative medicine-based therapeutics are restricted to thin and metabolically diffuse systems limited by the lack of perfused vascualuture.[59,153,154] Vascularization approaches that rely solely on implant anastomosis with the host are limited by slow host vessel ingrowth (tenths of micrometers/day[61]) and non-homogenous vessel distribution within the construct[155]. Often these insufficient transport regimes result in a necrotic core and a reduction in the construct's overall therapeutic potential.[62]

Engineering of microvascular networks *in vitro* prior to implantation, known as pre-vascularization, holds the promise to improve slow and insufficient host-implant anastomosis.[102] Despite pre-vascularization progress in natural and synthetic biomaterials, [95,156] microvascular network perfusion *in vitro* has remained absent from the literature. Perfusion of self-assembled microvascular networks through lumen supported convective transport followed by extra vessel diffusion holds the promise to recapitulate favorable biomimetic mass transport regimes in vitro and improve host-implant integration.[157] Perhaps more important and markedly absent from the pre-vascularization literature is self-assembled microvascular network integration with microfabricated channels. Fabricated microchannel integration with self-assembled microvascular networks allows for controlled convective transport to occur across large length scales in a wide range of vessel diameters and would result in improved anastomotic interfaces.

Herein we report the integration of multilayer microfluidic polydimethylsiloxane– polyethylene glycol (PDMS-PEG) hydrogel microdevice with a self-assembling pro-vasculogenic co-culture of human umbilical vein endothelial cells (HUVECs) and pericyte precursors (10T ½). We demonstrate that the device can be used to spatiotemporally control microvascular network self-assembly and system apoptotic activity. In addition, integration of self-assembled microvascular networks with microfabricated channels shifted the construct's transport regime to vessel supported convective transport followed by extra vessel diffusion. This work has direct implications towards the development of perfusable pre-vascularized tissues *in vitro* for cell culture and regenerative medicine applications.

7.2. Objectives

- Demonstrate and characterize microvascular network self-assembly within PDMS/PEG microfluidic device
- Integrate self-assembled microvascular networks with fabricated channel
- Perfuse self-assembled microvascular networks from fabricated channel
- Evaluate changes in transport between non-vascularized and vascularized system

7.3. Materials and Methods

7.3.1. Cell Maintenance

Human umbilical vein endothelial cells (HUVECs) (Lonza , Walkersville, MD) were grown in endothelial growth medium (EGM-2, Lonza , Walkersville,

MD) supplemented with 2mM L-glutamine, 1000 U mL^{-1} penicillin, and 100 mg L^{-1} streptomyocin (Sigma-Aldrich, St. Louis, MO) and used between passages 3-8. 10T ½ cells (American Type Culture Collection, Rockville, MD) were grown and maintained in Dulbecco's modified Eagle's medium (DMEM) supplemented with 10% fetal bovine serum (FBS), 2mM L-glutamine, 1000 U mL^{-1} penicillin, and 100 mg L^{-1} streptomyocin (Sigma-Aldrich, St. Louis, MO) and used at passages 16-20. All cells were incubated at 37° C in a 5% CO_2 environment.

7.3.2. Proteolytically Degradable PEG Pre-Polymer Synthesis

Extracellular matrix (ECM) derived peptide sequences have been shown to be specifically cleaved by matrix metalloproteases (MMP).[158] Conjugation of the collagen ECM mimetic peptide sequence (GGPQGIWGQGK) to non-proteolytically degradable synthetic polymers has been shown to result in complete degradation of the polymer network by specific MMPs and other broad acting proteases.[43] Furthermore, the conjugation of the GGPQGIWGQGK sequence to monoacrylate terminated photocrosslinkable PEG macromers in an ABA block co-polymer system has demonstrated the ability to promote polymer construct remodeling and support microvascular network formation by HUVECs and 10T ½ co-cultures.[43]

The peptide sequence GGPQGIWGQGK was synthesized by standard solid phase FMOC chemistry using an Apex396 peptide synthesizer (Aapptec; Louisville, KY). Following synthesis and purification, the peptide product was verified using matrix-assisted laser desorption ionization time of flight mass

spectrometry (MALDI-ToF; Bruker Daltonics, Billerica, MA). (see Appendix for MALDI –ToF results) A diacrylate terminated ABA block co-polymer of the peptide sequence was synthesized by reacting heterobifunctional acrylate-PEG-N-hydroxysuccinimide (Laysan; acrylate-PEG-NHS, 3400 Da) in a 1:2.2 (peptide:PEG) molar ratio in anhydrous dimethylsulfoxide (DMSO, Sigma-Aldrich, St. Louis, MO) in the presence of 15 mM N,N-Diisopropylethylamine (DIPEA, Sigma-Aldrich, St. Louis, MO) overnight. (Figure 43) This reaction conjugates a PEG monoacrylate to the amine terminus of the peptide sequence and to the lysine's amine side chain at the peptide's carboxy terminus using standard N-hydroxysuccinimide amine chemistry. The resulting product's reaction volume was slowly diluted 2:1 in an ice bath with ultrapure H_20 and dialyzed (5000 MWCO regenerated cellulose, Spectrum Laboratories, Rancho Dominguez, CA) for 48 hrs to remove DIPEA, DMSO, and un-reacted PEG and peptide moieties. The product was then frozen at -80°C, lyophilized for 72 hrs, and stored under argon at -80°C until further use. The cell adhesive ligand Arg-Gly-Asp-Ser, (RGDS, American Peptide Sunnyvale , CA) was conjugated to acrylate-PEG- N-hydroxysuccinimide in a 1:1.1 (PEG:RGDS) molar ratio under the same conditions as the PEG-Peptide-PEG block co-polymer.(Figure 43) (see Appendix for bioconjugate characterization)

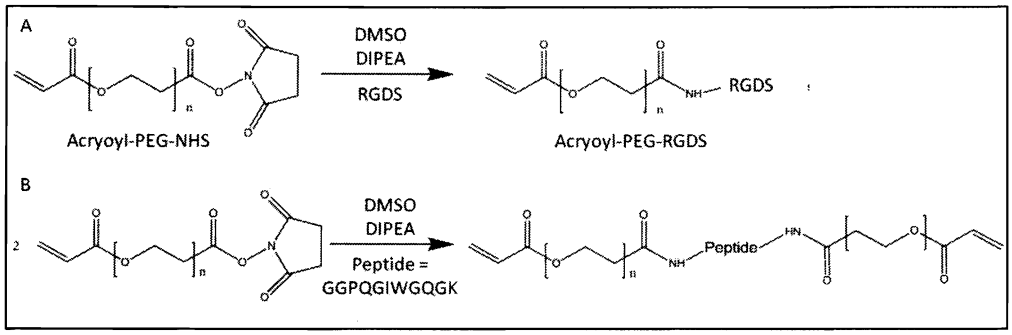

Figure 43: Reaction Schematic of Peptides with Heterobifunctional PEG linkers to form tethered adhesion peptides and a proteolytically degradable PEG derivative. (A) The amino acid sequence RGDS is reacted with acryoyl-PEG-N-hydroxysuccinimide. (B) A collagen derived ECM mimetic peptide sequence (GGPQGIWGQGK) was reacted in a 1:2 molar ratio with acryoyl-PEG-N-hydroxysuccinimide to form a degradable peptide sequence flanked by acrylate terminated PEG chains.

7.3.3. Multilayer Photolithographic Fabrication of Perfused PEG Scaffold

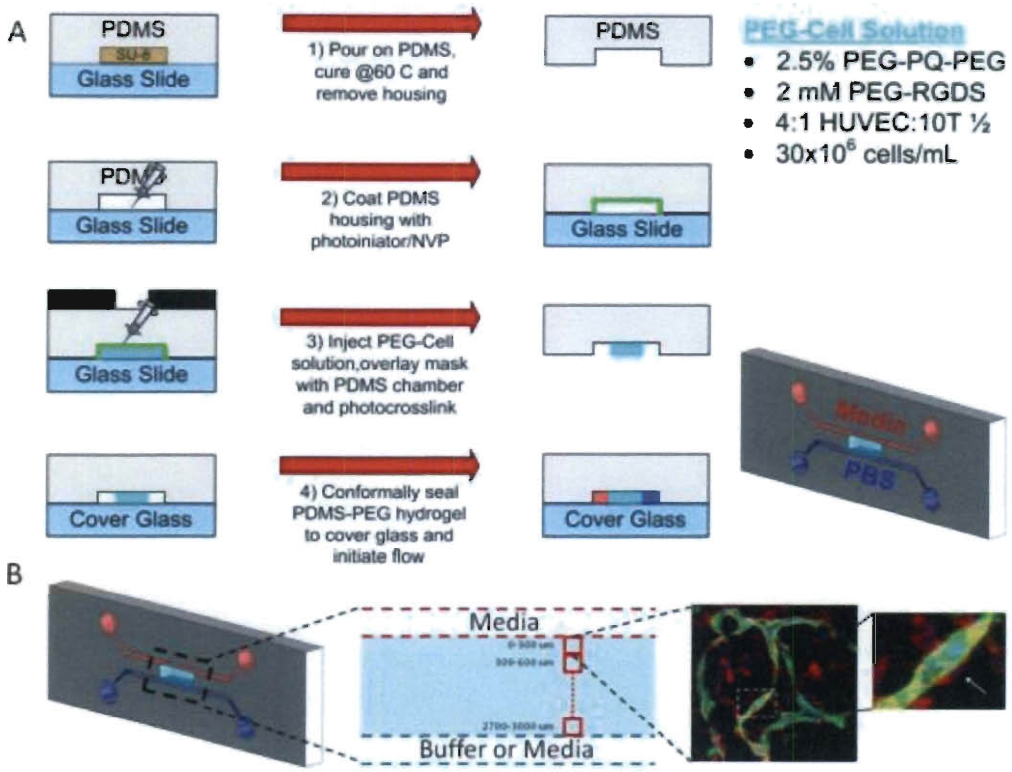

Figure 44: System Design Schematic and Microvascular Network Formation. (A) Device Fabrication and System Design Schematic. (B, Left) Photolithographic fabrication of PEG hydrogel slab in PDMS housing Transparent microfabricated PDMS housing (gray) with vasculogenic PEG hydrogel (cyan) located between two microchannels perfused with endothelial growth media (red) and buffer (blue). (Middle) Schematic showing relationship of PEG hydrogel to perfused media and buffer microchannels and the spatial relationships of tiled imaged regions to the two channels. (Bottom) Representative immunohistochemistry images of the self-assembled microvasculature in the 0-300 μm distance from the media microchannel. HUVECs (green; anti-PECAM) are shown forming connected microvascular networks and 10T ½ cells (red; anti-smooth muscle alpha actin) are shown acting as pericytes wrapping and stabilizing vessel networks (inset; arrow) (blue, DAPI).

Poly(dimethylsiloxane) (PDMS, Sylgard 184) housings were prepared using standard softlithographic techniques as previously described.[148] Briefly, PDMS housings (15:1, silicone elastomer: curing agent) were molded to photoresist masters (SU-8 2100, 350 um in height, Microchem, Newton, MA) to create a robust housing with perfusion access ports and transparent optical qualities for ease of imaging (see Figure 36). All PDMS housings were treated

with the photoinitiator acetophenone (2,2-dimethoxy-2-phenyl acetophenone in n-vinylpyrrolidone, 300 mg mL^{-1}, Sigma) for 5 min to promote free radical induced interfacial polymerization of the acrylate terminated PEG pre-polymer solution to the PDMS housing. Excess photoinitiator was removed via sequential rinsing with 100% ethanol and ultrapure H_2O and dried with filtered air. Acetophenone coated PDMS housings were sealed to glass slides treated with SigmaCote (Sigma-Aldrich, St. Louis, MO) aligned and overlaid with a transparency photomask (20,000 dpi, CAD/ART Services, Bandon, OR) to control spatial photopolymerization and hydrogel geometry within the PDMS housing. (Figure 44)

The MMP degradable PEG block copolymer and PEG-RGDS were dissolved in EGM-2 to final concentrations of 2.5% (w/v) and 2 mM respectively. The photoinitiator Irgracure-2959 (Ciba, 100 mg mL^{-1} in 200 proof ethanol) was added to the pre-polymer solution at 30 µL mL^{-1}. HUVECs and 10T ½ cells were suspended in the pre-polymer solution in a 4:1 ratio (HUVEC:10T ½) to a final concentration of $30x10^6$ cell mL^{-1}. The resulting cell-pre-polymer solution was injected into the PDMS housing through the perfusion access ports and exposed through the photomask to long wavelength UV light (365 nm, 10 mW cm^{2-1}) for 5 min to crosslink and fabricate the PEG hydrogel structures. The PDMS housing with the embedded photocrosslinked PEG hydrogel was gently rinsed with sterile phosphate buffered saline (PBS, pH 7.4), dried with canned air and sealed to #1 cover glass. The cell-hydrogel construct was perfused at 600 µL hr^{-1} with EGM-2 at one interface and sterile PBS on the opposite interface to establish a gradient

of growth factors, nutrients, and waste species across the construct (Media-Buffer configuration). (Figure 44) Some experiments were conducted in a Media–Media configuration where both hydrogel construct channel wall interfaces were perfused with EGM-2 in order to determine the maximum distance microvascular networks would develop form the perfused microchannel.

7.3.4. Immunohistochemistry Staining

Immunofluorescence staining was performed to determine spatiotemporal microvascular network characteristics and the cell-cell relationships within the co-culture. At 0, 48 and 96 hr perfusion was terminated and hydrogel microdevices were fixed, permeabilized and stained with primary and secondary antibodies (Figure 45). The primary antibodies used were mouse anti-SM α-actin (Sigma-Aldrich, St. Louis, MO) to label the 10T ½ cells and goat anti-PECAM (Santa Cruz Biotechnology, Santa Cruz, CA) to label the membranes of HUVECs. The secondary antibodies used were anti-mouse and anti-goat conjugated with either Alexa flour 488, Alexa flour 532, and or Alexa flour 647. DAPI (300 nM,Invitrogen) was used as a nuclei counter stain for all immunofluorescence images.

7.3.5. Spatiotemporal Microvascular Network Morphology Analysis

Spatiotemporal PECAM immunofluorescence images were analyzed at 0, 48 and 96 hr post device fabrication to determine the effects of perfusion time and distance from the EGM-2 perfused microchannel on microvascular network morphology (Figure 46). The PECAM immunofluorescence was imaged using a

confocal microscope (Zeiss LSM 5 Live, 20x/NA 0.8 objective, FOV 318x318 μm, vertical z-stack: 1 μm slices, 50 slices per region, Carl Zeiss Inc., Thornwood, NY). Regions were tiled at 300 μm intervals radially outward from the perfused media microchannel wall to the PBS microchannel wall for a total of 10 regions spanning the 3 mm thickness of the hydrogel construct.

Pre-processing of the LSM images was accomplished by first applying a maximum intensity projection to the z-stack using the image browser function in the LSM Image Examiner software (Carl Zeiss Inc., Thornwood, NY). After maximum intensity projection, channels were split and the PECAM immunofluorescence channel was thresholded to preserve the tubule elements, while decreasing the background signal. The resulting thresholded image was then used to measure the lengths of the tubule elements within the construct. Each tubule was measured manually using the image browser measurement tool, where single tubules were determined as starting at one branch and ending at another. Both the tubule lengths and the total number of tubules were recorded for each representative image at different locations within the constructs.

7.3.6. Spatiotemporal TUNEL Apoptosis Assay

Spatiotemporal apoptotic profiles at 48 and 96 hr of culture were analyzed using the Click-It TUNEL assay for DNA fragmentation (Invitrogen, Carlsbad, CA). Samples were fixed, permeabilized and labeled with the manufacture recommended protocols and counterstained wit DAPI (300 nM,Invitrogen).

Fragmented DNA fluorescence was imaged using a confocal microscope (Zeiss LSM 5 Live, 20x/NA 0.8 objective, FOV 318x318 μm, vertical z-stack: 1 μm slices, 50 slices per region, Carl Zeiss Inc., Thornwood, NY). Image regions were tiled at 300 μm intervals radially outward from the perfused media microchannel wall to the PBS microchannel wall for a total of 10 regions spanning the 3 mm thickness of the hydrogel construct. At each region and time point, the ratio of apoptotic cells (TUNEL positive) to total cells (DAPI positive) was analyzed and plotted to indicate percentage of apoptotic cells. Control samples treated with 70% ethanol were used to set the TUNEL positive imaging parameter values and to avoid false positive TUNEL signal. (Figure 47)

7.3.7. Analysis of Acellular and Vascularized Mass Transport

System mass transport properties were analyzed in acellular PEG hydrogel constructs and the vascularized constructs after 96 h of culture. High molecular weight fluorescent dextran (dextran- FITC, lysine fixable, 2 $x10^6$ Da; Invitrogen, Carlsbad, CA) was added to the perfusion media and flow was set at 600 μL hr^{-1}. Images of the region immediately adjacent to the microchannel wall were collected for 120 min via time lapse live-cell fluorescent confocal microscopy (Figure 48 A,B & C) (Zeiss LSM 5 Live, 20x/NA 0.8 objective, FOV 318x318 μm, vertical z-stack: 10 μm slices, 6 slices per region, Carl Zeiss Inc., Thornwood, NY). In some vascularized constructs, post time lapse imaging, the dextran was fixed using 4% paraformaldehyde and vessel structures were stained using anti-PECAM and DAPI to determine the spatial localization of dextran relative to vessel structures. (Figure 48D)

The rate of dextran transport in the acellular and vascularized systems was assessed by measuring the total fluorescence signal in regions 10, 50 and 80 μm from the channel wall over time using the Image Processing Toolbox in MatLab. (Figure 49) The difference in vascularized and acellular dextran accumulation (% Convective Transport) was determined by taking the difference of vascularized and acellular values at a time point and plotting as a percentage of the vascularized value.(see Equation 8) Differences in the dextran fluorescent intensity landscape of the acellular and vascularized images were assessed using the Plot Profile function in Image J. Raw intensity value were normalized to maximum intensity in order spatially overlay the data. To evaluate extra vessel diffusion, changes in vascularized intensity peak widths and peak aspect ratios (aspect ratio = peak height/peak width) were measured over time at a constant intensity value.

$$\%\ Convective\ Transport = \frac{Vascularized\ Intensity_t - Acellular\ \ Intensity_t}{Vascularized\ Intensity_t} \times 100$$

Equation 8: Equation for Calculation of % Convection Transport Trace

7.4. Results and Discussion

7.4.1. Multilayer PDMS/PEG Micro Device Characteristics and Advantages

PEG hydrogel incorporation within a robust PDMS housing addresses a number of the logistical challenges associated with handling microfluidic hydrogels and negates the need for complicated supporting apparatuses.[130] In addition, PDMS fluid access ports allow for transient and precise control over vascular bed concentration and pressure gradients while maintaining the

hydrogel in a sterile and non-dehydrating environment. Furthermore, this multilayer approach results in independent control over PDMS housing and PEG hydrogel geometry allowing for freeform user defined fabrication of tissue-mimetic PEG hydrogel structures within the PDMS housing. (Figure 44) A particularly advantageous characteristic of this microfabricated system is the ability to localize perfusion interfaces in close spatial proximity to self-assembled vessel networks within the hydrogel bulk. This allows for study of interfacial mass transport from fabricated channels 1 mm in diameter to microvascular networks 30 μm in diameter and enables integrated transport across large length scales (Figure 45).

7.4.2. Spatiotemporal control of co-culture self-assembly

Our group and others have previously shown that media perfused microfluidic channels within tissue engineered constructs can improve system mass transport properties and increase overall cell viability. Despite this technological advancement, cell viability and metabolic density decrease as a function of distance from the media perfused microchannel.[14, 15] Network design with reduced distances between microchannels has been shown to counteract necrosis and increase overall construct viability.[130] However, current hydrogel microfabrication technologies limit microchannel network complexity to 2D planar designs.[131] Formation and perfusion of 3D self-assembled microvascular networks between fabricated microchannels shifts the characteristic diffusion length from fabricated channel spacing to the much shorter distance between vessels controlled by microvascular network density. Therefore it is important to

determine the microfabricated channel spacing that supports microvascular network self-assembly and therefore minimizes overall system diffusion lengths.

Here we set out to determine the maximum distance, from a perfused media channel, that supports microvascular network self-assembly in the pro-vasculogenic PEG hydrogel. For this study, perfused microchannel systems were either configured in a Media-Buffer configuration analogous to capillary-lymphatic mass exchange or a Media-Media configuration analogous to inter-capillary exchange (Figure 44) Spatiotemporal microvascular network self-assembly was evaluated by anti-PECAM immunohistochemistry labeling of HUVEC membranes followed by morphological analysis of total tubule length and number (see Materials & Methods Immunohistochemistry Staining)

Microvascular network formation in the Media-Buffer configuration was highly dependent upon culture time and distance from the perfused media microchannel. A trend of decreasing total tubule length and total tubule number with increasing distance from the media microchannel was observed at both 48 and 96 h of culture. (Figure 45 & Figure 46) Both total tubule length and total tubule number at 96 h were significantly greater in the nutrient rich regions (< 600 μm from the media microchannel) when compared to all regions greater than 600 μm. ($p<0.05$, n=3,Figure 46) However, this trend was not present at early time points in microvascular network formation where cellular coalescence and self-assembly was relatively homogenous and did not vary significantly with distance from the media microchannel (Figure 45 & Figure 46; t= 48 h). Moreover, only microvascular networks within the region closest to the media microchannel (0-

300 μm from microchannel) experienced significant increases in total tubule number and length from 48 to 96 h ($p<0.05$, n=3, Figure 45 & Figure 46) while microvascular networks within the constructs interior regions (900-2100 μm from microchannel) experienced a significant decrease in total tubule number and length over the same time period ($p<0.05$, n=3, Figure 45 & Figure 46).

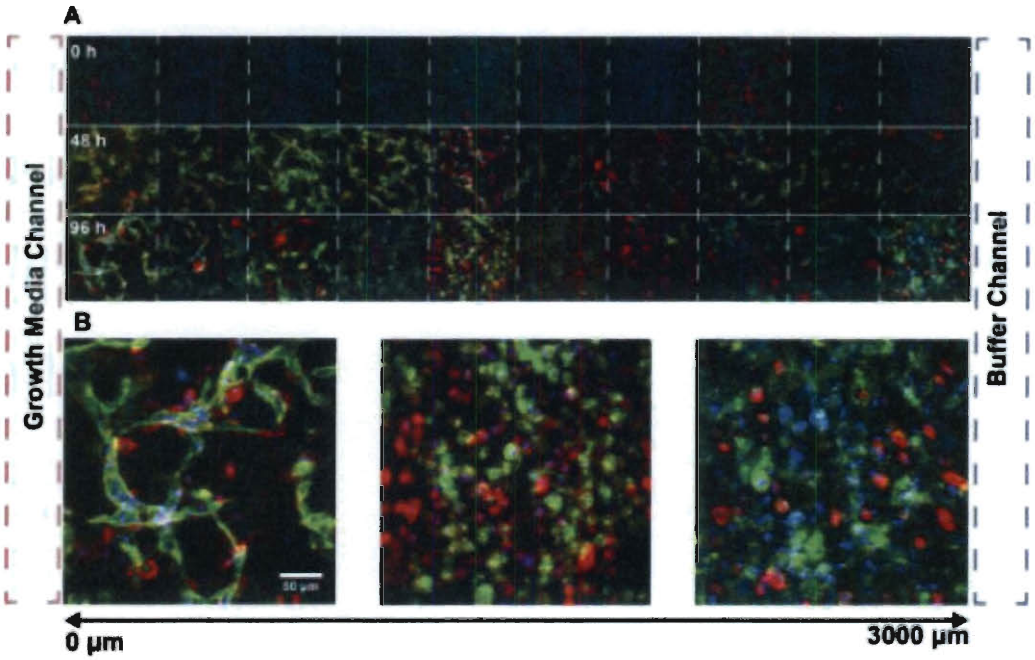

Figure 45: Spatiotemporal Microvascular Morphology. (A) Immunohistochemistry fluorescent micrographs of HUVECs (green; anti-PECAM) 10T ½ (red; anti-smooth muscle alpha actin) and DAPI (blue) as a function of culture time (0, 48, & 96 h) and distance (300 μm regions; 0-3000 μm) from the perfused media microchannel. Tubules start as homogenously seeded 3D co-culture suspensions at time 0 h and self organize to form tubules over 96 h. Interestingly at 48 h of culture initial tubule coalescence persist into the interior regions of the scaffold but by 96 h only the nutrient rich regions (0-600μm) support tubule formation. (B) Enlarged images of the 0-300 (left) 1200-1500 (center) and 2700-3000 μm (right) regions at 96 h.

The Media-Media configuration encouraged microvascular network formation at greater distances from the microchannel than the Media-Buffer configuration displaying high levels of self-assembly throughout the entire thickness of the construct at 96 h of culture (Figure 46; hashed bars). Perhaps

the most interesting characteristic of the Media-Media configuration is its ability to support robust microvascular network growth from 48-96 h. In the Media-Media configuration all regions experienced increases in tubule length and number from 48-96 h whereas in the Media-Buffer system this increase was only observed within the nutrient rich regions less than 300 μm from the perfused microchannel.

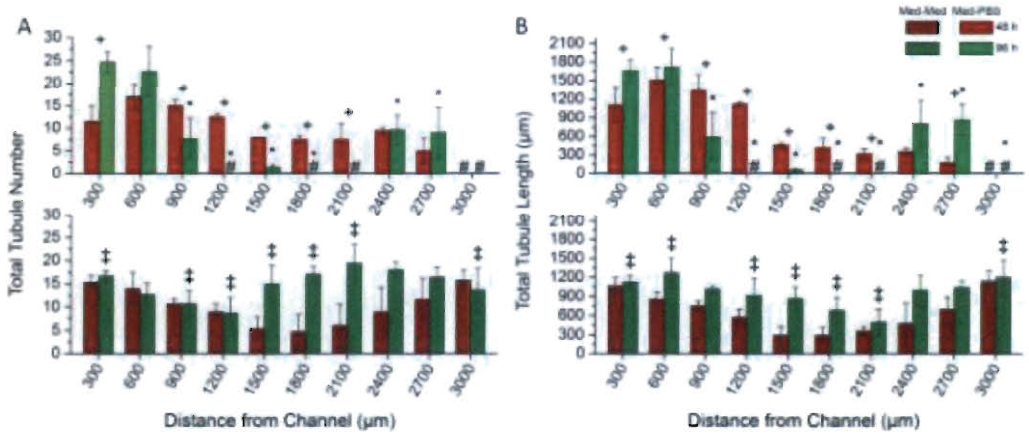

Figure 46: Spatiotemporal Self-Assembled Microvascular Network Morphology. Total tubule number (A) and total tubule length (B) in a Media-Buffer configuration (solid bars) and a Media-Media configuration (hashed bars) as a function of distance from the microchannel (0-3000 μm) and perfusion time 48 (red) and 96 h (green). Robust microvascular network formation (total tubule length and number) in the Media-Buffer system was confined to regions closest to the media microchannel (0-600 μm) with the interior regions (1200-2100 μm) not forming networks at 96 h. Interestingly the Media-Media configuration maintained microvascular network formation farther from the microchannel but with an overall lower number of total tubules and a decrease in total tubule length at each time and location when compared to the Media-Buffer configuration. ($p<0.05$, n=3, paired t-test, (+) indicates 48 h vs. 96 h temporal significance, (*)indicates spatial significance compared to the 0- 300 μm region, and ‡ indicates significance between Media-Media and Media-Buffer at 96 h.

7.4.3. Spatiotemporal Construct Apoptotic Activity

The lack of robust microvascular network self-assembly in regions farthest from the perfused media microchannel in the Media-Buffer configuration was thought to be due to necrosis driven by nutrient deprivation. To confirm that necrotic activity was the underlying mechanism for inhibited microvascular

network formation, a spatiotemporal TUNEL assay to quantify fragmented DNA and characterize late stage apoptotic activity was applied to the Media-Buffer system at 48 and 96 h of culture. The spatiotemporal apoptotic activity of the construct, as indicated by the fraction of TUNEL positive cells, was shown to be inversely related to microvascular network self-assembly. At 96 h of culture, the region nearest the media microchannel (Figure 48 A & B; 0-300 μm) had significantly lower fraction of TUNEL positive cells than nearly all other regions ($p<0.05$, n=3, Figure 48A). Furthermore the TUNEL positive fraction was shown to increase from 48 to 96 h in the same regions that total tubule length and number were shown to decrease. Interestingly the nutrient rich region (0-300 μm from channel) that experienced increases in total tubule number and length from 48 to 96 h also exhibited low but significant increases in apoptotic activity over the same time period ($p <0.05$, n=3, Figure 48A; 0-300 μm). This is thought to be due to cellular pruning that is characteristic of maturing microvascular networks.[66] These observations taken together are suggestive of initially high and homogenous self-assembly into a nascent capillary plexus from 0-48 h, followed by network maturation in the nutrient rich regions and network regression in necrotic regions from 48-96 h. Spatiotemporal control over microvascular network formation provides a valuable design parameter to optimize microvascular network self-assembly and by extension, minimize construct characteristic diffusion lengths.

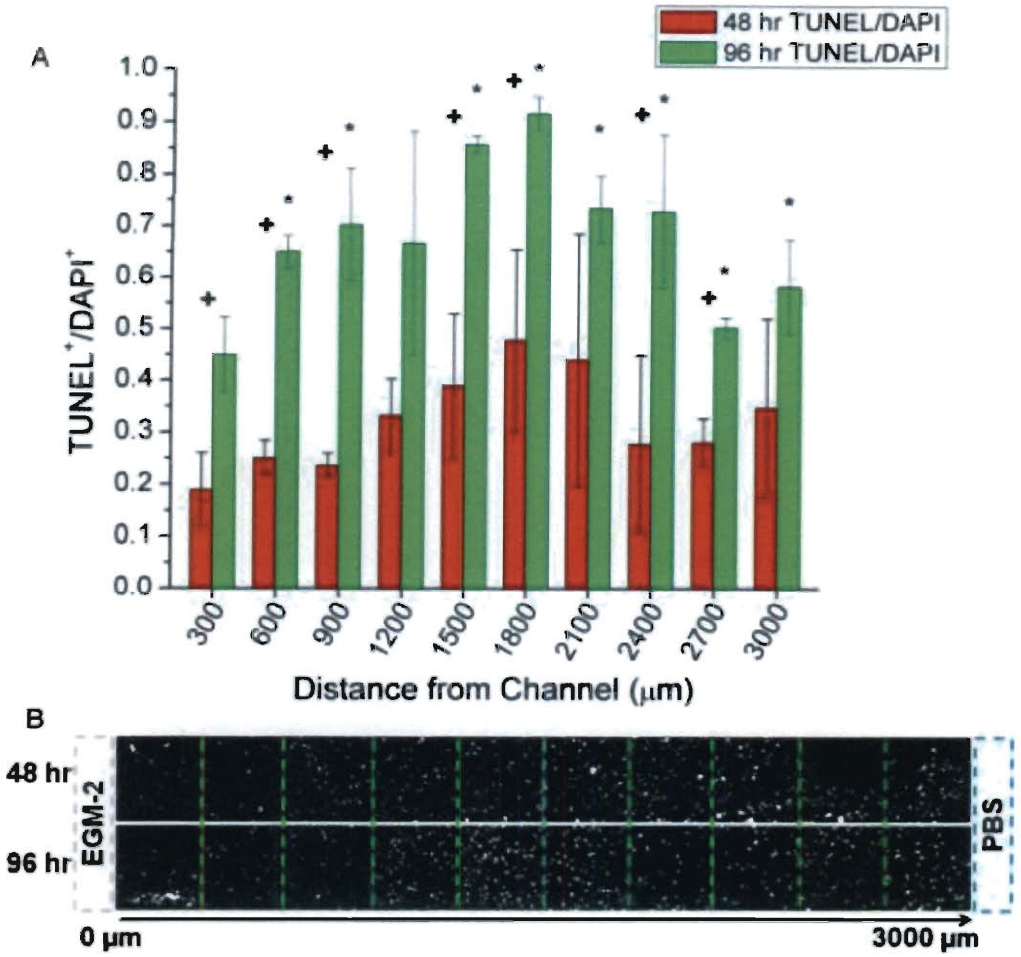

Figure 47: Spatiotemporal Scaffold Apoptotic Activity. (A) Spatiotemporal fraction of TUNEL positive cells normalized to DAPI. (B) Spatiotemporal fluorescent micrographs of TUNEL positive cells. Spatiotemporal construct apoptotic signal normalized to in the Media-buffer configuration. TUNEL signal increased with increasing distance from the media microchannel with interior regions (1500-1800 μm) showing the highest level of apoptotic activity at 96 h. (n=3, paired t-test, $p<0.05$, + indicates 48 vs. 96 h temporal significance at a given distance * indicates 96 h spatial significance compared to 0-300 μm)

7.4.4. Functional Convective Vessel Transport and Shifting Transport Regimes

Non-vascularized hydrogel mass transport regimes are limited to passive diffusion governed by the system concentration gradients and the effective diffusivity relationship of the solute and hydrogel matrix.[21] Diffusional distances in

these constructs are defined by the overall size of the construct or in the case of microfluidic hydrogel systems, the distance between channels. Transport within vascularized constructs is characterized by rapid, lumen-supported convection through the microvascular network followed by diffusion out of the vessel structures.[159] In addition, the characteristic diffusion length in vascularized systems is not the overall construct geometry, but the distance between vessels. Therefore transport in vascularized systems is much more efficient than a purely diffusional system because convection is used to transport mass across large distances while diffusion is only required to drive transport the short distance between vessels. Recapitulation of this transport regime within an *in vitro* construct is advantageous for the development of more robust tissue culture systems that can produce bulkier, more clinically relevant tissue-engineered therapeutics.

Here we set out to compare the mass transport characteristics of a non-vascularized, acellular hydrogel with a vascularized hydrogel containing the self-assembled microvascular networks. Pro-vasculogenic PEG hydrogels containing the high-density co-culture of HUVEC and 10T ½ cells were cultured in the Media-Media configuration for 96 h to drive microvascular network self-assembly. After 96 h of culture, growth medium was supplemented with high molecular weight fluorescent dextran (2 $x10^6$ Da) and time-lapse confocal microscopy was used to image dextran transport through the construct for 180 minutes at regular intervals. In a separate study, non-vascularized microfabricated constructs containing the same pro-vasculogenic PEG hydrogel but without cells were

perfused with dextran and imaged using time-lapse confocal microscopy. The diffusion rate and the spatiotemporal intensity landscape were analyzed and compared between the non-vascularized and vascularized system.

Non-vascularized hydrogels exhibited a uniformly advancing dextran intensity front characteristic of 1D Non-Steady State Fickian diffusion of a solute through a hydrogel matrix[129,148,160] (Figure 49A & Figure 50 and Figure 51A). Vascularized hydrogels displayed rapid, convective-like dextran transport in regions spatially coinciding with vessel structures (Figure 49B & C,Figure 50, Figure 51A). At each time point, fluorescent dextran can be seen at greater distances from the perfused channel in the vascularized construct when compared to the non-vascularized construct. (Figure 49 and Figure 50) Moreover, at a fixed distance from the channel, the rate of dextran accumulation in the vascularized system was significantly higher than the acellular system for the first 30 minutes of perfusion. ($p < 0.05$, $n=9$, Figure 50) Interestingly, this difference in vascularized and non-vascularized transport (Figure 50, % Convective Transport, blue trace) is greatest at early time points when convection is dominant and decreases over time as system transport becomes diffusion limited. These observations suggest that the vascularized system supports enhanced transport characterized by combination of convection and diffusion.

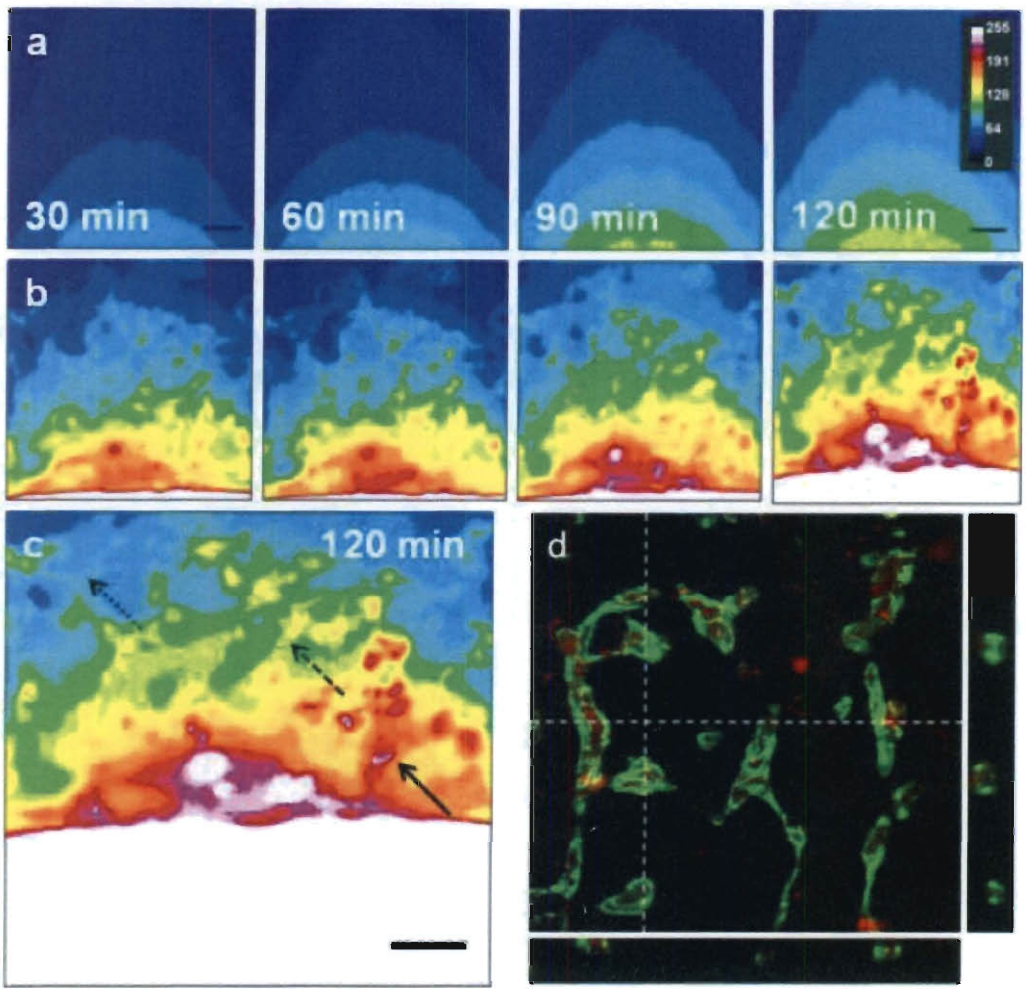

Figure 48: Mass Transport Regimes in Acellular and Vascularized PEG Scaffolds. (A) Time-lapse intensity maps of regions directly adjacent to the microchannel wall of high molecular weight dextran diffusion through acellular PEG scaffolds. Acellular transport profiles behave according to Fickian diffusion through a polymer matrix. (B) Time-lapse intensity maps of regions directly adjacent to the microchannel wall of high molecular weight dextran transport in vascularized scaffolds at 96 h of culture. Rapid convective like transport through the matrix in regions coinciding with vessel structures suggests a shift in transport from purely diffusional transport to convection through vessel structures. (C) Enlarged high molecular weight dextran intensity map at 120 h post perfusion. Dotted arrows indicating newly perfused vessels, dashed and solid arrows indicate progressively broadened intensity profiles suggesting diffusion out of vessels. (D) Orthogonal projection of fixed high molecular weight dextran (red) and anti-PECAM IHC (green) in vascularized scaffolds at 96 h of culture. Co-localization of dextran with PECAM suggests transport via vessel structures.

The dextran fluorescent intensity landscape or spatial dextran distribution in the vascularized system displayed rapid intensity increases occurring ahead of

the diffusion front which is indicative of convective, vessel-supported transport. (Figure 49c arrows and Figure 50A) This suggests a shift in transport regimes from entropically driven Fickian diffusion to rapid lumen supported convection through the vessel networks. To further validate that microvascular lumens supported convective transport, dextran perfused vascularized constructs were fixed and stained with anti-PECAM to determine the spatial proximity of perfused dextran relative to vessel lumens. Confocal imaging of the fixed dextran-perfused microvascular hydrogels show the dextran predominantly co-localized within the lumen of the microvascular structures. (Figure 48D)

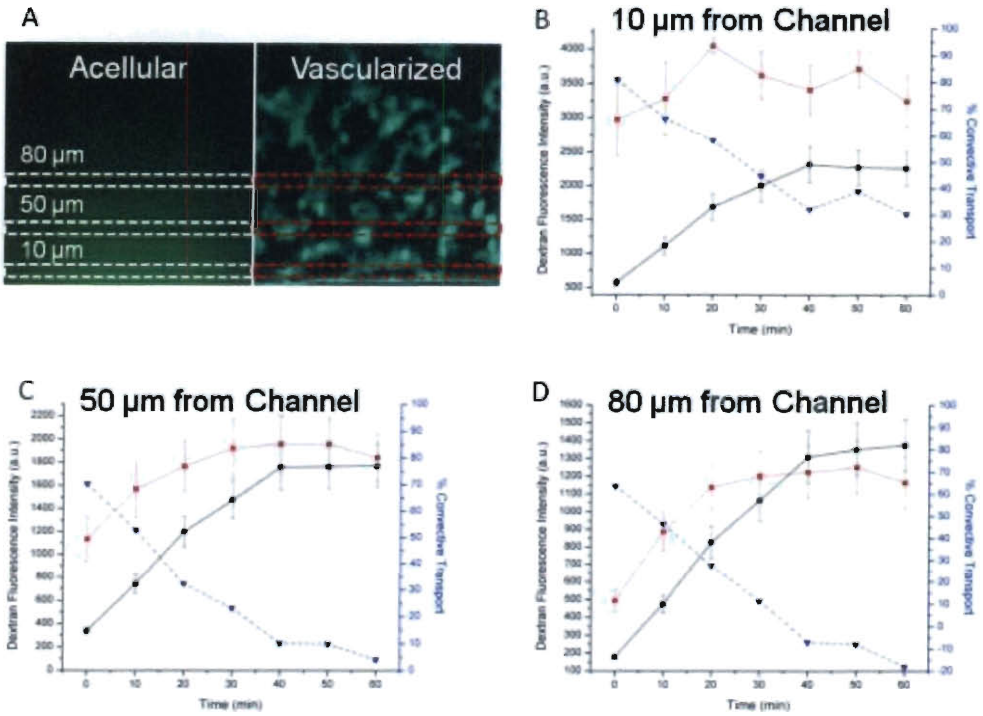

Figure 49: Dextran Spatial Fluorescence Intensity Profiles (A) Dextran fluorescence intensity micrographs in an acellular and vascularized hydrogel. Total dextran fluorescence accumulation in acellular (black trace) and vascularized hydrogels (red trace) at (B) 10, (C) 50 and (D) 80 µm from the microchannel corresponding to the regions analyzed panel A. The rate of accumulation is greater in the vascularized system (red trace) when compared to the acellular system (black trace) for all distances at early time points. The difference in vascularized and acellular transport or the % convective transport shown as a percentage of total intensity (blue dash trace). The contribution of convective transport is greatest at early time points.

In addition to supporting convective transport, vascularized constructs display a greatly reduced characteristic diffusion length (λ_V=67 µm) when compared to the acellular system (λ_D=3 mm). Diffusion lengths in the vascularized system are defined by vessel density or spacing and not overall construct geometry (Figure 51A). This is an important shift to a biomimetic transport regime where characteristic diffusion lengths are less than critical necrotic distances. Perhaps more significant, time lapse dextran intensity profiles show broadening of profile intensities and a decrease in peak intensity aspect

ratio over time. Together these observations suggest vascularized constructs support initial convective-like transport and extra vessel diffusion into the interstitial space. This represents an important step towards recapitulating an important functional mass transport property of the microvasculature.

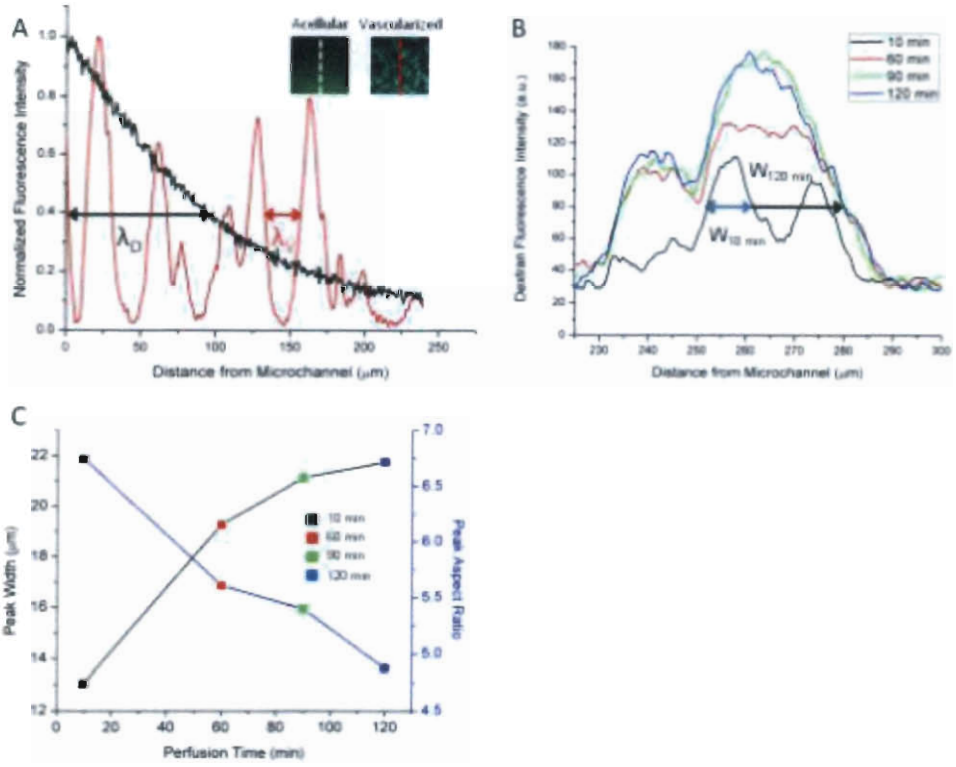

Figure 50: High Molecular Weight Dextran Intensity Profiles and Extravessel Diffusion. (A) High molecular weight dextan diffusion profiles in an acellular (black trace) and vascularized (red trace) hydrogels. Acellular hydrogels rely on diffusional transport with construct characteristic diffusion lengths (λ_D) limited to large distances between perfused microchannels. Vascularized hydrogels exhibit convective transport that rapidly penetrates hundreds of micrometers into the hydrogel with characteristic diffusion lengths (λ_V) limited to the small distance between vessels. (B) Time-lapse (0-120 min) high molecular weight dextran intensity profiles in a vascularized construct show diffusion out of vessel structures as indicated by (C) increases in peak width and a decrease in peak aspect ratio over time.

7.5. Conclusions

In conclusion, we report the integration of robust microfabrication technologies with a pro-vasculogenic hydrogel and co-culture that enables the perfusion of self-assembled microvascular networks within a multilayer microfluidic device. Spatiotemporal characterization of microvascular network self-assembly allowed for the determination of optimal microchannel spacing that promotes maximum microvascular network formation and minimizes necrotic activity. Perhaps the most significant finding for tissue engineering is the shift in dextran mass transport regimes from pure diffusion through a hydrogel matrix to microvasculature network supported convection and extra vessel diffusion. Combination of externally fabricated synthetic structures with self-assembled microvascular networks enables this shift and provides a valuable tool towards the recapitulation of vascular hierarchies across multiple length scales. This system has applicability towards the development of improved preclinical tissue models and more clinically relevant, pre-vascularized tissue engineered therapeutics.

8. Chapter 8: Softlithographically and Photolithographically Fabricated PEG Hydrogels

8.1. Introduction

Research activities in Chapter 7 & 8 developed technologies to build microfluidic networks within PEG hydrogels and demonstrated integration of these fabricated technologies with self-assembling microvascular networks. However, this research failed to address the incorporation of parenchymal elements within microvascular networks. (See Current Limitations in MVTE #3) Furthermore, previous work has failed to develop tool sets capable of fabricating multilayer tissue microstructures with heterogeneous cellular and matrix components. Therefore our recent efforts have focused on developing techniques to photolithographically pattern biomimetic tissue microstructures with heterogeneous cellular components.

8.1.1. Multimodal fabrication strategies

In order to fabricate multilayer heterocellular structures within PDMS perfusion housings, precise photolithographic alignment procedures must be developed. Precise multilayer alignment (tolerances < 1mm) often requires the use of imaging apparatuses coupled with micromanipulators.[161,162] A multilayer alignment system applicable to hydrogel photolithography was reported by Love *et al.*[163] as a technique to achieve sub-mask limited photoresist exposures and an as a means to fabricate precise multilayer photoresist structures. The technique known as Mask Projection Photolithography (MPP) uses a standard

epifluorescent microscope with a micromanipulator stage modified to incorporate a photomask in an optical conjugate plane to the sample. (Figure 52)

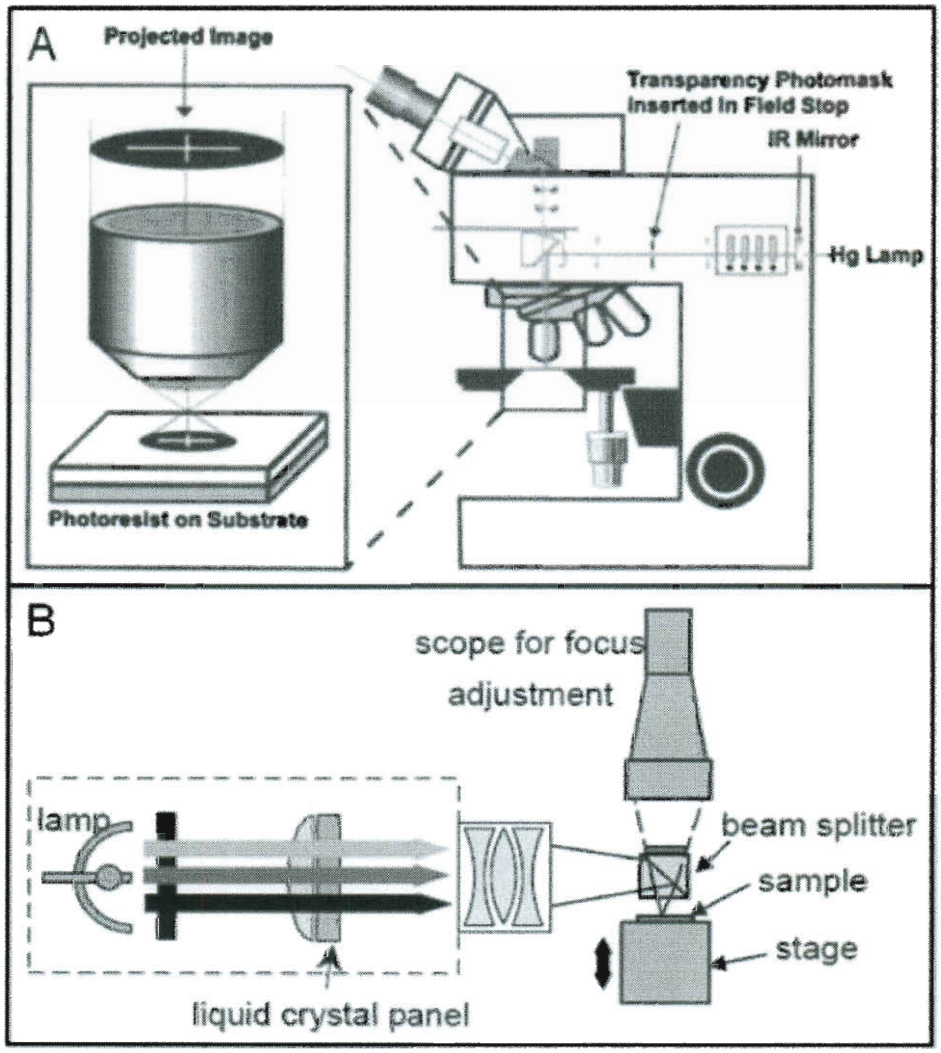

Figure 51: Schematic of Microscope Modified for Mask Projection Photolithography and an LCD Based Exposure System. (A) Schematic demonstrating insertion of the photomask, in a conjugate plane to the sample stage, at the Field Stop. (B) Schematic showing the use of a programmable LCD as a virtual mask photocrosslinking. Recreated from Love *et al*[163]. and Itoga *et al*[164].

This system is attractive for multilayer hydrogel photolithography due to its ability to align the photomask and reference structures under one wavelength of

light that does not initiate photocrosslinking followed by switching the light source and or filter set to expose the PEG hydrogel to a wavelength that drives photocrosslinking. This technique allows for precise, rapid, large and small structure fabrication and due to the prevalence of epifluorescent imaging systems this technique is highly amenable to the life science community.

8.1.2. Application of Multimodal Hydrogel Fabrication to Bioartificial Livers (BALs)

One of many potential tissues to mimic using multimodal heterocellular microfabrication strategies is the liver. Liver failure claims 70,000 lives annually in the U.S. and the clinical gold standard for treatment, orthotropic allograft transplantations, only addresses 10% of these patients.[165] These clinical shortcomings have driven the need for tissue engineered bioartificial livers (BALs). Further complicating BAL design for both extracorporeal and implantation applications, is a myriad of complex challenges requiring tissue engineers to integrate technologies across multiple disciplines. One particular challenging aspect is the efficient transfer of nutrients and waste from the metabolically dense hepatic tissue structure. Moreover, the liver is highly heterocellular and has a very distinct structure-function relationship[115] making it a tissue that requires complex fabrication schemes to recapitulate structure *in vitro*. (Figure 53) Together these factors have motivated great interest to apply and develop multimodal heterocellular hydrogel fabrication technologies to BAL design.

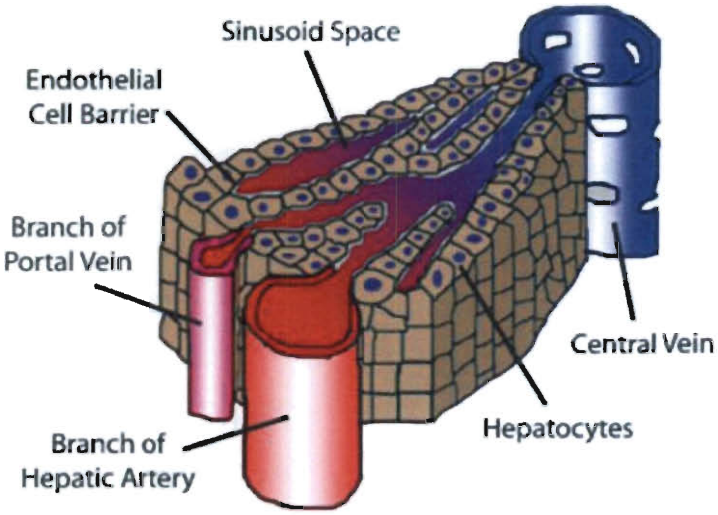

Figure 52: Schematic Diagram of Liver Functional Unit. The hepatic artery and portal vein deliver blood to the hepatocyte rich liver sinusoid. Hepatocytes, which make up 70-80% of the cytoplasmic mass, secret and store proteins, and modify or detoxify both exogenous and endogenous substances for excretion in the central vein. Recreated from Lee *et al.*[166]

Early implantable constructs employed to restore liver function focused on microparticles as cell carriers[167] or encapsulation of hepatocytes in 3D polymer scaffolds[168,169]. Unfortunately, large decreases in cell viability due to inadequate mass transport resulted in poor long-term functionality.[170] One approach to address inadequate mass transport in BALs is the fabrication of microfluidic conduits to perfuse BALs.[87] Several designs have been studied using standard softlithographic techniques to fabricate parenchymal and perfusion chambers separated by filtering membranes.[105,166] (Figure 54) One highly biomimetic multilayer approach employed a branched microvascular network compartment overlaid with a hepatocytes parenchymal compartment.[171] (Figure 54 A & B) Although this construct was highly biomimetic in structure, the material used to fabricate the device (PDMS) is not suitable for long-term implantation or tissue

integration and therefore these devices and similar technologies are limited extracorporeal applications.

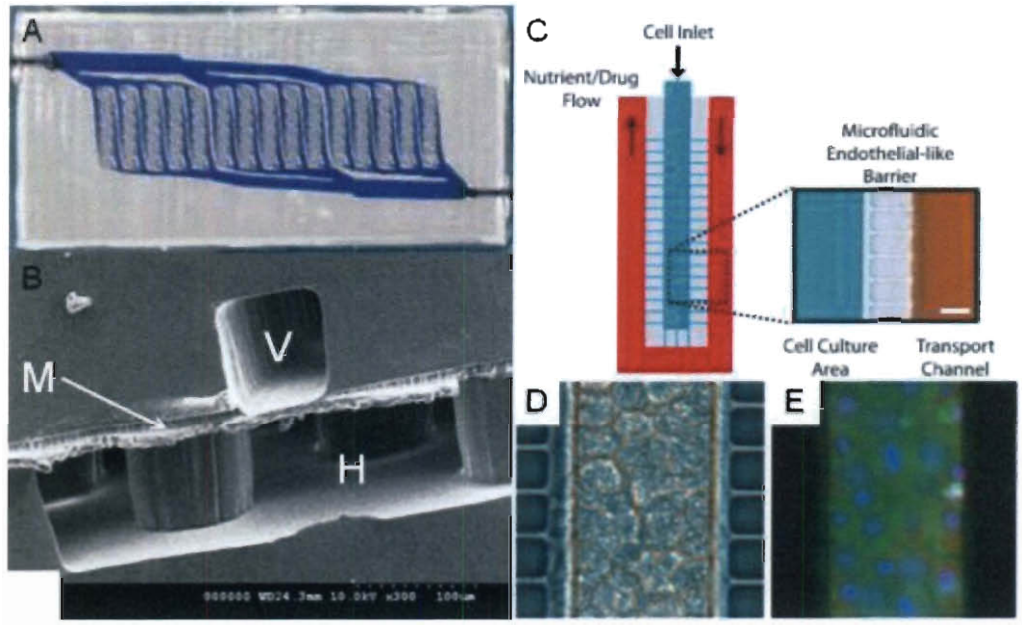

Figure 53: Microfabricated, Perfusable, Multi-compartment BAL Devices. (A) Macro view of perfused biomimetic microvascular networks in PDMS. (B) Cross section of PDMS chambers where the fabricated microvascular network channel, V, is separated from the hepatic compartment, H, by a nanoporous membrane, M. (C) Schematic showing design of a PDMS BAL with a cell chamber (blue) and a perfusion vasculature like chamber (red) separated by an endothelial like barrier (gray). (D) Light microscopy image of cell chamber and endothelial cell barrier. (E) Calcien AM stain (green) with Hoechst nuclei counter stain (blue) indicating high cell viability at 7 days. Recreated from Carraro *et al.*[171] and Lee *et al.*[166].

A more biocompatible BAL analog fabricated from materials suitable for implantation and tissue integration was reported by Tsang *et al.*[34] in 2007. This device utilized multilayer photolithographic fabrication of poly(ethylene glycol) diacrylate (PEGDA) hydrogels encapsulated with high density cultures of primary hepatocytes. (Figure 55) Although this construct demonstrated functional urea secretion and high initial cell viability, it did not integrate any perfusion conduits to address transport limitations nor did it incorporate heterocultures consisting of

supporting cellular components known to improve liver function and drive hepatic tissue formation. Furthermore, PEGDA hydrogels are not degradable by cellular proteases or by hydrolysis at physiologic pH. Therefore implantation of this construct would not likely result in adequate host-implant integration.

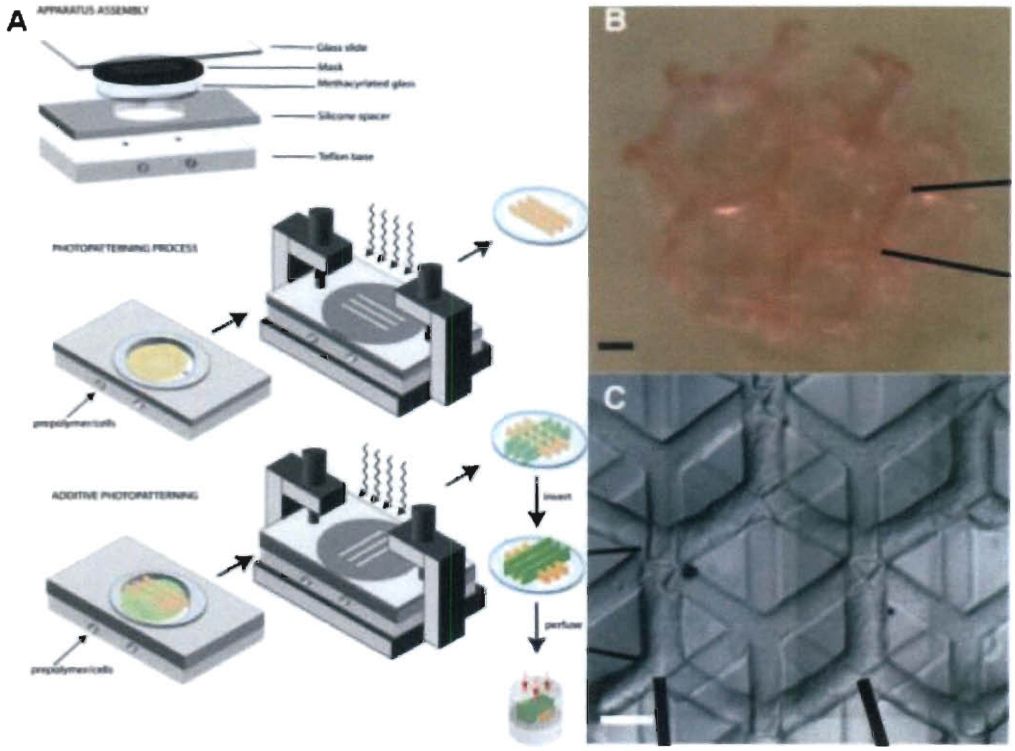

Figure 54: Multilayer Additive Photolithographic Fabrication of PEGDA Hydrogels with Encapsulated Hepatocytes. (A) Schematic showing mask alignment, injection ports and hydrogel structure fabrication in an additive fashion. (B) Light micrograph and (C) phase contrast micrograph of 3D hepatic tissue analog. Recreated from Tsang *et al.*[34]

The previous designs address the livers complex structure by developing novel microfabricated devices; however they neglect the liver's heterocellular nature and the effect of cell-cell signaling on hepatocytes phenotype and function. Hepatocytes morphology and function has been shown to be modulated by epithelial[172] and fibroblast[173] co-cultures. Early studies of these co-culture

effects focused on 2D substrates to assay the role of cell contacts[174] and trans-well assays to isolate the effects of soluble signals[175]. More recently microfabrication techniques, such as microcontact printing[176] and photolithographic patterning[177], have been used to specifically probe the nature of the co-culture interaction. (Figure 56)

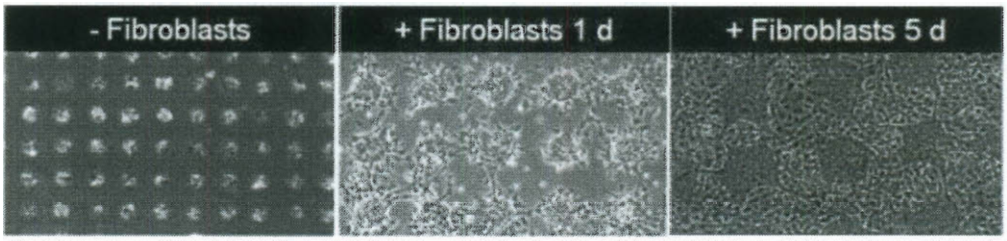

Figure 55:Hepatocyte Fibroblast Microfabricated Co-Culture. (left) Hepatocyte cell islands without fibroblasts (middle) with fibroblasts seeded as a backfill layer at day 1 and (right) co-culture at day 5 self organizes with interisland contacts. Recreated from Revzin *et al.*[177]

However, the effect of a pro-tubulogenic co-culture (HUVECs +10T ½ see Chapter 5) on hepatocyte function is less understood. A very interesting synergy when combining this co-culture with hepatocytes is due to the pluripotency of the 10T ½ mesodermal derived stem cell. It has been shown that in addition to acting as a vessel stabilizing pericyte[75], co-culture of 10T ½ with hepatocytes was shown to improve hepatocyte function within *in vitro* cultures.[178,179] Therefore this tri-culture system becomes a very interesting platform to improve hepatocyte function, and drive microvascular network formation that improves transport and likely in syncytium with others cell types may drive the self organization of hepatic tissue.

8.2. Objectives

- Combine softlithographic PDMS housing and PEG microfluidic channel fabrication methods with the ability to photolithographically pattern hydrogel structures in the PDMS housing
- Develop techniques to precisely align multiple photolithographically fabricated PEG structures within the PDMS perfusion housing
- Develop liver biomimetic heterocellular tri-culture techniques to both drive microvascular network formation from HUVECs and 10T ½ while maintaining hepatocytes viability and function

8.3. Materials and Methods

8.3.1. Cell Maintenance

Human hepatocellular liver carcinoma cell (HEP G2; ATCC) were cultured in Eagles Minimum Essential Medium (MEM) supplemented with 10% fetal bovine serum (FBS), 1000 U mL^{-1} penicillin, and 100 mg L^{-1} streptomyocin (PS) (Sigma-Aldrich, St. Louis, MO). 3T3 fibroblasts (ATCC) were cultured as previously described (see Section 6.3.1-3T3 Cell Maintenance) and used from passages 3-10. Human Umbilical Vein Endothelial cells (HUVEC; Lonza) were cultured as previously described (see Section **Error! Reference source not found.**-UVEC Cell Maintenance) and seeded between passages 2-6. Human mesodermal stem cells (10T ½ cells; ATCC) were cultured as previously described (see Section **Error! Reference source not found.**-10T ½ Cell Maintenance) nd seeded between passages 15-20.

8.3.2. Modification of Microscope for Mask Projection Photolithographic (MPP) Methods

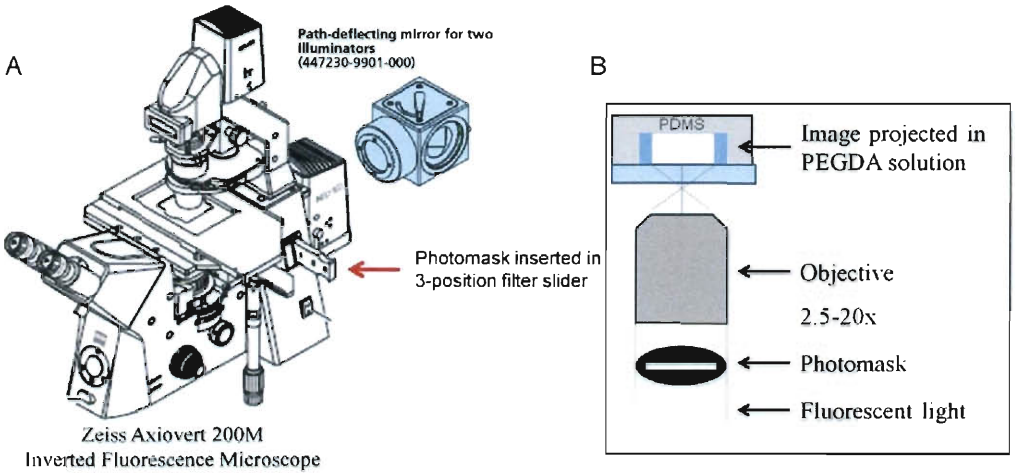

Figure 56: MPP System Schematic. (A) Modification of a Zeiss Axiovert 200M microscope with a transparency photomask inserted in a conjugate plain to the sample at the field-stop. Also a path-deflecting mirror for two illuminators is necessary for alignment under a non-crosslinking low intensity halogen light source and a high intensity mercury arc lamp that drives PEG hydrogel photocrosslinking and structure fabrication. (B) Schematic demonstrating projection of the transparency photomask image to the PEGDA pre-polymer solution in the PDMS housing at the sample stage.

A Zeiss Axiovert 200M inverted fluorescence microscope was modified with a path-deflecting mirror to toggle the aligning light source (halogen white light illuminator) and the photocrosslinking light source (broad band mercury arc lamp) for control over structure fabrication.(Figure 57) Microscope modification with a transparency photomask utilized a standard 15 mm 3-position filter slide to fix the mask at the field-stop location.

All light sources were allowed to warm up for at least 5 minute prior usage. The halogen light source for structure-mask alignment was set to the lowest intensity value. The mercury arc lamp was set to 50% lamp power. Band pass filter sets were designed for either peak intensity in the UV range (390 nm ± 10 nm) for use with the UV photoinitiator Irgacure 2959 or peak intensity in the white

light range (530 nm ± 10 nm) for eosin Y based photoinitiator systems. Transparency photomasks were fabricated as previously described in Section 6.3.5.1 Fabrication of SU-8 Photoresist Masters.mPDMS housing and SU-8 Photoresist Master Preparation for Multimodal Microfluidic Hydrogel Device Fabrication.

SU-8 2100 photoresist masters for the PDMS housing and SU-8 2050 photoresist masters for PEG microchannel fabrication were prepared as previously described in Section 6.3.5.1 - Fabrication of SU-8 Photoresist Masters. PDMS housings were prepared as previously described in Section 6.3.5.2 - PDMS Housing Fabrication. Briefly PDMS (15:1;silicone elastomer: curing agent) was replica molded and cured to SU-8 2100 photoresist masters to fabricate PDMS housings 350 µm in height. Perfusion access ports were bored with 1 mm biopsy punch and treated with acetophenone/NVP solution for 5 minutes immediately prior to use.

8.3.3. PEG-Pre-polymer Preparation for Proof of Concept Structure Fabrication

6kDa PEGDA synthesized as previously described (see Section 6.3.2 - Poly(ethylene glycol) diacrylate synthesis) was dissolved in phosphate buffered saline (PBS, pH 7.4) to yield a final pre-polymer concentration of 10% (wt/vol). The photoinitiator Irgacure 2959 (100mg/mL in 200 proof ethanol) was added to the hydrogel pre-polymer solution to yield a final concentration of 3% wt/vol. 10 µm fluorescent polystyrene microspheres (Invitrogen) of various spectral

properties were added to the hydrogel pre-polymer solution at 10 million spheres/mL to allow for structure visualization.

8.3.4. PEGDA Hydrogels Fabricated using Mask Projection Photolithography and Soft lithography

Acetophenone coated PDMS housings were placed on the microscope stage and secured using a standard microscope slide holder. The halogen alignment light source was then turned on and the projected mask structure was aligned to the desired location within the PDMS housing using the micromanipulator stage. The alignment light source was turned off and the PEG pre-polymer solution corresponding to Structure #1 was injected into the housing. The proper band pass filter was selected and the optical path splitter was switched to the mercury arc lamp to expose the sample for 5 min and photocrosslink the hydrogel (Figure 58; Step #3). The remaining un-crosslnked pre-polymer solution was rinsed from the housing by repeated flushing with phosphate buffered saline. The photomask for Structure #2 was aligned to the first set of structures using the alignment light source. The pre-polymer solution for Structure #2 was injected and the proper band pass filter was selected and the optical path splitter was switched to the mercury arc lamp to expose the sample for 5 min and photocrosslink the hydrogel (Figure 58; Step #4). Finally for fabrication of the microfluidic channel networks, the PDMS housing is aligned by eye with the SU-8 2050 photoresist masters. The third and final PEG pre-polymer solution was injected in the housing and the entire housing is exposed to photocrosslink the microfluidic channels (Figure 58; Step #5). The PDMS

housing was peeled from the microchannel mold ,sealed to coverglass, and connected to the perfusion apparatus.

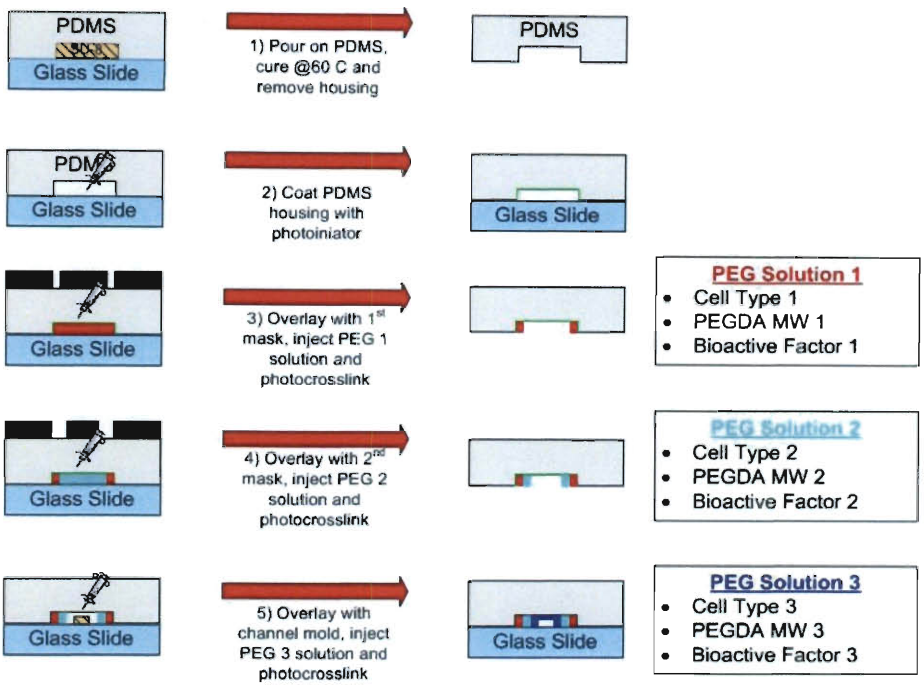

Figure 57: Multilayer Photolithographic and Softlithographic Fabrication Schematic of PDMS/PEGDA Microdevices. Standard softlithographic fabrication methods are used to fabricate the PDMS housing (Step #1). Serial mask directed photopolymerization of PEGDA pre-polymers produces hydrogel structures with various physical and biochemical content. (Steps 3 & 4) Softlithographic replica molding of PEG hydrogels to a photoresist master produces a perfusable microfluidic channel to support construct transport needs.

8.3.5. Photoinitiator Effects on Structure Formation

The effect of photoinitiator concentration and solvent type (200 proof ethanol or n-vinylpyrrolidone) on the ability to fabricate PEGDA structures was evaluated. All PDMS housings were prepared as described in Section 6.3.5.2. 6kDa PEGDA was dissolved in PBS at 10% wt/vol. Irgacure 2959 was dissolved in either ethanol or n-vinylpyrrolidone (NVP) at 100 mg /mL. Photoinitiator was added to the hydrogel solutions at various volumes to prepare final

concentrations of 0.3, 0.6, 0.9, 1.2, and 1.5% wt/vol. Samples were exposed for 5 min at 50% lamp power and imaged immediately after exposure to determine structure fabrication.

8.3.6. Photoinitiator Effects on Cell Viability

The effects of Irgacure 2959 concentration on cell viability were assessed using the Live/Dead assay (calcein AM/ethidium homodimer; Invitrogen). Cells were exposed to Irgacure 2959 in 200 proof ethanol (100mg/mL) at final concentrations varying from 0.3 to 1.5% wt/vol for 5 min. The ratio of live cells (Calcein AM positive) to total cells (Calcein AM + Ethidium homodimer) was calculated for each condition using a fluorescent plate reader.

8.3.7. Heterocellular Culture Effects on Hepatocyte Cytochrome P450 Enzyme Function

Heterocultures were seeded at a constant hepatocyte density (1000 cells/cm^2) and a fixed overall density of non-parenchymal cells (500 cell/cm^2) as described in Table 3. Heterocultures were cultured at 37 °C and 5% CO_2 with eagles minimum essential medium MEM supplemented with 10% FBS and 1% PS. As a fluorescent metabolic marker of cytochrome P450 activity, 7-ethoxy-4-trifluoromethylcoumarin (EFC) was added to the HEP G2 media to a final concentration of 100 μM. EFC is common marker of hepatocyte function due to its ability to become fluorescent upon exposure to cytochrome P450 enzymes. Media from well plates with various cellular compositions was removed and

analyzed using a fluorescent plate reader at 24 and 72 h using filters set at (ex385/em502).

Table 3: Ratios and Density of Heterocellular Culture Conditions

Experimental Condition	Hepatocytes (cells cm^2)	3T3 Fibroblast (cells cm^2)	HUVEC (cells cm^2)	10T ½ (cells cm^2)
#1	1000	-	-	-
#2	1000	500	-	-
#3	1000	-	400	100
#4 Control	-	500		
#5 Control			400	100

8.3.8. Media Formulation Effects on Hepatocyte Cytochrome P450 Function

The effects of media formulation on hepatocyte CYP450 function was analyzed to determine optimal media blends. HEP G2, HUVEC and10 T ½ cells were sub-cultured to 80-90% confluence prior to seeding as described in Section 8.3.7. Tri-cultures of HEP G2, HUVECs and 10T1/2 were seeded in tissue culture polystyrene plates at 2,000, 37,500 and 12,500 cells/cm^2 respectively. Media formulations consisting of hepatocyte growth media (MEM), endothelial growth media (EGM-2) and blends of the two media (1/3 MEM: 2/3 EGM-2 and 2/3 MEM and 1/3 EGM-2) were supplemented with 100 µM EFC to assay effects of media formulation on hepatocyte function. Negative controls (co-culture without hepatocytes) at each media condition were used to control for cellular autofluorescence and baseline EFC metabolism. Media was removed from the well plates and analyzed using a fluorescent plate reader at 24 h with filters set at (ex385/em502).

The transient effects of media formulations were analyzed to determine the ability to recover hepatocyte function after initial exposure to endothelial growth conditions that are known to form tubules. Tri-cultures were sub-cultured and seeded in well plates as previously described. All media formulations were supplemented with 100 μM EFC to allow for monitoring of hepatocyte function. Tri-cultures were maintained in either hepatocyte media (MEM), endothelial growth media (EGM-2), or a blend of the two (1/2 MEM:1/2 EGM-2) for 72 hr. The original media was then replaced with MEM and hepatocyte function recovery was assessed every 24 h for 72 h. A positive control where MEM media was maintained throughout the 6 day culture and a negative control where EGM-2 media was maintained throughout were employed to determine a top and bottom limit for EFC metabolism.

8.4. Results and Discussion

8.4.1. PEGDA Hydrogels Fabricated using Mask Projection Photolithography and Softlithography

Combination of softlithography and photolithography allows for microfluidic conduits to be rapidly fabricated over large length scales using soft lithographic techniques followed by photolithographic fabrication of high fidelity hydrogel microstructures. (Figure 59 C) This multimodal fabrication scheme couples the advantages of a robust PDMS housing with the biomimetic capabilities of hydrogel biomaterials. A specific embodiment of these multimodal devices consist of softlithographically fabricated outer PDMS housing providing larger macroscale conduits, with an inlaid layer of softlithographically fabricated

hydrogel microchannels to provide efficient mass transport and interface with cells in between microchannels (Figure 59 C). Finally photolithographically patterned structures or biomolecule patterns within regions between microfluidic conduits can be used to mimic heterogeneous tissue microstructures. This is a highly biomimetic organization capable of mimicking complex tissue microenvironments.

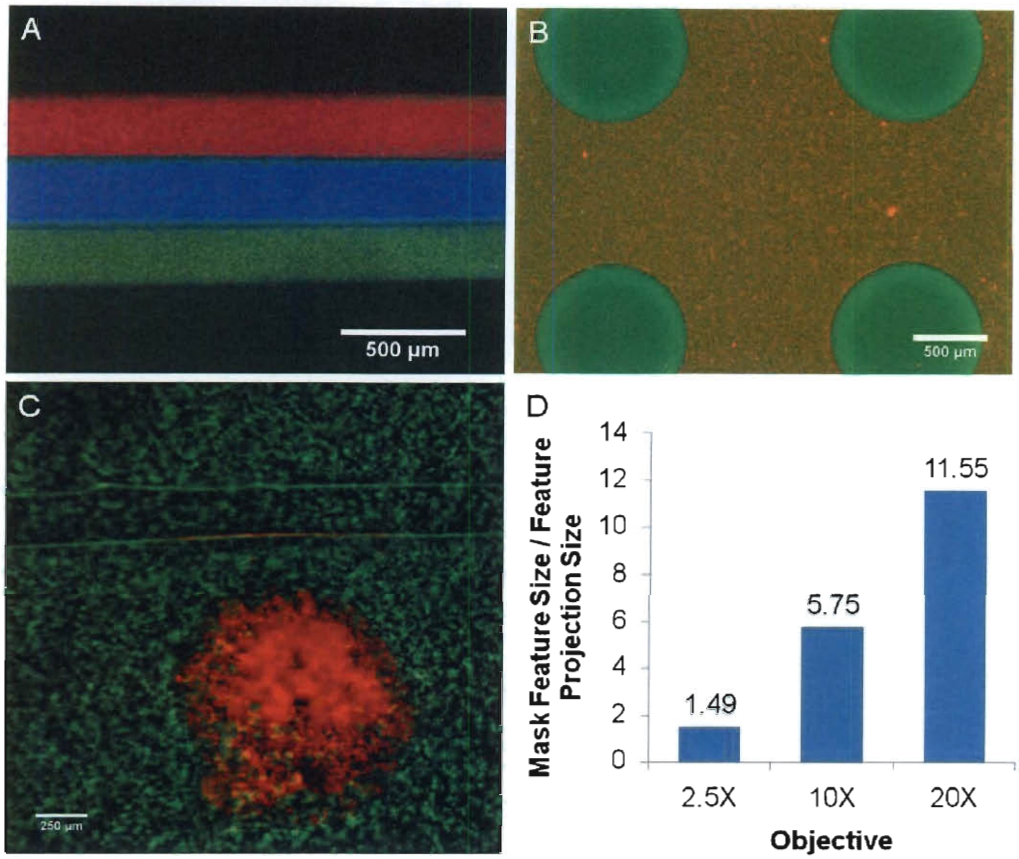

Figure 58: Multilayer PEGDA Hydrogels Fabricated using Mask Projection Photolithography and Softlithography. Multilayer PEGDA hydrogels fabricated using Mask Projection Photolithography to fabricate a (A) heterogeneous tri-layer structure and (B) an array of pillars surrounded by a backfill solution. PEGDA pre-polymer solutions were doped with 10 µm fluorescent microspheres to allow for structure visualization and to model cell encapsulation (C) Multimodal fabrications strategy combining a photolithographically fabricated pillars with encapsulated mouse hippocampus progenitor cells (MHP 36; red) with a softlithographically molded microchannel backfill solution containing human umbilical vein endothelial cells (HUVECs; green).(D) MPP feature size reduction demonstrates that mask features are reduced from 1.55x to11.55x between a 2.5x or 20x objective.

The ability to photolithographically fabricate multilayer micron level structures requires precise alignment capabilities. The application of mask projection photolithography (MPP) provides a valuable tool pattern to rapidly photopolymerize PEG hydrogels with micron level precision over large areas. (Figure 59 A&B) Minimal modification of standard epifluorescent microscope

systems makes this technique an attractive option for a large number of researchers interested in patterning multilayer structures (see Figure 57).

8.4.2. Photoinitiator Effects on Structure Formation and Cell Viability

Other groups have reported the ability to photolithographically pattern poly(ethylene glycol) diacrylate (PEGDA) hydrogels with micron level precision in PDMS housings.[140] However, the choice of hydrogel formation (MW = 575, and concentration > 20% wt/vol) and photoinitiator concentration (>3% wt/ vol) is not conducive to high cell viability and does not provide a hydrogel system capable of robust cellular remodeling and tissue formation. We set out to determine photolithographic fabrication conditions that optimize structure fabrication while maintaining hydrogel formulations (6 kDa and 10% wt/vol) and photoinitiator concentrations that preserve high cell viability.

The type of solvent used to dissolve the photoinitiator was shown to play an active role in improving the efficiency of photoinitiator on structure fabrication. Ethanol is commonly used as a solvent for the photoinitiator Irgacure 2959 due to its high solubility limit. However, ethanol is passive in the photopolymerization process and only acts to improve photoinitiator solubility in the final highly aqueous hydrogel solution. Therefore, we sought to investigate the effects of a potentially non-passive solvating reagent on structure fabrication. N-vinylpyrrolidone (NVP) contains a vinyl end-group similar to the terminal acrylate moiety on PEGDA. It was recently reported that the presence of hydrophobic acrylate micelles prior to network photopolymerization is one of the key

mechanisms in the crosslinking of PEGDA hydrogels.[30] Therefore we hypothesized that the addition of NVP as a solvent would have a stabilizing effect on micelle formation and therefore improve the efficiency of photopolymerization as indicated by the minimum concentration of photoinitiator needed to form a structure.

It was observed that Irgacure 2959 in ethanol only formed structures at the highest concentrations tested (1.5% wt/vol; Table 4) while Irgacure 2959 dissolved at the same concentration in NVP displayed structure formation at greater than half the effective concentration of Irgacure 2959 (0.6% wt/vol; Table 4). This is an important finding because cell viability increased significantly when Irgacure 2959 concentration is decreased to within this range. (Figure 60)

Table 4: Effects of Photoinitiator Concentration and Solvent Type on Structure Formation

Photoinitiator Concentration in Hydrogel (%wt/vol)					
+ Structure Formed × No Structure Formation	0.3	0.6	0.9	1.2	1.5
Irgacure 2959/Ethanol	×	×	×	×	+
Irgacure 2959/NVP	×	+	+	+	+

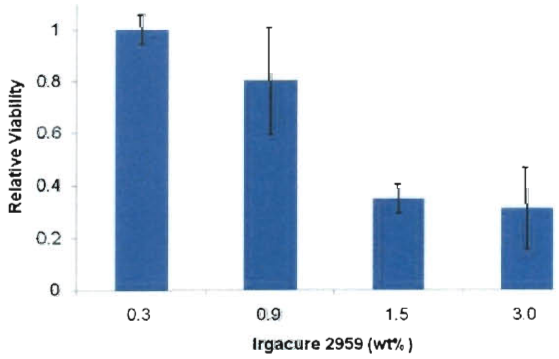

Figure 59: Effects of Photoinitiator Concentration on Cell Viability. Irgacure 2959 in 200 proof ethanol was shown to decrease cell viability in a dose dependent manor.

8.4.3. Heterocellular Culture on Hepatocyte Cytochrome P450 Function

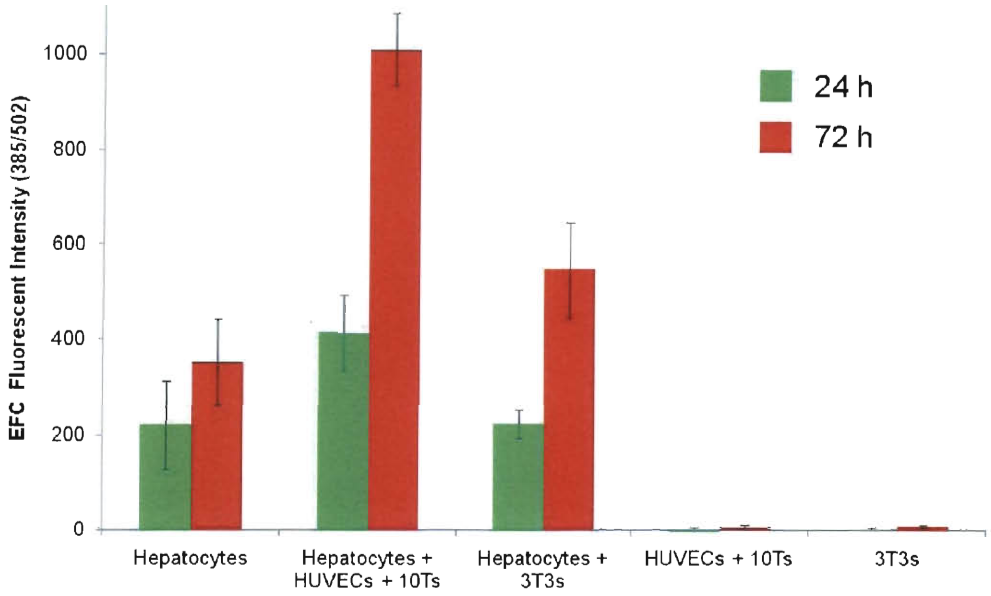

Figure 60: Heteroculture Composition Effects on Hepatocyte Cytochrome p450 Function. P450 enzyme function as measured by EFC metabolism was assayed in hepatocytes alone, tri-cultures containing hepatocytes, HUVECs and 10T ½ cells and a co-culture with hepatocytes and fibroblasts at 24 and 72 h of culture.

The effect of heterocultures on hepatocyte EFC metabolism was assessed by analyzing CYP450 activity through EFC fluorescence. It was demonstrated that tri-cultures of hepatocytes with HUVECs and 10T ½ cells had the greatest effect on CYP450 activity with a greater than a twofold increase in EFC fluorescence over hepatocytes alone at 72 h of culture. Interestingly this amount was greater than the well characterize synergistic co-culture with NIH 3T3 fibroblasts. (Figure 61) This happened despite the fact that total number of non-parenchymal cells was held constant (see Table 3). Therefore this suggests that both the endothelial and 10T ½ cells are enhancing hepatocyte function via separate and potentially synergistic paths. The specific mechanism of enhancement is not clear and requires further study.

8.4.4. Media Formulation Effects on Hepatocyte Cytochrome P450 Function

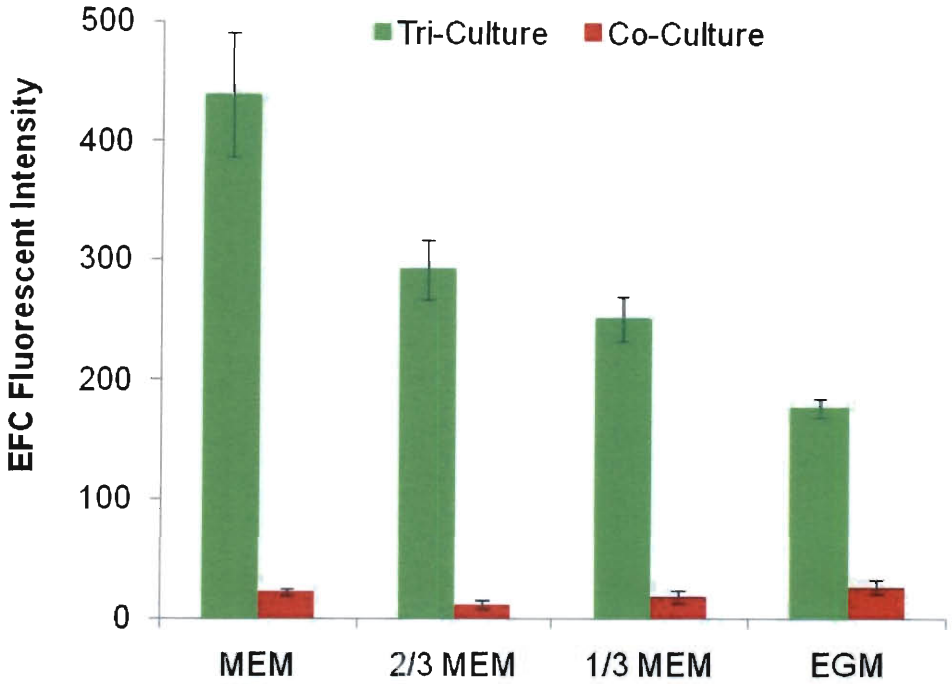

Figure 61: Effect of Media Formulation on Hepatocyte Cytochrome P450 Function. Tri-cultures were cultured in either MEM alone, EGM-2 alone, or blends of MEM and EGM-2 for 24 h. EFC fluorescence was measured using a plate reader to determine cytochrome P450 activity.

One major limitation of complex heterocellular cultures is the wide variation in nutrient and signaling needs required to maintain cellular phenotype and function. Therefore much of our efforts have focused on determining culture conditions that drive microvascular formation from the pro-tubulogenic co-culture while still preserving hepatocyte functionality. It was shown that culturing of the tri-culture in endothelial growth media (EGM) media decreased CYP450 metabolism as indicated by greater than a twofold decrease in EFC fluorescence. (Figure 62) Addition of hepatocyte recommended media (MEM) to EGM at final concentrations of 33% and 66% vol/vol improved EFC fluorescence in a dose dependent manor in proportion to the volume of MEM (Figure 62).

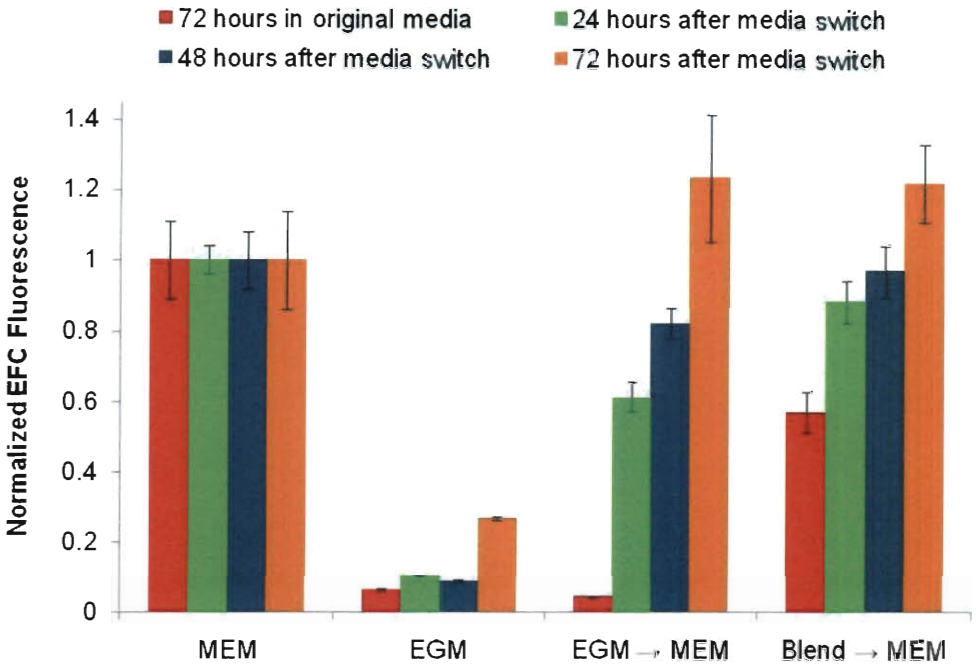

Figure 62: Transient Media Conditioning on Hepatocyte Cytochrome P450 Function. Tri-cultures were cultured in either MEM, EGM-2, or a MEM:EGM-2 blend (red bar) for 72 h. Media formulations were switched to MEM and hepatocyte function was analyzed every 24 h for 72 h to determine ability to recover cytochrome P450 function.

The ability to recover hepatocyte function after culturing in pro-tubulogenic media was assessed via a dynamic culture condition experiment. It was shown that by culturing tri-cultures in EGM media for 72 h, CYP450 function decreased by 90%. (Figure 63, Red bar) However, by switching to MEM media, the CYP450 activity was fully recovered by 48 h and was greater than the MEM only control by 72 h. (Figure 63, Blue and orange bar) This is very interesting finding that suggests an initial period of tubule growth conditions to facilitate microvascular network formation can be followed by a period where hepatocyte function can be restored and improved due the increase in cell numbers. (Figure 63) This agrees with findings in the literature that show the addition of epidermal growth factor (EGF) and fibroblast growth factor (FGF), both components in EGM, to

hepatocyte cultures decreases CYP450 and albumin gene expression in favor of driving hepatocyte mitogenesis and clonal expansion.[180,181] Confirming these findings our results, demonstrated that removal of the FGF and EGF from the media (Figure 63, EGM-MEM or Blend-MEM) restored hepatocyte function.

8.5. Conclusions

In conclusion we have demonstrated the ability to integrate multilayer soft and photolithographic fabrication techniques. In particular we have shown the ability to apply mask projection photolithography to the fabrication of multilayer PEG hydrogel structures. These technologies provide a valuable tool set to recapitulate complex heterogeneous cellular microenvironments within *in vitro* microdevices. Furthermore, we have shown the ability to adapt these technologies to fabrication conditions that are conducive to high cell viability and hydrogel compositions that allow for cell remodeling and tissue formation. These are important strides toward the merging of microfabrication technologies with highly bioactive PEG hydrogels.

In addition we have begun to investigate heteroculture methods to combine parenchymal cell types with pro-vasculogenic co-cultures. In particular we have demonstrated a tri-culture formulation that enhances hepatocyte cytochrome P450 function greater than other co-cultures. This is a very interesting finding that demonstrates the potential of incorporating a single pluripotent cell source that can differentiate into multiple, functionally distinct phenotypes. We have also determined the optimal media formulation and

transient culture conditions that allows for initial tubule growth while still maintaining the ability to recover hepatocyte function. This finding highlights the plasticity of hepatocytes and emphasizes the need to provide distinct and dynamic signaling regimes at different times in tissue development. Together these findings lay the groundwork to fabricate and culture a BAL with cellular components that have highly biomimetic structure function relationships.

9. Chapter 9: Strategic Directions in Microvascular Tissue Engineering

1. Engineering interfaces

Developing fabrication technologies to build multilayer devices is an important step towards recapitulating tissue microstructures. However, beyond developing multiple layers it is important to carefully design and integrate the interfaces between layers. Interfacial engineering in microfabricated hydrogel systems should focus on (1) the interface between the flowing solution in the microchannel and the hydrogel microchannel wall (sol-gel interface) and (2) the interface between heterogeneous hydrogel structures (gel-gel interface). Furthermore, interface engineering should account for both biochemical design motifs and control over the physical microenvironment.

In the case of the perfused microfluidic channel and the hydrogel matrix channel wall there is sol-gel interface. One design choice that needs to be considered is developing flow regimes that are diffusion limited (Peclet Number >> channel length/channel height) but have acceptable microvascular shear stress values (5-15 dyne/cm^2) for cells that are present at the interface. This optimization becomes non-convergent if you also constrain channel diameter and solution viscosity. Therefore it is important to consider whether the application of the system places emphasis on optimal mass transport, physiological shear, or biomimetic channel geometries.

Another sol-gel design consideration focuses on the functionalization of the interface for controlled anastomosis or encapsulated cell interaction with the solution. Tools to address this challenge include patterning of biochemical cell-cell proteins, such as Ephrin A1, or cell-matrix ligands, such as RGDS or IKVAV peptides, that control where cells in the hydrogel bulk can interact with the channel wall (see Section 4.2 and 4.3). Another method that can be used in conjunction with biochemical functionalization is developing structural modifications to the interface that can control anastomosis. Some possible designs include microvilli like protrusions into or out of the channel wall or non-degradable pillars at the interface that can spatially confine cellular interaction with the flowing solution. Combination of biochemical and physical interface design provides a mechanism to better control integration across lengths scales and fabricated structure-cellular element assimilation.

When engineering the gel-gel tissue structure interface *in vitro* it is unclear whether it is advantageous to pattern heterogeneous tissue mimetic structures or to homogenously mix multiple cell types know to be present in the native tissue and allow for self-assembly to drive tissue formation. It is likely that a combination of fabricated structures guidance followed by self-assembly will be required to generate tissue mimetic structure-functional relationships *in vitro*. Therefore gel-gel interface design should employ both biochemical and physical designs in integrate cellular self-assembly with fabricated structures. Some potential design ideas could involve patterned pro-migratory regions between interface with decreased matrix density and increases adhesive or pro-mitogenic

signals. Other simpler designs could be the encapsulation or loading of biochemical signals within structures as a tool to control signaling gradients and drive cell migration to and from structures. Also fabricated structures acting as signaling or nutrient gradient sinks or sources provides another order of control over tissue pattern formation beyond initial fabricated structures.

2. Freeform 3D fabrication methods

With the exception of photocleavable PEG derivative work reported by Kloxin *et al*[123], (see Figure 24) most fabrication methods reported in the literature are restricted to planar designs. Even the photocleavable technologies are limited by long writing or exposure times with a costly and uncommon two-photon confocal microscope system. Other softlithographic designs may be amenable to scaling in the third dimension, via layer-by-layer approaches, however robust technologies to microfabricate hydrogels using 3D free form fabrication have not been reported to the best of our knowledge.

The lack of progress in this area is likely due to a combination of material property limitations and means to convey spatial information to the material. Fabrication of high aspect ratio hydrogel structures that do not collapse or deform under their own weight is difficult due to the relatively low elastic modulus of the highly aqueous materials. Rapid prototyping techniques have applied removable filler substrates to support structures during fabrication followed by steps to dissolve away the support structures. This outside-in approach is a potential option for 3D free form fabrication as long as the filling support structure can be removed under conditions that do not damage the hydrogel and more importantly

maintain cell viability. A similar but converse inside-out approach could involve initially building dissolvable structures and backfilling around the structures with the final hydrogel material. This would be followed by dissolving the interior sacrificial structures in a "lost wax" or sacrificial poragen process. This technique, like the outside-in approach, must apply highly cell and hydrogel compatible dissolution processes.

One potential materials fabricating scheme could apply an enzymatically degradable material as either the filling support structure or the sacrificial poragen. This would allow for aqueous and cell compatible degradation conditions. However, this approach requires that the support or poragen dissolution enzyme does not have cross reactivity with the final hydrogel scaffold. Progress in 3D free-form fabrication technologies will likely have broad implications to all materials fabrication sectors and will improve the state of the art for developing 3D microstructures.

3. **Multipotent cellular elements and clinically viable cell sources**

Incorporation of multiple terminally differentiated cell types into tissue engineered constructs is one approach to recapitulate complex tissues *in vitro*. However, this approach is plagued by the need to provide unique signals and culture environments for each cell type. This is difficult to not possible if the cells of interest are not plastic enough to recover function upon termination of orthogonal culture conditions. Furthermore, this approach is not well suited to the clinically preferred autologous cell source due to the need to harvest from

multiple tissues, the lack of donor site availability and unacceptable damage to the donor site.

An interesting and intense area of research to address this limitation is the use of a single multipotent cell type to drive formation of both parenchymal and functional cellular elements. This approach would closely mimic native tissue development and would allow for harvesting of cells from a single source tissue. Furthermore the use of a single, multipotent cell type improves the feasibility of cell cryostorage banks as a long term cell source. It is important that continued progress in stem cell and developmental biology research result in multidisciplinary collaborations that drive improvements in knowledge and cell sources available to tissue engineers.

10. Chapter 10: Bibliography

1. Langer, R. & Vacanti, J. Tissue engineering. *Science* **260**, 920-926(1993).

2. Sen, C. & Sekhar, L.N. Direct vein graft reconstruction of the cavernous, petrous, and upper cervical internal carotid artery: lessons learned from 30 cases. *Neurosurgery* **30**, 732-42; discussion 742-3(1992).

3. Steiner, M.E. et al. Anterior cruciate ligament graft fixation. Comparison of hamstring and patellar tendon grafts. *The American journal of sports medicine* **22**, 240-6; discussion 246-7

4. Schmidt, C.E. & Leach, J.B. Neural tissue engineering: strategies for repair and regeneration. *Annual review of biomedical engineering* **5**, 293-347(2003).

5. Naughton, G.K. From lab bench to market: critical issues in tissue engineering. *Annals of the New York Academy of Sciences* **961**, 372-85(2002).

6. Tsigkou, O. et al. Engineered vascularized bone grafts. *Proceedings of the National Academy of Sciences of the United States of America* **107**, 3311-6(2010).

7. Kuberka, M. et al. Magnification of the pore size in biodegradable collagen sponges. *The International journal of artificial organs* **25**, 67-73(2002).

8. Watanabe, E. et al. Cardiomyocyte transplantation in a porcine myocardial infarction model. *Cell transplantation* **7**, 239-46

9. Marler, J.J. et al. Soft-tissue augmentation with injectable alginate and syngeneic fibroblasts. *Plastic and reconstructive surgery* **105**, 2049-58(2000).

10. Shireman, P.K. & Greisler, H.P. Mitogenicity and release of vascular endothelial growth factor with and without heparin from fibrin glue. *Journal of vascular surgery : official publication, the Society for Vascular Surgery [and] International Society for Cardiovascular Surgery, North American Chapter* **31**, 936-43(2000).

11. Ratner, B.D. et al. *Biomaterials Science, Second Edition: An Introduction to Materials in Medicine*. (Elsevier Academic Press: San Diego, 2004).

12. Moon, J.J. & West, J.L. Vascularization of engineered tissues: approaches to promote angio-genesis in biomaterials. *Current topics in medicinal chemistry* **8**, 300-10(2008).

13. Murphy, W.L. et al. Salt Fusion : An Approach to Improve Pore Interconnectivity within Tissue Engineering Scaffolds. *Tissue Engineering* **8**, 43-52(2002).

14. Ma, P.X. & Zhang, R. Synthetic nano-scale fibrous extracellular matrix. *Vacuum* 27-30(1998).

15. Harris, L.D., Kim, B.S. & Mooney, D.J. Open pore biodegradable matrices formed with gas foaming. *Journal of biomedical materials research* **42**, 396-402(1998).

16. Pham, Q.P., Sharma, U. & Mikos, A.G. Electrospun poly(epsilon-caprolactone) microfiber and multilayer nanofiber/microfiber scaffolds: characterization of scaffolds and measurement of cellular infiltration. *Biomacromolecules* **7**, 2796-805(2006).

17. Baker, B.M. & Mauck, R.L. The effect of nanofiber alignment on the maturation of engineered meniscus constructs. *Biomaterials* **28**, 1967-77(2007).

18. Baker, B.M. et al. The potential to improve cell infiltration in composite fiber-aligned electrospun scaffolds by the selective removal of sacrificial fibers. *Biomaterials* **29**, 2348-58(2008).

19. SILVA, M. et al. The effect of anisotropic architecture on cell and tissue infiltration into tissue engineering scaffolds. *Biomaterials* **27**, 5909-5917(2006).

20. Nguyen, K.T. & West, J.L. Photopolymerizable hydrogels for tissue engineering applications. *Biomaterials* **23**, 4307-4314(2002).

21. Peppas, N. a et al. Hydrogels in Biology and Medicine: From Molecular Principles to Bionanotechnology. *Advanced Materials* **18**, 1345-1360(2006).

22. Peppas, N. Biomaterials Science: An Introdcution to Materials in Medecine. 105(2004).

23. Hern, D.L. & Hubbell, J. a Incorporation of adhesion peptides into nonadhesive hydrogels useful for tissue resurfacing. *Journal of biomedical materials research* **39**, 266-76(1998).

24. West, J.L. & Hubbell, J.A. Polymeric Biomaterials with Degradation Sites for Proteases Involved in Cell Migration. *Macromolecules* **32**, 241-244(1999).

25. Hubbell, J. a Bioactive biomaterials. *Current opinion in biotechnology* **10**, 123-9(1999).

26. Lutolf, M.P. & Hubbell, J. a Synthesis and physicochemical characterization of end-linked poly(ethylene glycol)-co-peptide hydrogels formed by Michael-type addition. *Biomacromolecules* **4**, 713-22(2003).

27. Metters, A. & Hubbell, J. Network Formation and Degradation Behavior of Hydrogels Formed by Michael-Type Addition Reactions. *Society* 290-301(2005).

28. Zisch, A.H. et al. Cell-demanded release of VEGF from synthetic, biointeractive cell ingrowth matrices for vascularized tissue growth. *The FASEB journal : official publication of the Federation of American Societies for Experimental Biology* **17**, 2260-2(2003).

29. Vernon, B. et al. Water-borne , in situ crosslinked biomaterials from phase-segregated precursors. *In Situ* **13**, (2002).

30. Beamish, J.A. et al. The effects of monoacrylated poly (ethylene glycol) on the properties of poly (ethylene glycol) diacrylate hydrogels used for tissue engineering. *Journal of Biomedical Materials Research Part A* (2009).doi:10.1002/jbm.a.32353

31. Nemir, S., Hayenga, H.N. & West, J.L. PEGDA hydrogels with patterned elasticity: Novel tools for the study of cell response to substrate rigidity. *Biotechnology and bioengineering* **105**, 636-44(2010).

32. Temenoff, J.S. et al. Thermally cross-linked oligo(poly(ethylene glycol) fumarate) hydrogels support osteogenic differentiation of encapsulated marrow stromal cells in vitro. *Biomacromolecules* **5**, 5-10(2004).

33. Bryant, S.J. & Anseth, K.S. Photopolymerization of Hydrogel Scaffolds. *Scaffolds in Tissue Engineering* 71-90(2006).

34. Tsang, V.L. et al. Fabrication of 3D hepatic tissues by additive photopatterning of cellular hydrogels. *The FASEB Journal* **21**, 790-801(2007).

35. Hahn, M.S., Miller, J.S. & West, J.L. Laser Scanning Lithography for Surface Micropatterning on Hydrogels. *Advanced Materials* **17**, 2939-2942(2005).

36. Hahn, M.S., Miller, J.S. & West, J.L. Three-Dimensional Biochemical and Biomechanical Patterning of Hydrogels for Guiding Cell Behavior. *Advanced Materials* **18**, 2679-2684(2006).

37. Miller, J. & West, J. Biomimetic Hydrogels to Support and Guide Tissue Formation. *Micro and Nanoengineering of the Cell Microenvironment* 101-120(2008).

38. Mellott, M.B., Searcy, K. & Pishko, M.V. Release of protein from highly cross-linked hydrogels of poly (ethylene glycol) diacrylate fabricated by UV polymerization. *Biomaterials* **22**, 929–941(2001).

39. Lin, C.-C. & Metters, A.T. Hydrogels in controlled release formulations: network design and mathematical modeling. *Advanced drug delivery reviews* **58**, 1379-408(2006).

40. Mann, B.K. et al. Modi " cation of surfaces with cell adhesion peptides alters extracellular matrix deposition. *Evaluation* **20**, 2281-2286(1999).

41. Mann, B. Smooth muscle cell growth in photopolymerized hydrogels with cell adhesive and proteolytically degradable domains: synthetic ECM analogs for tissue engineering. *Biomaterials* **22**, 3045-3051(2001).

42. DeLong, S.A., Moon, J.J. & West, J.L. Covalently immobilized gradients of bFGF on hydrogel scaffolds for directed cell migration. *Biomaterials* **26**, 3227-34(2005).

43. Moon, J.J. et al. Biomimetic hydrogels with pro-angiogenic properties. *Biomaterials* **31**, 3840-7(2010).

44. West, J. Photopolymerized hydrogel materials for drug delivery applications. *Reactive Polymers* **25**, 139-147(1995).

45. Gobin, A.S. & West, J.L. Smooth muscle cell adhesion and specificity. *October* (2003).

46. Gobin, A.S. & West, J.L. matrix analogues. *The FASEB Journal* (2002).

47. Morpurgo, M. & Veronese, F. Conjugates of Peptides and Protiens to Polyethylene Glycols. *Bioconjugate Protocols* 45-70(2004).

48. Lutolf, M.P. et al. Systematic modulation of Michael-type reactivity of thiols through the use of charged amino acids. *Bioconjugate chemistry* **12**, 1051-6(2001).

49. Arakawa, T. et al. The importance of Arg40 and 45 in the mitogenic activity and structural stability of basic fibroblast growth factor: effects of acidic amino acid substitutions. *Journal of protein chemistry* **14**, 263-74(1995).

50. Taite, L.J. et al. Nitric oxide-releasing polyurethane-PEG copolymer containing the YIGSR peptide promotes endothelialization with decreased platelet adhesion. *Journal of biomedical materials research. Part B, Applied biomaterials* **84**, 108-16(2008).

51. Zisch, A.H. et al. growth. *The FASEB Journal* (2003).

52. Saik, J.E. et al. Covalently Immobilized Platelet Derived Growth Factor-BB Promotes Angiogenesis in Biomimetic Poly(ethylene glycol) Hydrogels. *Acta biomaterialia* **7**, 133-143(2010).

53. Massia, S.P. & Hubbell, J. a An RGD spacing of 440 nm is sufficient for integrin alpha V beta 3-mediated fibroblast spreading and 140 nm for focal contact and stress fiber formation. *The Journal of cell biology* **114**, 1089-100(1991).

54. Lutolf, M.P. et al. Synthetic matrix metalloproteinase-sensitive hydrogels for the conduction of tissue regeneration : Engineering cell-invasion characteristics. *Building* (2003).

55. Miller, J.S. et al. Bioactive hydrogels made from step-growth derived PEG-peptide macromers. *Biomaterials* **31**, 3736-43(2010).

56. Moon, J.J., Lee, S.-H. & West, J.L. Synthetic biomimetic hydrogels incorporated with ephrin-A1 for therapeutic angiogenesis. *Biomacromolecules* **8**, 42-9(2007).

57. West, J.L. & Hubbell, J.A. Polymeric Biomaterials with Degradation Sites for Proteases Involved in Cell Migration. *Macromolecules* **32**, 241-244(1999).

58. Lysaght, M.J. & Reyes, J. The growth of tissue engineering. *Tissue engineering* **7**, 485-93(2001).

59. Atala, A. et al. Tissue-engineered autologous bladders for patients needing cystoplasty. *Regenerative Medicine* 1241-1246doi:10.1016/S0140-6736(06)68438-9

60. Jain, R.K. et al. Engineering vascularized tissue. *Nature biotechnology* **23**, 821-3(2005).

61. Clark, E.R. & Clark, E.L. Microscopic observations on the growth of blood capillaries in the living mammal. *American Journal of Anatomy* **64**, 251-301(1939).

62. Malda, J. et al. Oxygen Gradients in Tissue-Engineered PEGT / PBT Cartilaginous Constructs : Measurement and Modeling. *Biotechnology* (2004).doi:10.1002/bit.20038

63. Colton, C.K. Implantable biohybrid artificial organs. *Cell transplantation* **4**, 415-36

64. Folkman, J. & Hochberg, M. Self-regulation of growth in three dimensions. *The Journal of experimental medicine* **138**, 745-53(1973).

65. Hirschi, K.K. et al. Vascular assembly in natural and engineered tissues. *Annals of the New York Academy of Sciences* **961**, 223-42(2002).

66. Jain, R.K. Molecular regulation of vessel maturation. *Nature medicine* **9**, 685-93(2003).

67. Asahara, T. et al. Isolation of putative progenitor endothelial cells for angiogenesis. *Science (New York, N.Y.)* **275**, 964-7(1997).

68. Adams, R.H. & Alitalo, K. Molecular regulation of angiogenesis and lymphangiogenesis. *Nature reviews. Molecular cell biology* **8**, 464-78(2007).

69. Miquerol, L., Langille, B.L. & Nagy, A. Embryonic development is disrupted by modest increases in vascular endothelial growth factor gene expression. *Development (Cambridge, England)* **127**, 3941-6(2000).

70. Dyer, M.A. et al. Indian hedgehog activates hematopoiesis and vasculogenesis and can respecify prospective neurectodermal cell fate in the mouse embryo. *Development (Cambridge, England)* **128**, 1717-30(2001).

71. Noveroske, J.K. et al. Quaking is essential for blood vessel development. *Genesis (New York, N.Y. : 2000)* **32**, 218-30(2002).

72. Folkman, J. & Haudenschild, C. Angiogenesis in vitro. *Nature* **288**, 551-556(1980).

73. Kamei, M. et al. Endothelial tubes assemble from intracellular vacuoles in vivo. *Nature* **442**, 453-456(2006).

74. Hirschi, K.K. & D□ Amore, P.A. Pericytes in the microvasculature. *Cardiovascular research* **32**, 687-98(1996).

75. Hirschi, K.K. PDGF, TGF-beta , and Heterotypic Cell-Cell Interactions Mediate Endothelial Cell-induced Recruitment of 10T1/2 Cells and Their Differentiation to a Smooth Muscle Fate. *The Journal of Cell Biology* **141**, 805-814(1998).

76. Ruhrberg, C. et al. Spatially restricted patterning cues provided by heparin-binding VEGF-A control blood vessel branching morphogenesis. *Genes & development* **16**, 2684-98(2002).

77. Kamei, M. et al. Endothelial tubes assemble from intracellular vacuoles in vivo. *Nature* **442**, 453-6(2006).

78. Grunewald, M. et al. VEGF-induced adult neovascularization: recruitment, retention, and role of accessory cells. *Cell* **124**, 175-89(2006).

79. Guyton, A. & Hall, J. Text Book of Medical Physiology. 162-166(2000).

80. Rippe, B. & Haraldsson, B. Transport of macromolecules across microvascular walls: the two-pore theory. *Physiological reviews* **74**, 163-219(1994).

81. Kobayashi, I. et al. Platelet-activating factor modulates microvascular transport by stimulation of protein kinase C. *The American journal of physiology* **266**, H1214-20(1994).

82. Michel, C.C. & Curry, F.E. Microvascular permeability. *Physiological reviews* **79**, 703-61(1999).

83. Michel, C.C. REVIEW ARTICLE STARLING : THE FORMULATION OF HIS HYPOTHESIS OF MICROVASCULAR FLUID EXCHANGE AND ITS SIGNIFICANCE AFTER 100 YEARS. *The Journal of Physiology* **1996**, 1-30(1997).

84. Levick, J.R. & Michel, C.C. Microvascular fluid exchange and the revised Starling principle. *Cardiovascular research* **87**, 198-210(2010).

85. Ishaug, S.L. et al. Bone formation by three-dimensional stromal osteoblast culture in biodegradable polymer scaffolds. *Journal of biomedical materials research* **36**, 17-28(1997).

86. Kellner, K. et al. Determination of Oxygen Gradients in Engineered Tissue Using a Fluorescent Sensor. *October* 73-83(2002).doi:10.1002/bit.10352

87. Kaihara, S. et al. Silicon micromachining to tissue engineer branched vascular channels for liver fabrication. *Tissue engineering* **6**, 105-17(2000).

88. Khademhosseini, A. et al. Layer-by-layer deposition of hyaluronic acid and poly-L-lysine for patterned cell co-cultures. *Biomaterials* **25**, 3583-92(2004).

89. Tayalia, P. et al. 3D Cell-Migration Studies using Two-Photon Engineered Polymer Scaffolds. *Advanced Materials* **20**, 4494-4498(2008).

90. Almany, L. & Seliktar, D. Biosynthetic hydrogel scaffolds made from fibrinogen and polyethylene glycol for 3D cell cultures. *Biomaterials* **26**, 2467-77(2005).

91. Frenkel, S.R. & Di Cesare, P.E. Scaffolds for articular cartilage repair. *Annals of biomedical engineering* **32**, 26-34(2004).

92. West, J.L. Bioactive Hydrogels: Mimicking the ECM with Synthetic Materials. *Scaffolds in Tissue Engineering* 275-281(2006).

93. Richardson, T.P. et al. Polymeric system for dual growth factor delivery. *Nature biotechnology* **19**, 1029-34(2001).

94. Sakiyama-Elbert, S.E. & Hubbell, J.A. Development of fibrin derivatives for controlled release of heparin-binding growth factors. *Journal of controlled release : official journal of the Controlled Release Society* **65**, 389-402(2000).

95. Silva, E. a & Mooney, D.J. Effects of VEGF temporal and spatial presentation on angiogenesis. *Biomaterials* **31**, 1235-41(2010).

96. Zhang, Y. et al. The impact of proliferative potential of umbilical cord-derived endothelial progenitor cells and hypoxia on vascular tubule formation in vitro. *Stem cells and development* **18**, 359-75(2009).

97. Durr, E. et al. Direct proteomic mapping of the lung microvascular endothelial cell surface in vivo and in cell culture. *Nature biotechnology* **22**, 985-92(2004).

98. Santos, M.I. et al. Crosstalk between osteoblasts and endothelial cells co-cultured on a polycaprolactone-starch scaffold and the in vitro development of vascularization. *Biomaterials* **30**, 4407-15(2009).

99. Wang, Z.Z. et al. Endothelial cells derived from human embryonic stem cells form durable blood vessels in vivo. *Nature biotechnology* **25**, 317-8(2007).

100. Koike, N. et al. Tissue engineering: creation of long-lasting blood vessels. *Nature* **428**, 138-9(2004).

101. Kannan, R.Y. et al. The roles of tissue engineering and vascularisation in the development of micro-vascular networks : a review. *Angiogenesis* **26**, 1857-1875(2005).

102. Rouwkema, J., Rivron, N.C. & Blitterswijk, C. a van Vascularization in tissue engineering. *Trends in biotechnology* **26**, 434-41(2008).

103. Jeong, S.I. et al. Mechano-active tissue engineering of vascular smooth muscle using pulsatile perfusion bioreactors and elastic PLCL scaffolds. *Biomaterials* **26**, 1405-11(2005).

104. Hahn, M.S. et al. Physiologic pulsatile flow bioreactor conditioning of poly(ethylene glycol)-based tissue engineered vascular grafts. *Annals of biomedical engineering* **35**, 190-200(2007).

105. Leclerc, E. Perfusion culture of fetal human hepatocytes in microfluidic environments. *Biochemical Engineering Journal* **20**, 143-148(2004).

106. Sachlos, E. et al. Novel collagen scaffolds with predefined internal morphology made by solid freeform fabrication. *Biomaterials* **24**, 1487-97(2003).

107. Shepherd, B.R. et al. Rapid perfusion and network remodeling in a microvascular construct after implantation. *Arteriosclerosis, thrombosis, and vascular biology* **24**, 898-904(2004).

108. Jackson, Z.S. Wall Tissue Remodeling Regulates Longitudinal Tension in Arteries. *Circulation Research* **90**, 918-925(2002).

109. Sullivan, C.J. Flow-Dependent Remodeling in the Carotid Artery of Fibroblast Growth Factor-2 Knockout Mice. *Arteriosclerosis, Thrombosis, and Vascular Biology* **22**, 1100-1105(2002).

110. Pries, a R. & Secomb, T.W. Microcirculatory network structures and models. *Annals of biomedical engineering* **28**, 916-21(2000).

111. Pries, a R., Reglin, B. & Secomb, T.W. Structural response of microcirculatory networks to changes in demand: information transfer by shear stress. *American journal of physiology. Heart and circulatory physiology* **284**, H2204-12(2003).

112. Pries, a R., Reglin, B. & Secomb, T.W. Structural adaptation of microvascular networks: functional roles of adaptive responses. *American journal of physiology. Heart and circulatory physiology* **281**, H1015-25(2001).

113. Price, G.M., Chrobak, K.M. & Tien, J. Effect of cyclic AMP on barrier function of human lymphatic microvascular tubes. *Microvascular research* **76**, 46-51(2008).

114. Levenberg, S. et al. Engineering vascularized skeletal muscle tissue. *Nature biotechnology* **23**, 879-84(2005).

115. Bhatia, S.N. et al. Effect of cell-cell interactions in preservation of cellular phenotype: cocultivation of hepatocytes and nonparenchymal cells. *The FASEB journal : official publication of the Federation of American Societies for Experimental Biology* **13**, 1883-900(1999).

116. Blau, H.M. & Banfi, A. The well-tempered vessel. *Nature medicine* **7**, 532-4(2001).

117. Lee, R.J. et al. VEGF gene delivery to myocardium: deleterious effects of unregulated expression. *Circulation* **102**, 898(2000).

118. Monolayers, C.-adhesive S.-assembled et al. Laser-Scanning Lithography (LSL) for the Soft Lithographic Patterning of. *Biotechnology* (2006).doi:10.1002/bit

119. Itoga, K. et al. Maskless liquid-crystal-display projection photolithography for improved design flexibility of cellular micropatterns. *Biomaterials* **27**, 3005-9(2006).

120. Luo, Y. & Shoichet, M.S. A photolabile hydrogel for guided three-dimensional cell growth and migration. *Nature materials* **3**, 249-53(2004).

121. Lee, S.-H., Moon, J.J. & West, J.L. Three-dimensional micropatterning of bioactive hydrogels via two-photon laser scanning photolithography for guided 3D cell migration. *Biomaterials* **29**, 2962-8(2008).

122. Liu, V. & Bhatia, S.N. Three-Dimensional Photopatterning of Hydrogels Containing Living Cells. *Biomedical Microdevices* **4**, 257(2002).

123. Kloxin, A.M. et al. Photodegradable hydrogels for dynamic tuning of physical and chemical properties. *Science (New York, N.Y.)* **324**, 59-63(2009).

124. Weibel, D.B., Diluzio, W.R. & Whitesides, G.M. Microfabrication meets microbiology. *Nature reviews. Microbiology* **5**, 209-18(2007).

125. Rohde, C.B. et al. Microfluidic system for on-chip high-throughput whole-animal sorting and screening at subcellular resolution. *Proceedings of the National Academy of Sciences of the United States of America* **104**, 13891-5(2007).

126. Gómez-Sjöberg, R. et al. Versatile, fully automated, microfluidic cell culture system. *Analytical chemistry* **79**, 8557-63(2007).

127. Koh, W.-G., Itle, L.J. & Pishko, M.V. Molding of hydrogel microstructures to create multiphenotype cell microarrays. *Analytical chemistry* **75**, 5783-9(2003).

128. Yadavalli, V. Microfabricated protein-containing poly(ethylene glycol) hydrogel arrays for biosensing. *Sensors and Actuators B: Chemical* **97**, 290-297(2004).

129. Ling, Y. et al. A cell-laden microfluidic hydrogel. *Lab on a chip* **7**, 756-62(2007).

130. Choi, N.W. et al. Microfluidic scaffolds for tissue engineering. *Nature materials* **6**, 908-15(2007).

131. Bettinger, C.J. et al. Three-Dimensional Microfluidic Tissue-Engineering Scaffolds Using a Flexible Biodegradable Polymer. *Advanced materials (Deerfield Beach, Fla.)* **18**, 165-169(2005).

132. Gillette, B.M. et al. In situ collagen assembly for integrating microfabricated three-dimensional cell-seeded matrices. *Nature materials* **7**, 636-40(2008).

133. Golden, A.P. & Tien, J. Fabrication of microfluidic hydrogels using molded gelatin as a sacrificial element. *Lab on a chip* **7**, 720-5(2007).

134. Chung, S. et al. Cell migration into scaffolds under co-culture conditions in a microfluidic platform. *Lab on a chip* **9**, 269-75(2009).

135. Wong, A.P. et al. Partitioning microfluidic channels with hydrogel to construct tunable 3-D cellular microenvironments. *Cell* **29**, 1853-1861(2008).

136. Fidkowski, C. et al. Endothelialized microvasculature based on a biodegradable elastomer. *Tissue engineering* **11**, 302-9(2005).

137. Chrobak, K.M., Potter, D.R. & Tien, J. Formation of perfused, functional microvascular tubes in vitro. *Microvascular research* **71**, 185-96(2006).

138. Zervantonakis, I.K. et al. Concentration gradients in microfluidic 3D matrix cell culture systems. *International Journal of Micro-Nano Scale Transport* **1**, 27-36(2010).

139. Khademhosseini, A. et al. Molded polyethylene glycol microstructures for capturing cells within microfluidic channels. *Lab on a chip* **4**, 425-30(2004).

140. Cheung, Y.K. et al. Direct patterning of composite biocompatible microstructures using microfluidics. *Lab on a chip* 7, 574-9(2007).

141. Yeh, J. et al. Micromolding of shape-controlled, harvestable cell-laden hydrogels. *Biomaterials* **27**, 5391-8(2006).

142. Panda, P. et al. Stop-flow lithography to generate cell-laden microgel particles. *Lab on a chip* **8**, 1056-61(2008).

143. Du, Y. et al. Directed assembly of cell-laden microgels for fabrication of 3D tissue constructs. *Proceedings of the National Academy of Sciences of the United States of America* **105**, 9522-7(2008).

144. Murray, C.D. The Physiological Principle of Minimum Work: I. The Vascular System and the Cost of Blood Volume. *Proceedings of the National Academy of Sciences of the United States of America* **12**, 207-14(1926).

145. Lim, D. et al. Fabrication of microfluidic mixers and artificial vasculatures using a high-brightness diode-pumped Nd:YAG laser direct write method. *Lab on a chip* **3**, 318-23(2003).

146. Borenstein, J.T. et al. Microvascular Engineering: Design, Modeling, and Microfabrication. *Micro and Nanoengineering of the Cell Microenvironment* 295-315(2008).

147. Janakiraman, V., Mathur, K. & Baskaran, H. Optimal planar flow network designs for tissue engineered constructs with built-in vasculature. *Annals of biomedical engineering* **35**, 337-47(2007).

148. Cuchiara, M.P. et al. Multilayer microfluidic PEGDA hydrogels. *Biomaterials* **31**, 5491-7(2010).

149. Fournier, R.L. Basic Tranport Phenomena in Biomedical Engineering. 27-30(1998).

150. Langer, R. & Peppas, N.A. Advances in biomaterials, drug delivery, and bionanotechnology. *AIChE Journal* **49**, 2990-3006(2003).

151. Chow, D.C. et al. Modeling pO (2) distributions in the bone marrow hematopoietic compartment . I .... *Science* (2001).

152. Chow, D.C. et al. Modeling pO (2) distributions in the bone marrow hematopoietic compartment . II ... *Science* (2001).

153. Gentzkow, G.D. et al. Use of dermagraft, a cultured human dermis, to treat diabetic foot ulcers. *Diabetes care* **19**, 350-4(1996).

154. Temenoff, J.S. & Mikos, A.G. Review: tissue engineering for regeneration of articular cartilage. *Biomaterials* **21**, 431-40(2000).

155. Carmeliet, P. & Jain, R.K. Angiogenesis in cancer and other diseases. *Nature* **407**, 249-57(2000).

156. Phelps, E.A. et al. Bioartificial matrices for therapeutic vascularization. *Proceedings of the National Academy of Sciences of the United States of America* **107**, 3323-8(2010).

157. Griffith, L.G. & Swartz, M. a Capturing complex 3D tissue physiology in vitro. *Nature reviews. Molecular cell biology* **7**, 211-24(2006).

158. Imper, V. & Van Wart, H. Substrate Specificity and Mechanisms of Substrate Recognition of the Matrix Metalloproteinases. 219-240(1998).

159. Gerlowski, L.E. & Jain, R.K. Microvascular permeability of normal and neoplastic tissues. *Microvascular research* **31**, 288-305(1986).

160. Choi, N.W. et al. Microfluidic scaffolds for tissue engineering. *Nature materials* **6**, 908-15(2007).

161. Moraes, C., Sun, Y. & Simmons, C.A. Solving the shrinkage-induced PDMS alignment registration issue in multilayer soft lithography. **065015**, (2009).

162. Moraes, C. et al. A microfabricated platform for high-throughput unconfined compression of micropatterned biomaterial arrays. *Biomaterials* **31**, 577-84(2010).

163. Love, J.C. et al. Microscope Projection Photolithography for Rapid Prototyping of Masters with Micron-Scale Features for Use in Soft Lithography. *Langmuir* **17**, 6005-6012(2001).

164. Itoga, K. Cell micropatterning using photopolymerization with a liquid crystal device commercial projector. *Biomaterials* **25**, 2047-2053(2004).

165. Department of Health and Human Services, Health Resources and Services Adminsitration, Health Care Systems Bureau, D. of T. *UNOS, Annual Report of the U.S. Organ Procurement and Transplantation Network and the Scientific Registry of Trasnplant Receipients: Transplant Data 1994-2006*. (Rockville, MD, 2007).

166. Lee, P.J., Hung, P.J. & Lee, L.P. An Artificial Liver Sinusoid With a Microfluidic Endothelial-Like Barrier for Primary Hepatocyte Culture. *Biotechnology* **97**, 1340-1346(2007).

167. Demetriou, A.A. et al. Replacement of liver function in rats by transplantation of microcarrier-attached hepatocytes. *Science (New York, N.Y.)* **233**, 1190-2(1986).

168. Mooney, D.J. et al. Long-term engraftment of hepatocytes transplanted on biodegradable polymer sponges. *Journal of biomedical materials research* **37**, 413-20(1997).

169. Vacanti, J.P. et al. Selective cell transplantation using bioabsorbable artificial polymers as matrices. *Journal of pediatric surgery* **23**, 3-9(1988).

170. Davis, M.W. & Vacanti, J.P. Toward development of an implantable tissue engineered liver. *Biomaterials* **17**, 365-72(1996).

171. Carraro, A. et al. In vitro analysis of a hepatic device with intrinsic microvascular-based channels. *Biomedical microdevices* **10**, 795-805(2008).

172. Guguen-Guillouzo, C. et al. Maintenance and reversibility of active albumin secretion by adult rat hepatocytes co-cultured with another liver epithelial cell type. *Experimental cell research* **143**, 47-54(1983).

173. Michalopoulos, G., Russell, F. & Biles, C. Primary cultures of hepatocytes on human fibroblasts. *In Vitro* **15**, 796-806(1979).

174. Rojkind, M. et al. Characterization and functional studies on rat liver fat-storing cell line and freshly isolated hepatocyte coculture system. *The American journal of pathology* **146**, 1508-20(1995).

175. Schrode, W., Mecke, D. & Gebhardt, R. Induction of glutamine synthetase in periportal hepatocytes by cocultivation with a liver epithelial cell line. *European journal of cell biology* **53**, 35-41(1990).

176. Kidambi, S. et al. Patterned co-culture of primary hepatocytes and fibroblasts using polyelectrolyte multilayer templates. *Macromolecular bioscience* **7**, 344-53(2007).

177. Revzin, A. et al. Designing a hepatocellular microenvironment with protein microarraying and poly(ethylene glycol) photolithography. *Langmuir : the ACS journal of surfaces and colloids* **20**, 2999-3005(2004).

178. Utesch, D. et al. Differential stabilization of cytochrome P-450 isoenzymes in primary cultures of adult rat liver parenchymal cells. *In vitro cellular & developmental biology : journal of the Tissue Culture Association* **27A**, 858-63(1991).

179. Donato, M.T., Gómez-Lechón, M.J. & Castell, J.V. Drug metabolizing enzymes in rat hepatocytes co-cultured with cell lines. *In vitro cellular & developmental biology : journal of the Tissue Culture Association* **26**, 1057-62(1990).

180. Michalopoulos, K. Liver regeneration : control molecular mechanisms of growth. *The FASEB Journal* 176-187

181. Block, G.D. et al. Population expansion, clonal growth, and specific differentiation patterns in primary cultures of hepatocytes induced by HGF/SF, EGF and TGF alpha in a chemically defined (HGM) medium. *The Journal of cell biology* **132**, 1133-49(1996).

182. Jain, R.K. Normalization of tumor vasculature: an emerging concept in antiangiogenic therapy. *Science (New York, N.Y.)* **307**, 58-62(2005).

11. Chapter 11: Appendices

11.1. Bioconjugate Synthesis Characterization

11.1.1. Gel Permeation Chromatography (GPC)

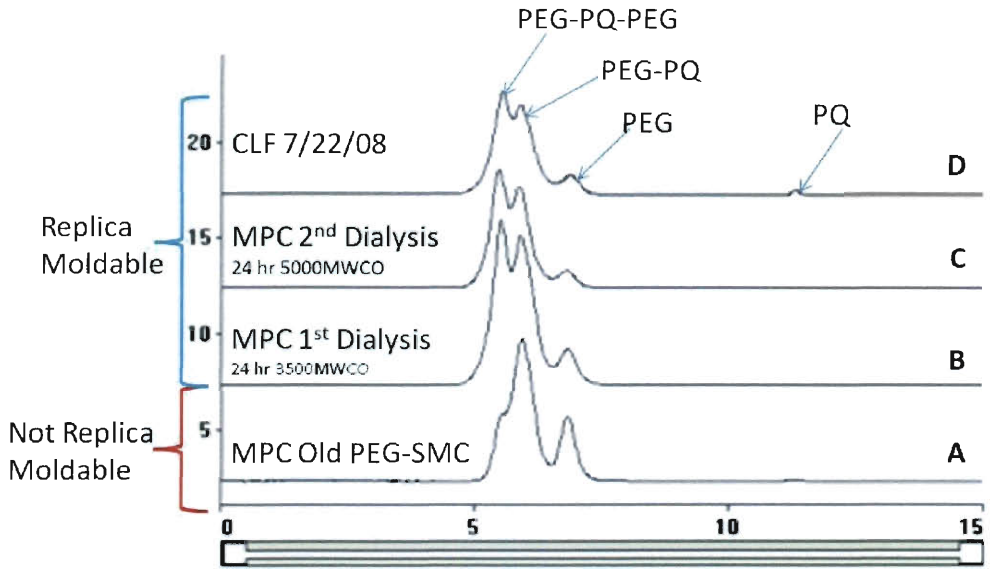

Figure 63: Gel Permeation Chromatography (GPC) of Laysan-PEG-NHS conjugation to PQ peptide. (A) No dialysis purification and (B) one dialysis purification step (C) two-stage dialysis purification and (D) Christy Franco batch with no dialysis. Conjugation batched (B-D) were able to be replica molded to 50 µm photoresist masters.

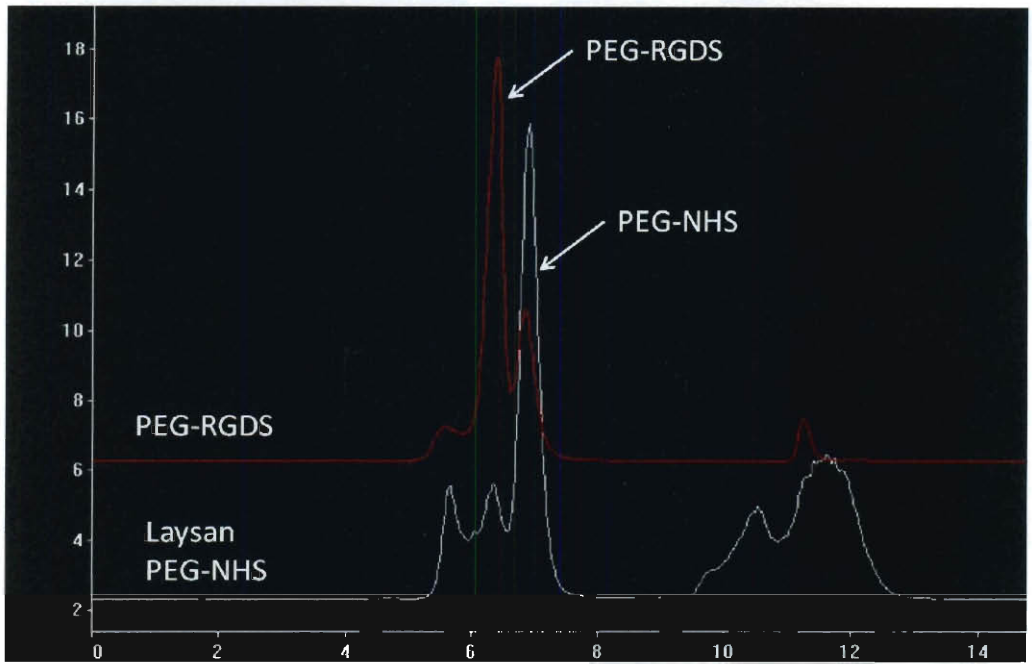

Figure 64: Gel Protein Chromatography (GPC) of Laysan-PEG-NHS conjugation to RGDS. (White Trace) Acryoyl-PEG-NHS from Laysan Bio. Inc. show a peak for PEG-NHS eluting at 7.25 min. (Red Trace) Conjugation of RGDS to PEG-NHS show a the shift in the PEG –RGDS peak to elution at 6 min.

11.1.2. Matrix Assisted Laser Desorption/Ionization Time of Flight Mass Spectroscopy (MALDI TOF)

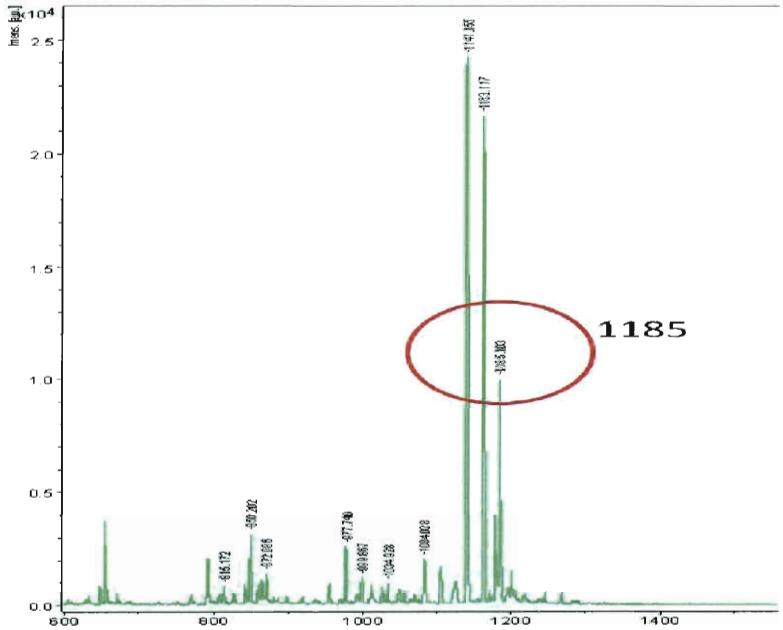

Figure 65: Matrix Assisted Laser Desorption/Ionization Time of Flight Mass Spectroscopy (MALDI TOF) of solid state peptide synthesis product for the collagen derived PQ peptide. Peak at 1185 is the target molecular weight for the peptide.

11.2. Raw Diffusion Data For Studies Reported in Chapter 6

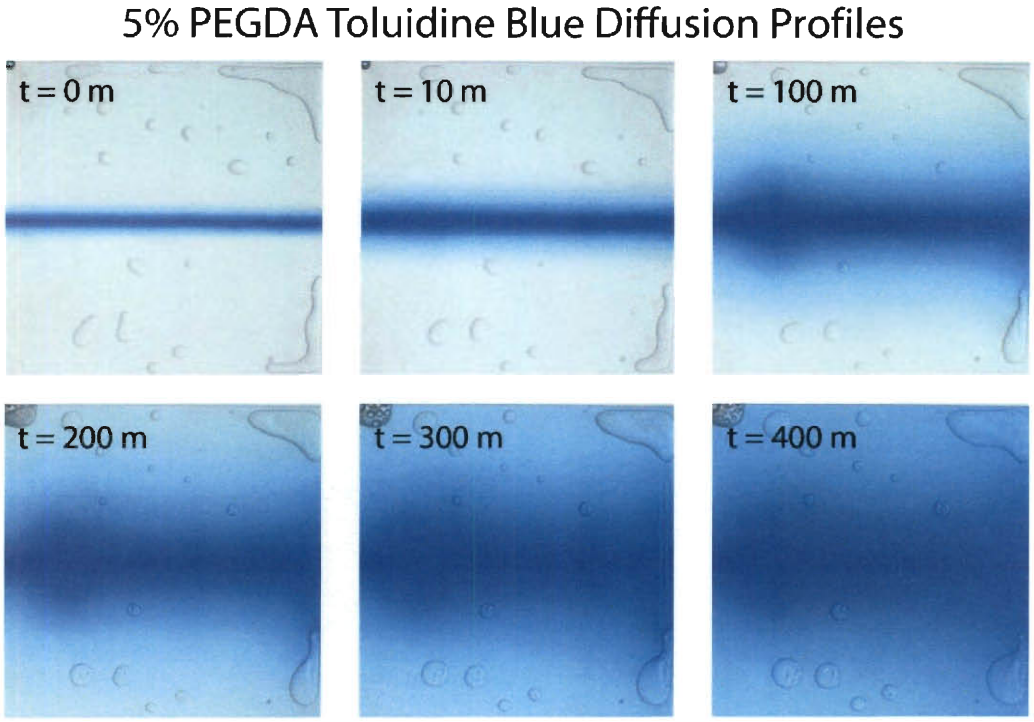

Figure 66: Representative Images of 5% PEGDA Toluidine Blue Diffusion Profiles

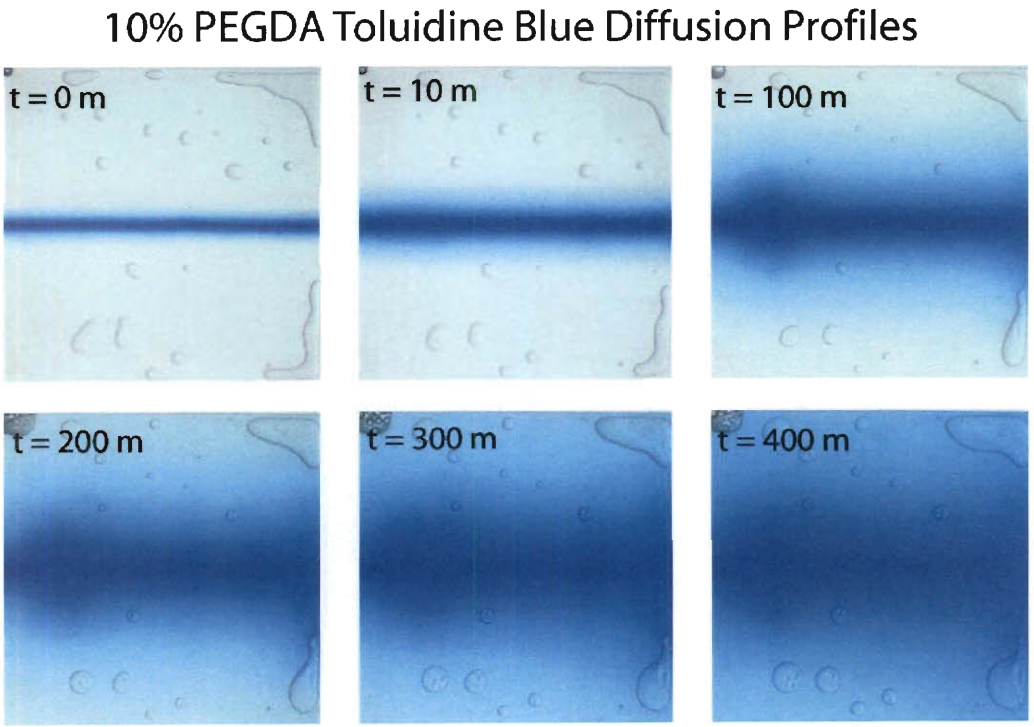

Figure 67: Representative Images of 10% PEGDA Toluidine Blue Diffusion Profiles

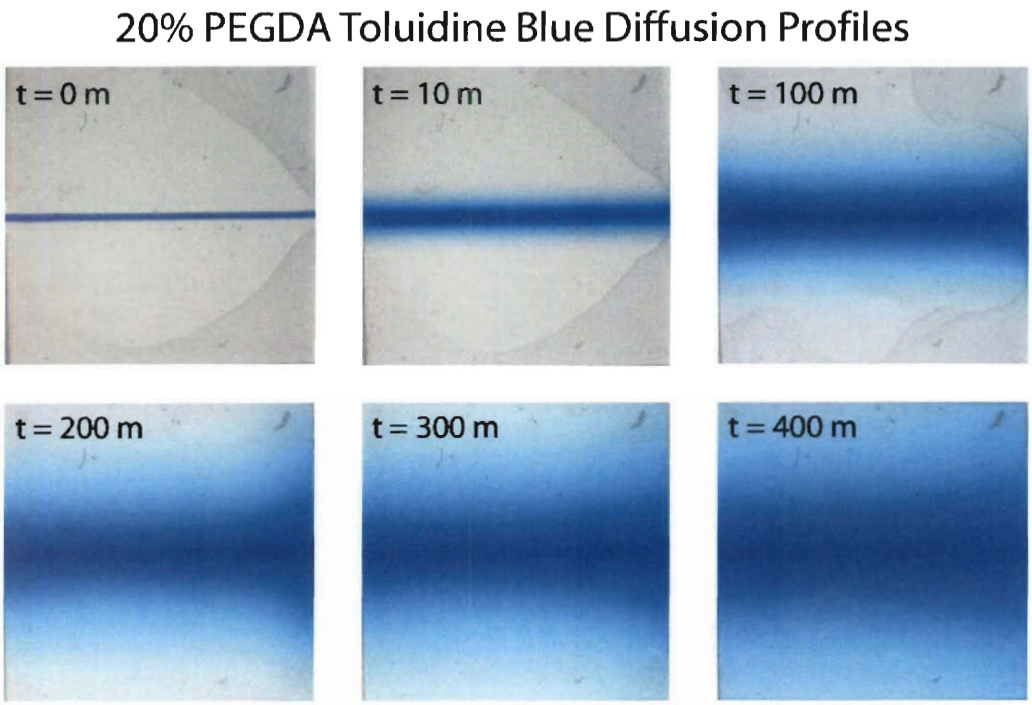

Figure 68: Representative Images of 20% PEGDA Toluidine Blue Diffusion Profiles

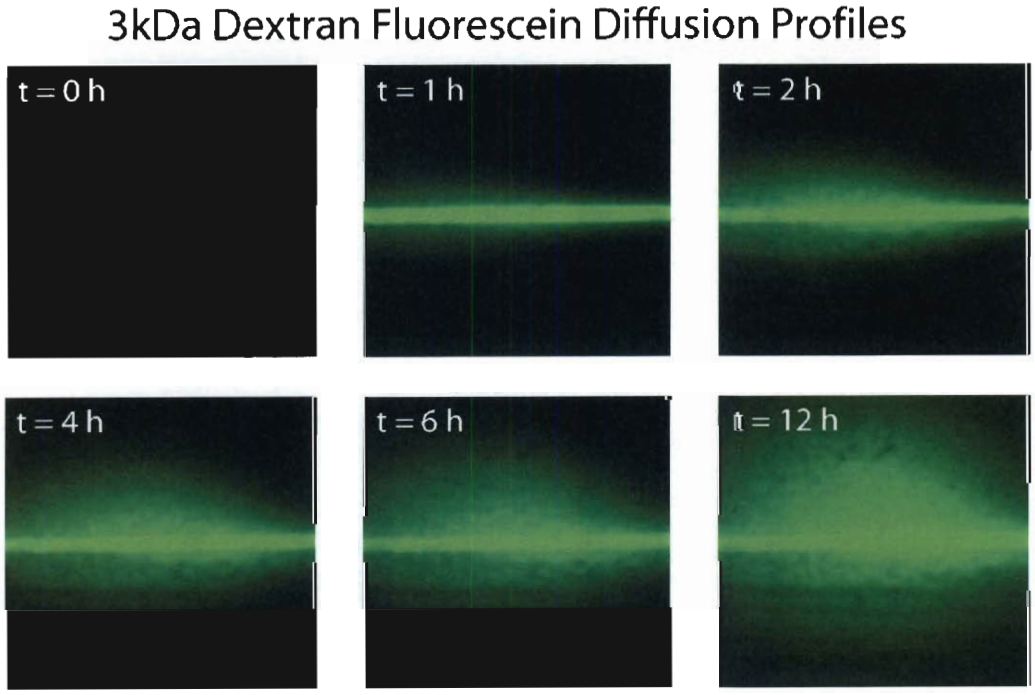

Figure 69: Representative Images of 10% PEGDA 3kDa Dextran Fluorescein Diffusion Profiles

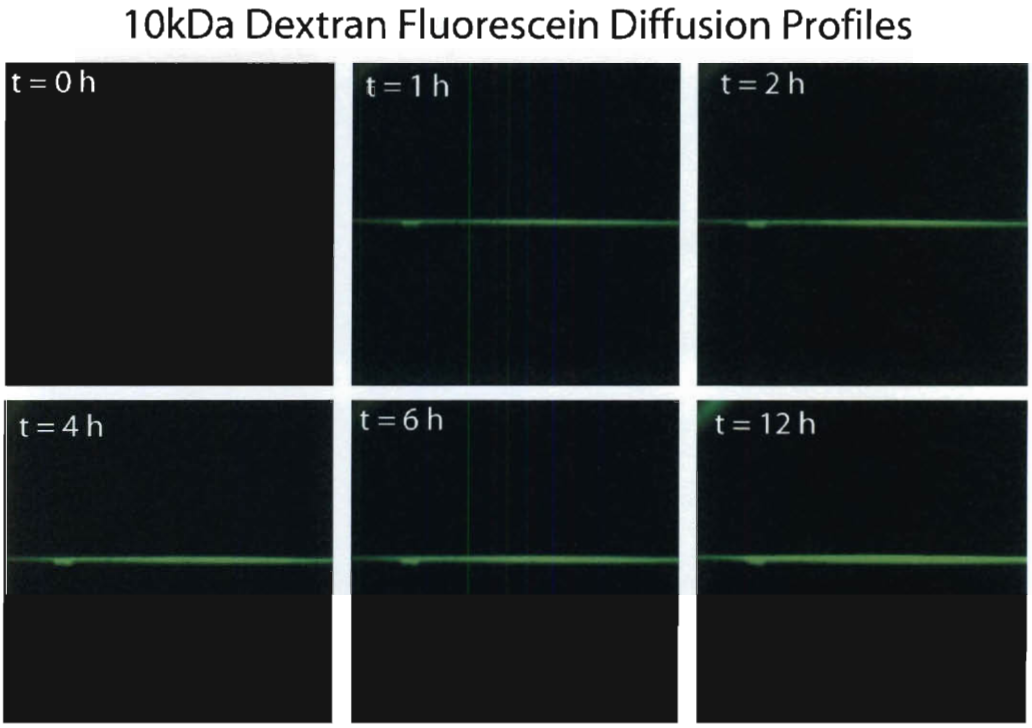

Figure 70: Representative Images of 10% PEGDA 10kDa Dextran Fluorescein Diffusion Profiles